

Sublimation Kinetics for Individual Graphite and Graphene Nanoparticles (NPs): NP-to-NP Variations and Evolving Structure-Kinetics and Structure-Emissivity Relationships

Bryan A. Long, Chris Y. Lau, Daniel J. Rodriguez, Susanna An Tang, and Scott L. Anderson*

Department of Chemistry, University of Utah, 315 S. 1400 E., Salt Lake City, Utah 84112, USA

*Corresponding author: anderson@chem.utah.edu

KEYWORDS: *graphite, graphene, nanoparticle, sublimation, kinetics, emissivity*

ABSTRACT: A single nanoparticle (NP) mass spectrometry method was used to measure sublimation rates as a function of nanoparticle temperature (T_{NP}) for sets of individual graphite and graphene NPs. Initially, the NP sublimation rates were ~ 400 times faster than that for bulk graphite, and there were large NP-to-NP variations. Over time, the rates slowed substantially, though remaining well above the bulk rate. The initial activation energies (E_a values) were correspondingly low and doubled as a few monolayer's worth of material were sublimed from the surfaces. The high initial rates and low E_a values are attributed to large numbers of edge, defect, and other low coordination sites on the NP surfaces, and the changes are attributed to atomic-scale "smoothing" of the surface by preferential sublimation of the less stable sites. The emissivity of the NPs also changed after heating, most frequently increasing. The emissivity and sublimation rates were anti-correlated, leading to the conclusion that high densities of low-coordination sites on the NP surfaces enhances sublimation but suppresses emissivity

INTRODUCTION

Chemistry on the surface of nanoparticles (NPs) is important in catalysis and in many applications of polycrystalline nanomaterials, yet most measurements of nano surface chemistry average over many NPs or crystallites. Because NPs in any ensemble are expected to have different distributions of surface sites (*e.g.*, facets, vertices, defects, ...), and in many cases, large variations in NP size and shape, there is reason to expect that the surface chemistry of individual NPs may deviate substantially from ensemble-averaged chemistry. Understanding these deviations, and associating them with variations in NP structure, is important in developing structure-reactivity relationships for nano surface reactions.

Here we present results from a new method we have developed to measure reaction kinetics and emission spectroscopy for individual NPs at well-defined temperatures. Previous work toward this goal is briefly reviewed in the SI. We apply the technique to sublimation kinetics for graphite and graphene NPs and report on the NP-to-NP variations in the kinetics, the evolu-

tion of rates and activation energies (E_a values) that occurs as the NPs sublime, and on correlations between changes in the distribution of surface sites, and the brightness and wavelength dependence of the thermal emission spectra for individual NPs.

There have been many studies over the last 70 years of the equilibrium vapor pressure of graphite at temperatures >2300 K,¹⁻⁴ including some with mass analysis of the vapor.⁵⁻⁷ The vapor consists of C_n clusters, with partial pressures in the following ratio: $C_3 : C_1 : C_2 = \sim 77.4 : 20.2 : 2.4$, with much smaller contributions from larger clusters. These data have been used to derive C_n heats of formation, $\Delta_f H(C_n)$, which are: $C = 716.7$ kJ/mol, $C_2 = 837.7$ kJ/mol, $C_3 = 820.1$ kJ/mol. Unusually, the sticking coefficients for C_n in collisions with hot graphite are well below unity,^{4, 7-8} thus equilibrium data do not give the C_n sublimation rates or activation energies (E_a values).

Graphite sublimation in vacuum has also been studied,⁹⁻¹² providing total sublimation rates averaged over the C_n species and over the surfaces of the polycrystalline samples. As shown in **Figure S1**, an effective E_a

for sublimation can be estimated by fitting the literature data to a rate law of the form $R = A \cdot \exp(-E_a/kT)$, resulting in a value near 862 kJ/mol, substantially in excess of the $C_n \Delta_f H$ values. A laser-heated sublimation mass spectrometry study measured C_n species distributions.¹³ As in the equilibrium vapor, C_3 was the most abundant, but the C/C_3 and C_2/C_3 ratios were significantly higher than in the equilibrium vapor.

Both our graphite/graphene NPs, and the bulk graphite materials used in the above experiments, have distributions of exposed surface sites, including perfect basal planes, vacancies and other basal plane defects, exposed basal plane edges, and for polycrystalline materials, grain boundaries. Previous results regarding the energetics of such sites and for site diffusion and annealing, are summarized in the Discussion. Fully-coordinated, basal plane sites are the most stable, hence have the highest E_a for sublimation. Basal plane edges, vacancies, and other defects expose atoms in under-coordinated and/or strained geometries, with lower stabilities, hence lower E_a values for sublimation. The sublimation rates and E_a values for both bulk graphite and for our NPs are weighted averages over the distributions of exposed surface sites. The bulk measurements also averaged over large ensembles of crystallites in the polycrystalline samples.

Our single NP measurements are, in essence, looking at individual crystallites, thus allowing the effects of NP-to-NP heterogeneity on sublimation rates to be observed. In addition, as the NPs sublime, the site distributions evolve, and we are able to observe the effects of this structural evolution on the rates and E_a values. For the bulk measurements, enough material was sublimed to ensure that the rates, averaged over many crystallites, reached steady state. For individual NPs, one question is whether anything like steady state can be reached.

Finally, we previously observed that when graphite and other carbon NPs are heated above ~ 1900 K, the intensities of their emission spectra change significantly over time, sometimes brightening by up to a factor of two.¹⁴ Here we characterize the changes in NP spectral intensities and wavelength dependence as NPs sublime, and are able to extract a correlation between the emission brightness and the sublimation rate that provides insight into the structural factors that control emissivity.

EXPERIMENTAL METHODS

The instrument and methods used for trapping a single nanoparticle (NP), and for measuring its charge (Q), mass (M), and temperature (T_{NP}), have been discussed previously.¹⁴⁻¹⁶ In brief, electrospray ionization (ESI) is used to get charged NPs into the gas phase, and after passage through hexapole and quadrupole ion guides, the NPs are passed through a split ring-electrode electrodynamic trap (SRET),¹⁷ where single NPs can be trapped. Argon in the 1 mTorr range is added to damp NP motion. A radio frequency voltage of frequency, F_{RF} , and amplitude, V_0 , is applied across the trap, creating an effective potential minimum at the trap center. Any NP that becomes trapped is heated by a laser focused through the trap, and trapping is detected by observing the thermal emission from the hot NP using a Si avalanche photodiode (APD).

A trapped NP undergoes simple harmonic motion about the trap center, with well-defined frequencies associated axial and radial motion. The axial frequency, F_z , is given by:

$$F_z = \left(\frac{|Q|}{M} \right) \left(\frac{\sqrt{2}V_0}{4\pi^2 F_{RF} z_0^2} \right), \quad \text{Equation 1}$$

where $z_0 = 2.96$ mm. F_z is measured every 30 seconds by a resonance excitation technique, thus giving Q/M . To determine Q , F_z is measured repeatedly as a vacuum ultraviolet lamp is used to induce single electron changes in Q , resulting in F_z steps that are fit to determine Q . F_z measurement precision is $\sim 0.03\%$, which is sufficient to determine Q exactly for $Q \leq \sim 70$ – typical of the small NPs studied here. Given Q , M can be extracted from the F_z measurements. Spontaneous thermionic emission charge steps, sometimes seen at high T_{NP} , are taken into account in calculating M .

To measure kinetics, M is monitored vs. time as the NP is held at constant T_{NP} , or at a series of T_{NP} values. The M vs. time data is fit to determine the mass-loss rate at each T_{NP} . Rates are expressed as numbers of C atoms lost *per* second, but note that our measurements provide no information about the desorbing C_n species. The NPs were heated by a continuous 532 nm laser, loosely focused through the trap center, such that the beam waist was more significant than the amplitude of the NP motion. We previously showed that there are no significant differences if, instead, a 10.6 μm laser is used for heating.¹⁴ The laser power was measured and controlled in order to stabilize T_{NP} .

Uncertainty in Mass Measurements: For NPs with $Q \leq 70$ (most NPs here) we are generally able to determine Q exactly, and in that case, the uncertainty in the M values extracted from equation 1 is primarily due to the uncertainty in z_0 , which depends on the accuracy with which the trap was machined and assembled. This factor gives uncertainty in the absolute mass calibration of roughly $\pm 1.3\%$. For a few of the larger NPs where Q was too large to determine exactly, there is additional uncertainty in the absolute mass calibration of roughly $\pm 0.6\%$. The precision or relative uncertainties in comparing M measurements is much better, $\sim \pm 0.18\%$, from a combination of the uncertainties in measuring V_0 and F_z . Each sublimation rate was determined by fitting at ~ 20 mass measurements to extract the slope of M vs. time.

Uncertainties in the absolute mass calibration cancel, at least partially, for some quantities reported. In the NP volume ratios used to correct spectral intensities, the absolute uncertainty cancels exactly. To allow rates to be compared for NPs of different sizes, we normalize them to a nominal NP surface area, calculated from M , assuming spherical shape with bulk density (2.265 g/cm^3).¹⁸ Thus, the area-normalized rates are proportional to $(\Delta M)/M^{2/3}$, with $\pm 0.4\%$ uncertainty.

NP Temperature Determination: Emission spectra covering the 600 to 1600 nm range were recorded simultaneously with the mass measurements, using an optical system described previously, along with the calibration methodology, and the uncertainties in T_{NP} values.^{14, 16} Briefly, light emitted by the trapped NP was collected and split into $\lambda < 980 \text{ nm}$ and $\lambda > 980 \text{ nm}$ beams, which were dispersed by a pair of spectrographs, equipped with cooled Si CCD and InGaAs photodiode array cameras, respectively. The sensitivity of the optical system vs. wavelength, $S(\lambda)$, is measured using a CO_2 laser-heated micro-thermocouple (type C) as a calibration emitter, allowing NP spectra to be corrected for non-idealities in the optical system. A few example spectra are shown in **Figure S2**.

The NP spectra are fit to a thermal emission model function consisting of Planck's function for ideal blackbodies, multiplied by an emissivity function, ϵ :

$$I(\lambda, T_{\text{NP}}) = \frac{2c \cdot \epsilon(\lambda, T_{\text{NP}})}{\lambda^4 \cdot \left(\exp\left(\frac{hc}{\lambda k T_{\text{NP}}}\right) - 1 \right)} \quad \text{Equation 2}$$

The $\epsilon(\lambda, T_{\text{NP}})$ function accounts for non-idealities due both to the properties of the emitting material and to optical coupling with NPs much smaller than the emitted wavelengths. According to Mie theory, the emissivity for small spherical particles is:¹⁹

$$\epsilon(\lambda, T_{\text{NP}}) = \frac{8\pi r}{\lambda} \text{Im} \left(\frac{(n + ik)^2 - 1}{(n + ik)^2 + 2} \right), \quad \text{Equation 3}$$

where r is the NP radius, and $n + ik$ is the complex index of refraction of the material, which depends on both λ and T_{NP} . Even for bulk materials, n and k are generally not known over our wavelength range at high temperatures, and for NPs there are additional factors such as quantum confinement and large numbers of surface sites that may affect the optical properties. Therefore, as is commonly done for carbonaceous NPs,²⁰⁻²⁴ we use a power-law approximation to the emissivity, $\epsilon(\lambda) \propto \lambda^{-n}$, with n as a fitting parameter, resulting in the thermal emission model function:

$$I(\lambda, T_{\text{NP}}) = \frac{K}{\lambda^{(4+n)} \cdot \left(\exp\left(\frac{hc}{\lambda k T_{\text{NP}}}\right) - 1 \right)} \quad \text{Equation 4}$$

Here, K is a normalization constant, and the two parameters that affect the wavelength dependence are T_{NP} and n . The fit quality is generally good, as can be seen in **figure S2**. We estimated¹⁴ that the extracted T_{NP} values have roughly $\pm 6.2\%$ absolute uncertainty, with $\pm 2\%$ relative uncertainty in comparing extracted T_{NP} values.

Other Experimental Considerations: Details of the NP feedstocks and steps taken to ensure that the NPs are pure carbon are discussed in the SI. The conclusion is that contaminants from ESI or from air exposure are desorbed long before the kinetics experiments start, and that metal contamination should be negligible. **Figure S3** shows an experiment testing possible effects on sublimation rates from background O_2 . The worst-case effects are estimated to be $< 5\%$ at our lowest T_{NP} where sublimation is slow, dropping to $< 0.1\%$ above $\sim 1950 \text{ K}$.

RESULTS

Sublimation kinetics were studied in a series of experiments on individual graphite and graphene NPs. We first present a typical experiment and its analysis, and then summarize the results for sets of graphite and

graphene NPs, focusing on both NP-to-NP variability, and the evolution of NP properties as the NPs are heated to drive sublimation.

Single NP Data: **Figure 1** shows a typical experiment on a single multilayer graphene platelet NP of initial mass 64.03 MDa. The graphene feedstock has reported average thickness of ~ 5 nm, corresponding to ~ 15 layers. The NP temperature (T_{NP}) was ramped in 100 K steps from 1800 K to 2100 K, back down to 1800 K, and finally back up to 2100 K. An initial period during which the NP was held at ~ 1300 K for Q determination is not shown. Gaps in the data indicate periods when T_{NP} was unstable, and these periods were

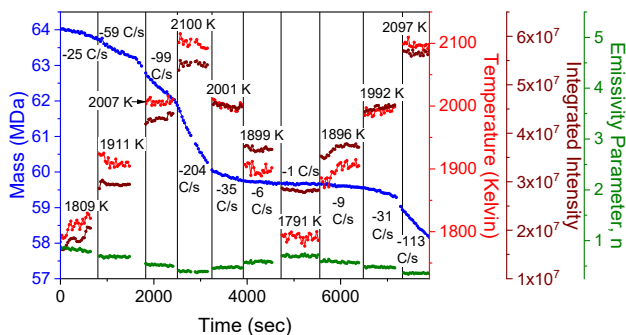


Figure 1: Typical experiment in which a single graphene NP of initial mass of 64.03 MDa was heated in step-wise fashion from ~ 1800 K to ~ 2100 K, back down to ~ 1800 K, then back to ~ 2100 K. The T_{NP} and sublimation rates (given as C atoms/sec) indicated in boxes, are the values averaged over the time intervals defined by the vertical black lines.

omitted from further analysis. With the exception of a few excursions, T_{NP} was generally stable to $\sim \pm 10$ K ($\pm 0.5\%$) during the constant T_{NP} periods, and even the largest excursions were only ~ 30 K (1.5%).

M and T_{NP} were measured repeatedly during each constant T_{NP} time interval, which are indicated by solid vertical lines. The T_{NP} values shown are simply the averages over these time intervals. Mass loss rates were determined by linear fits to M vs. time over the same time intervals, thus giving the average rates, which are indicated in terms of C atoms lost/second. As noted, the experiment gives no information about the desorbing C_n product distribution.

In addition to M and T_{NP} , the figure shows the integrated emission intensity (emitted photons/second/sr over the 600 – 1600 nm range) and the value of the n parameter in the power law emissivity function. Note that n decreased as T_{NP} increased, and then increased again as the NP cooled, indicating that emissivity is

temperature dependent. The integrated emission intensity, I , increased by a factor of ~ 2.6 as T_{NP} increased by a factor of ~ 1.17 (~ 1800 to ~ 2100 K), corresponding to $I \propto T_{NP}^6$.

The sublimation rates (slopes of M vs. time) increased with increasing T_{NP} , as expected, however, note that the rates at similar T_{NP} values measured at the beginning and end of the experiment were significantly different, generally slowing over time. For example, at ~ 2007 K during the initial heat ramp up, the NP sublimated at a rate of 99 C/sec, but at ~ 2001 K during the ramp down, the rate was only 35 C/sec. As NPs sublime, some rate slowing is expected due to loss of NP surface area, however, the mass loss over the entire experiment was only $\sim 9\%$, thus the surface area loss ($\propto M^{2/3}$) would have been on the order of 6%, i.e., far too small to account for the rate slowing.

To allow the kinetic and emission behavior to be observed more easily, it is useful to convert the raw results into more concise and comparable forms, and this process is illustrated in **figure 2** for the NP in **figure 1**. The T_{NP} values, emission intensities, and n parameters are the average values for each time interval in **figure 1**, and the rates are the average slopes in each interval. The uncertainties in mass, rates, T_{NP} , etc. are discussed above, and **figure 2** illustrates these using error bars. In this experiment, T_{NP} was ramped up, down, then up again, but for other NPs, different T_{NP} programs were examined. The order and direction of heat ramps applied to each NP are indicated using the following terminology: 1st Ramp: Up, 2nd Ramp: Down, etc.

The emission intensity changes are summarized in **figure 2A**. Ideal blackbody emission intensity scales with emitter surface area, but the emissivity for small NPs (**equation 3**) introduces another factor of r , thus intensity should scale with r^3 . Therefore, to compensate for the expected effects of decreasing NP size during experiments (and to allow comparisons between different size NPs), the intensities in **figure 2** and all figures below, have been scaled by the NP mass ($\propto r^3$) measured simultaneous with the spectra. In this case, the intensity increased and decreased with T_{NP} as noted, but note that the intensities tended to increase over the course of the experiments.

The horizontal error bars represent the estimated $\pm 2\%$ relative uncertainty in T_{NP} values, because this is what affects trends extracted from comparing data points. Intensity error bars are not shown because they would be smaller than the height of the symbols.

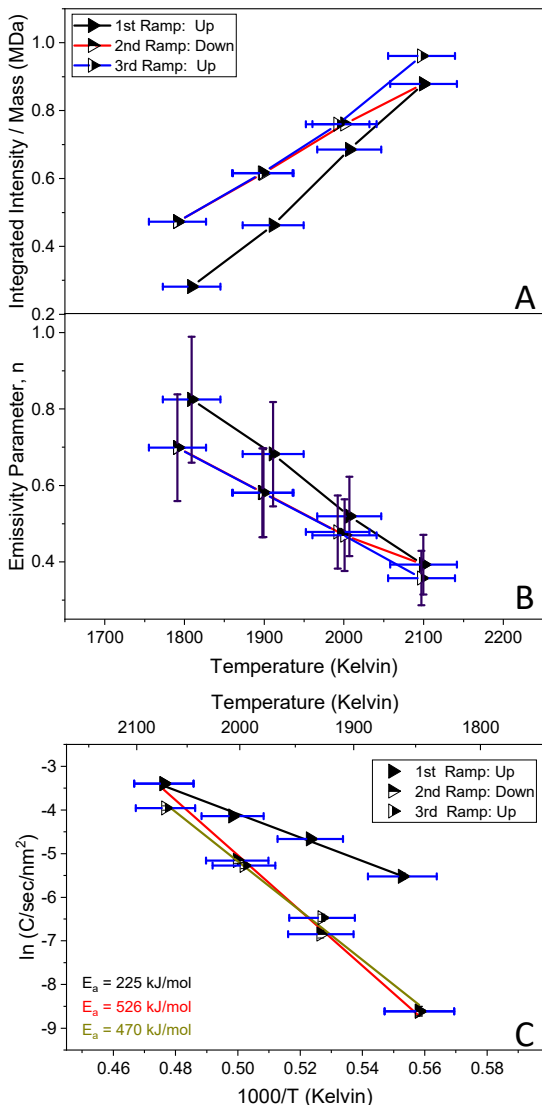


Figure 2: Analysis of the graphene experiment in **figure 1**. A: Integrated emission intensity averaged over each constant T_{NP} period. B: Emissivity parameter, n , averaged over each constant T_{NP} interval. C: Area-normalized sublimation rate vs. T_{NP} for each heat ramp, with fits to extract the effective E_a values shown.

Figure 2B plots the n parameter, which decreased with increasing T_{NP} , then recovered as the T_{NP} dropped, but only to $\sim 80\%$ of its initial value, again indicating an irreversible change during the experiment. The vertical error bars represent the estimated $\sim \pm 20\%$ uncertainty in the n parameter¹⁴ – large because it takes a large change in n to cause significant change in spectrum fit quality.

Figure 2C plots the sublimation rates measured at each T_{NP} during the three heat ramps. Vertical error bars ($\sim \pm 0.4\%$) are not shown because they would be smaller than height of the symbols. To correct for the

$\sim 6\%$ surface area loss during the experiment, and to allow comparisons with other NPs, we would ideally normalize rates to the NP surface areas, but these are unknown. Therefore, we have approximated the area-normalized rates assuming that the NPs are spherical with the bulk density. Obviously, this gives lower limits on the surface areas, hence upper limits on the area-normalized rates, given as $C/\text{sec}/\text{nm}^2$. The data for all three heat ramps are reasonably linear when plotted as $\ln(C/\text{sec}/\text{nm}^2)$ vs. $1000/T$, thus the fit lines can be used to extract activation energies, E_a , and prefactors, A , in rate expressions of the type: $R = A \exp(-E_a/RT_{\text{NP}})$.

For this data, the E_a value extracted from 1st ramp up was 225 kJ/mol. The E_a extracted from the 2nd ramp down was 526 kJ/mol, and the 3rd ramp up gave $E_a = 470$ kJ/mol. We discuss the interpretation of the extracted E_a values, below, after summarizing the results for sets of graphene and graphite NPs.

Because the uncertainties in the mass loss rates are small, the uncertainty in the E_a values comes almost entirely from the $\pm 2\%$ relative uncertainty in T_{NP} measurements. We estimated the E_a uncertainty by simulating the effect of applying random gaussian T_{NP} perturbations to each point in the heat ramps, with 2% standard deviation, refitting the data to extract the E_a values associated with the perturbed T_{NP} values. The simulation was repeated $\sim 10,000$ times for each heat ramp to obtain the corresponding spread in E_a . The spreads vary somewhat from heat ramp to heat ramp, but average $\sim \pm 20\%$ of the extracted E_a values, and we take this as our estimate of the uncertainty in E_a .

Figures S4 and **S5** present a similar experiment and analysis for a single graphite NP, with initial mass of 38.93 MDa. As with the graphene NP in **figures 1** and **2**, irreversible changes in the graphite NP's kinetic and spectroscopic properties were observed over the course of the experiment. The volume-weighted emission intensity increased, the n parameter decreased, and the sublimation kinetics slowed substantially over the course of the experiment, with a substantial increase in the E_a values from the first to second heat ramps.

Before presenting summaries of sublimation experiments on sets of graphite and graphene NPs, we present an example of a simpler kind of experiment, monitoring kinetic and emission behavior over longer time periods at constant T_{NP} , as shown in **figures 3** and **S6**, for two graphite NPs held at different T_{NP} values. The NP in **figure 3** had initial mass of 82.88 MDa, and was held at 1900 K for ~ 9 hours (an initial period for Q determination at low T_{NP} is not shown). This experiment was

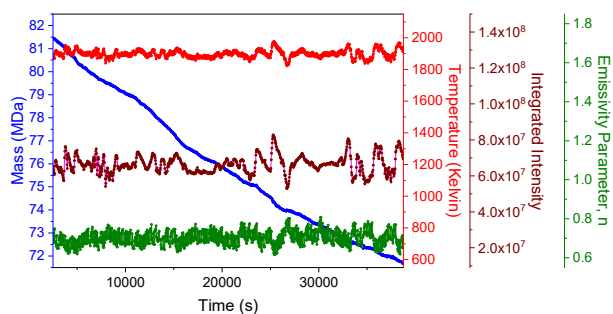


Figure 3: Long exposure heating experiment of a graphite NP with initial mass 82.88 MDa. The T_{NP} was held at 1900 K for ~ 10.8 hours.

done using the 532 nm heating laser, augmented by a cw CO_2 laser run at nominally constant power. T_{NP} had good long-term stability, but there were short term fluctuations, from power fluctuations of the CO_2 laser, which the T_{NP} control program was not able to compensate completely. The emission intensity fluctuated with the T_{NP} fluctuations, as expected from the strong dependence of intensity on T_{NP} . The mass loss rate also

fluctuated, but much more slowly, and some fluctuations (e.g. between 10,000 and 20,000 seconds), were not obviously correlated with variations in T_{NP} . More importantly, there was a gradual slowing of the mass loss rate from an average of 368 C/sec over the first three hours, to an average of 189 C/sec over the final three hours. This $\sim 50\%$ decrease is far larger than can be rationalized by the $\sim 12\%$ loss in total mass ($\sim 9\%$ in surface area). More dramatic mass loss rate slowing was observed for a graphite NP at 2000 K, as shown in **figure S6**.

Comparison Data: **Figure 4** plots aggregated data for emission properties from 15 graphite NPs with initial masses ranging from ~ 5 to ~ 120 MDa (~ 19 to 56 nm, if spherical), and for 7 graphene NPs with initial masses ranging from ~ 10 to ~ 70 MDa. A consistent set of symbols is used in **figures 4-7, S7, and S8**; color and shape indicate particular NPs, while symbol filling indicates the 1st, 2nd, or 3rd heat ramps. The arrows after the legend symbols indicate whether each heat ramp was up or down, *i.e.*, to increasing or decreasing T_{NP} .

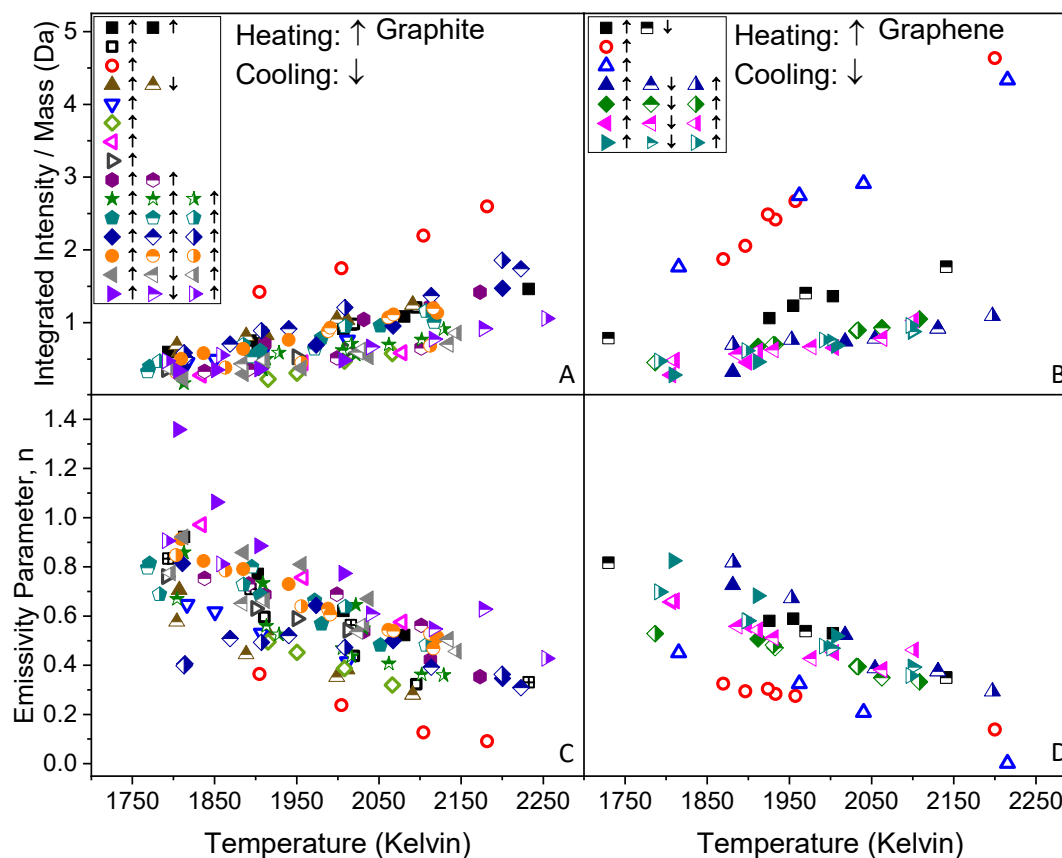


Figure 4: A and B: Integrated emission intensity for all graphite and graphene NPs in each heat ramp. Consistent symbol shapes are used for each NP. The symbol fill indicates the heat ramp. The arrows in the legend indicate whether the heat was ramped up or down. C and D: Emissivity parameter n for each NP in all heat ramps.

For some experiments, indicated by open symbols, we were only able to run a single heat ramp (always up) before losing the NP from the trap. The vertical scales are identical for the graphite and graphene NPs, allowing direct comparison of the emission properties.

The top half of the figure shows the integrated emission intensities, scaled by the NP masses measured at the same time as the emission, *i.e.*, approximately corrected for the effects expected from varying NP volume, both from NP-to-NP and for each NP as it sublimed. Error bars are not shown, but would be the same as in **figure 2A** ($\pm 2\%$ horizontal, negligible vertical).

The main observations were:

1. The volume-corrected emission intensity increased with increasing T_{NP} for all NPs, but with substantial NP-to-NP variation.

2. One graphite and two graphene NPs stood out as having substantially higher-than-average volume-corrected emission intensities, even though their masses were similar to those of other NPs (see below).

3. The graphite and graphene NPs had similar emission intensities, *i.e.*, while there were large NP-to-NP variations within each data set, the intensity ranges for graphite and graphene NPs overlapped.

4. Examples were seen where the emission brightness increased, decreased, or did not change significantly between the heat ramps.

The bottom half of **figure 4** shows data for the n parameter, which controls the shape of the thermal emission model function used in spectral fitting. Low (high) n corresponds to flatter (sharper) λ dependence. Error bars are not shown, but would be the same as in **figure 2B** ($\pm 2\%$ horizontal, $\pm 20\%$ vertical). The main observations were:

1. The n parameter tended to decrease with increasing T_{NP} but with NP-to-NP variation of more than a factor of 2.

2. The one graphite and two graphene NPs that had unusually high emission intensity also had unusually low n parameters, *i.e.*, less λ -dependent spectra.

3. The graphite and graphene NPs had n parameters in overlapping ranges, but graphite had slightly higher n parameters on average.

Figure 5 summarizes the sublimation rates, R , plotted as $\ln(R)$ vs. $1000/T$, such that the slopes are proportional to the activation energies (E_a). Data points are the experimental rates for each NP, and lines are single exponential fits to the data. As in **figures 2C** and **S5C**,

the raw sublimation rates (C atoms/sec) have been normalized to nominal NP surface areas, calculated assuming spherical shape with the bulk density. Error bars are not shown, but would be the same as those in **figure 2C** ($\pm 2\%$ horizontal, negligible vertical).

Rates are reported separately for the 1st heat ramp (always up) and for the 2nd and 3rd heat ramps, the direction of which can be seen in the legend for **figure 4**. The masses of the NPs in each heat ramp can be seen by comparison to **figure 6**, and the charges can be seen by comparison to **figure S8**. Also plotted for comparison in each frame of **figure 5** is an estimate of the sublimation rate for bulk graphite from measurements at temperatures above 2300 K (see **figure S1**).⁹⁻¹²

Most of the data are reasonably well fit by single exponential functions, but during the 1st heat ramps, the fits for some NPs deviated by up to a factor of ~ 5 at the lowest or highest T_{NP} points. In those cases, the fit lines shown are the best single exponential fits to the remaining points. In the 2nd and 3rd ramps, the data are generally well fit by single exponential rate laws.

To facilitate comparisons between different heat ramps and with the rates for bulk graphite, we also show the ensemble-averaged rates as solid red dots with red fit lines. Calculating the ensemble averages is complicated by the fact that the measured T_{NP} values varied from NP-to-NP. To obtain the average rate, we used the single exponential fits to each NP data set to estimate what the rates for each NP would have been at 1800, 1900, 2000, and 2100 K. These estimated rates were ensemble-averaged to obtain the red dots, which were then fit to single exponentials (red lines).

There are several important points to note:

1. During the 1st heat ramp, the average area-normalized rate for graphite NPs at 1800 K was ~ 400 times faster than the bulk graphite rate, and that for graphene was ~ 360 times faster. Our assumption of spherical shape in calculating the NP surface area gives an upper limit on the rate *per* nm^2 , however, the actual NP surface areas are certainly not underestimated by anything like a factor of 400. Thus, we conclude that the NPs had substantially higher inherent sublimation rates *per* unit area than bulk graphite.

2. The NP sublimation rates increased more slowly with increasing T_{NP} than that for bulk graphite, such that for $T_{\text{NP}} = 2100$ K, the averaged NP rates were only a factor of \sim three higher than that for bulk graphite.

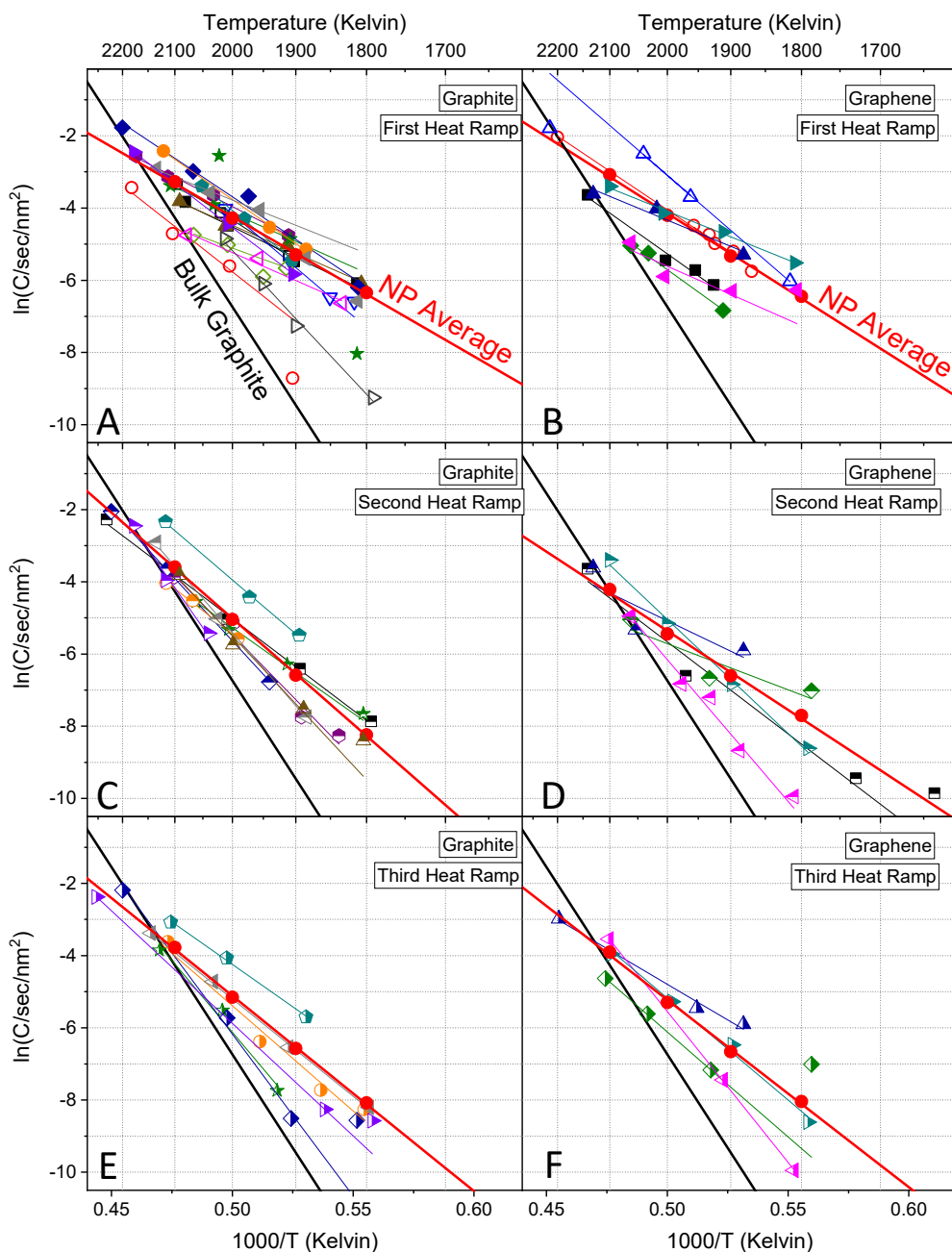


Figure 5: Top: Area-normalized rates vs. T_{NP} for graphite (right) and graphene (left) NPs. Points indicate measured rates using the same symbols as in **figure 4**, and lines through each set of points are single exponential fits. The solid red circles show the average rates, and the red lines are fits to the average rates. The solid black line is the extrapolated rate for bulk graphite. Middle and bottom rows: Analogous plots for the 2nd and 3rd heat ramps.

3. The anomalously bright graphite NP (red circles) had the slowest sublimation rates and the steepest slope of any of the graphite NPs. The two anomalously bright graphene NPs (red circles, blue triangles) also

had somewhat steeper-than-average slopes, but had higher-than-average sublimation rates.

4. The rates at low T_{NP} in the 2nd and 3rd heat ramps were substantially lower than those in the 1st heat ramp,

although still substantially higher than the bulk graphite rate. For example, at 1800 K the averaged rate for graphite NPs in the 2nd heat ramp was ~ 6.6 times slower than in the 1st heat ramp, but still ~ 60 times higher than that for bulk graphite.

5. The rates in the 2nd and 3rd heat ramps increased substantially faster with T_{NP} compared to the 1st heat ramp so that for $T_{NP} > 2100$ K, the rates for all three heat ramps were similar and also similar to that for bulk graphite.

6. The area-normalized rates at low T_{NP} in the different heat ramps varied from NP to NP by factors of up to 10 for the graphite NPs, and by factors of up to 20 for the graphene NPs. The variability of the rates decreased at higher T_{NP} but still exceeded a factor of 4.

7. The NP-to-NP variability in the sublimation rate was much larger than the differences between the ensemble-averaged rates for graphite and graphene, *i.e.*, there was no significant difference between graphite and graphene NPs.

Finally, the activation energies (E_a values) extracted from the single exponential fits in **figure 5** are plotted in **figure 6** against the NP mass, measured at the beginning of each heat ramp. To maintain readability, error bars are not shown, however, the uncertainties in mass are negligible, and as discussed above, the uncertainties in the E_a values are roughly $\pm 20\%$. **Figure S7** in the SI gives the prefactors (A) using the same format. For NPs where only a single heat ramp was completed, a single point is shown (open symbols). For NPs where multiple ramps were completed, filled symbols connected with lines are used. For a few of the more massive NPs, arrows are superimposed on the lines to show the order of the heat ramps (1 \rightarrow 2 \rightarrow 3). For other NPs, the E_a values can be associated with the 1st, 2nd, and 3rd heat ramps by recognizing that the NP mass always decreased from 1st to 2nd to 3rd heat ramp. The NP-ensemble-averaged E_a values, and the value for bulk graphite are shown as horizontal dashed lines.

The important points for this figure are:

1. There were no obvious trends in E_a with NP mass.
2. In 1st heat ramp for each NP, the E_a values varied significantly from NP-to-NP, and many were unexpectedly low. For graphite NPs, the E_a values ranged from 202 to 597 kJ/mol, with an ensemble-averaged E_a of 322 kJ/mol. For graphene, the E_a values ranged from 224 to 482 kJ/mol with average of 352 kJ/mol. (The ensemble-averaged values given in the figure include

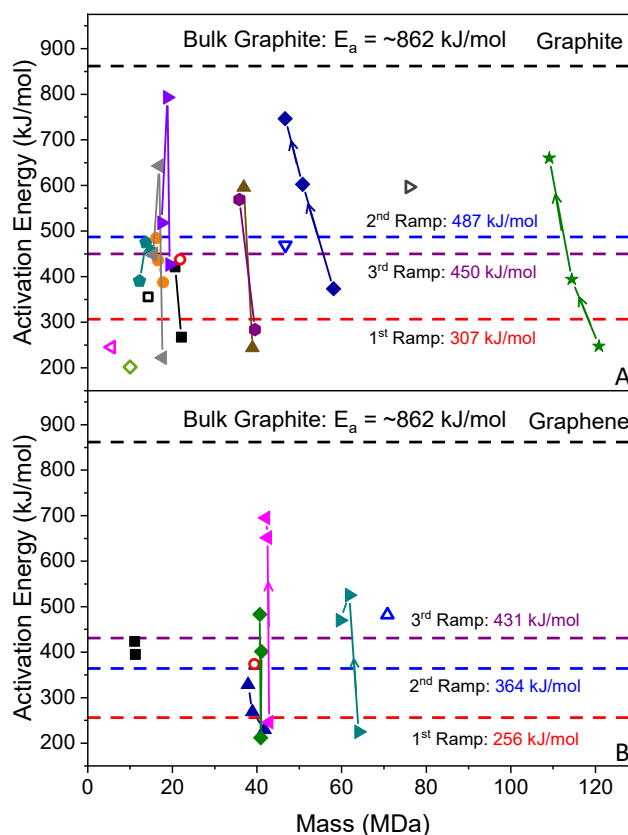


Figure 6: E_a values extracted from fits to the rates in **figure 5** for graphite (top) and graphene (bottom). Pre factor values are found in **figure S6**. Also shown in all figures are the average values for the NPs and the values obtained by fitting bulk graphite data.

only NPs for which at least two heat ramps are available).

3. These spreads in E_a values are not uncertainties, but rather indicate the inherent variations between different NPs. Measuring this NP-to-NP variability is one of the motivations for studying single NP kinetics.

4. In the 2nd heat ramp, the E_a values increased for all NPs, but there were still substantial NP-to-NP variations (394 to 792 kJ/mol for graphite, 212 to 652 kJ/mol for graphene). The ensemble-averaged E_a values increased to 487 kJ/mol and 364 kJ/mol for graphite and graphene, respectively.

5. In the 3rd heat ramp, the E_a values for a few of the graphite NPs approached the bulk graphite value, but most remained well below, and for a few NPs, the E_a values decreased, in one case substantially. As a result, the average E_a decreased slightly for graphite.

6. On average, the E_a values for graphene NPs were lower than those for graphite NPs, but the differences

were much smaller than the NP-to-NP variations within each data set.

DISCUSSION

The results presented here show that there are substantial NP-to-NP variations in volume-scaled emission intensities, n parameters, area-normalized sublimation rates, and activation energies, and that all these properties evolve significantly as the NPs sublime. It is not so obvious what factors influence the emission properties, however, the sublimation kinetics clearly must depend on the distribution of sites present on each NP's surface. Sites with different structures have different energetics, hence different E_a values and rates for sublimation, and the measured rates for each NP are averages over the site distributions present at the time of measurement. The substantial NP-to-NP variation in sublimation behavior is attributed to the heterogeneity of the graphene and graphite feedstocks, which have distributions of size, shape, and presumably of atomic-scale surface structure. The mass losses during each experiment correspond to removing several monolayer's worth of material, thus it is reasonable to expect that the surface structures should evolve, thereby accounting for the observed evolution of the kinetics. Before discussing the structure-kinetics relationship, we need to consider two other properties which varied significantly from NP-to-NP, and thus could conceivably have affected sublimation: the NP size/mass and the charge.

Effects of NP Mass on Sublimation Rates: Figure 5 shows that the surface-area-normalized rates for the NPs in each heat ramp varied substantially and that they changed from one heat ramp to the next. The mass of each NP at the start of each heat ramp can be identified by comparison to figure 6, where the same symbols are used. Close examination shows no correlation between mass and rates in the 1st heat ramp – some NPs with similar masses had very different rates, and some NPs with very different masses had similar rates. In the 2nd and 3rd heat ramps, the NP-to-NP rate variations were smaller, and one apparent anomaly emerged. Most of the graphite NPs had rates within a factor of ~two of the average rate, and these showed no correlation to the NP mass. One graphite NP (turquoise pentagons) had distinctly higher rates, and it happened to be the lowest mass graphite NP (initial mass ~17.5 MDa) for which multiple heat ramps were completed. Note, however, that there were four other graphite NPs with an initial mass just a few percent higher, and these had rates at or below the average. Therefore, we discount

the possibility that the high rates for this NP resulted from an inherent effect of mass on sublimation.

Figure 6 plots E_a vs. NP mass in each heat ramp on each NP. E_a varied substantially for the set of NPs, but there is no obvious correlation with NP mass. It is true that the E_a values generally increased during the three heat ramps, while M decreased, but the mass changes are small compared to the differences in masses between different NPs. Therefore, the changes in E_a as each NP sublimed are attributed to evolution of the NP surface site distributions, rather than to any inherent effect of the small changes in mass.

Effects of NP Charge on Sublimation Rates: In these experiments, the NP charge, Q , varied from +30e to +110e, generally increasing with NP mass. We previously showed that changing Q has no effect on emission spectra or T_{NP} ,¹⁴ and here the question is whether Q might have effects on sublimation kinetics. In fact, such effects would be quite surprising because Q/M is so low – between 7×10^{-7} and 6×10^{-6} e/Da, corresponding to between 8×10^{-6} and 7×10^{-5} e/carbon atom. Figure S8 shows the measured E_a values for the graphite NPs plotted against the Q values measured at the beginning of each heat ramp. A comparison of figures 5 and S8 allows the rates for each graphite NP to be associated with its charge. As discussed in the SI, we conclude that there are no direct effects of Q on either sublimation rates or extracted E_a values.

Effects of NP Surface Site Distributions on Sublimation Rates: For graphitic NPs, the two major classes of sites are perfect basal planes where all atoms are fully coordinated with unstrained bonds, and less stable sites such as basal plane defects or edges. Because such sites are less stable, they have lower heats of sublimation, and because they have fewer or strained C-C bonds, the transition states for sublimation should also be lower in energy (*i.e.*, lower E_a values), compared to those for loss of C_n from perfect basal planes.

For both graphite and graphene NPs, the rates measured at low T_{NP} during the 1st heat ramps averaged about 400 times faster than the rate for bulk graphite, indicating that the NPs initially had large numbers of defective or under-coordinated surface sites. At low T_{NP} during the 2nd heat ramps, the rates were much slower, indicating that the numbers of such sites decreased when the NPs were heated, driving sublimation. For most, but not all NPs, the rates in the 3rd heat ramps were slower yet, indicating that sublimation tends to drive the NPs toward more stable surface structures.

This evolution of the surface site distributions explains why the E_a values extracted from the 1st heat ramp data were so low – below 300 kJ/mol for many NPs. Such low E_a values are unphysical because any sites with such low E_a values would have sublimed away long before the start of the kinetics experiments, during the >20 minutes that each NP was held at ~1300 K for Q determination. For example, assuming a 1st order desorption rate constant of the form, $k_1 = v_1 \cdot \exp(-E_a/RT)$, and $v_1 \approx 10^{14} \text{ sec}^{-1}$, in the range typically seen for surface desorption,²⁵⁻²⁶ we can estimate the lifetime ($1/k_1$) for a site with $E_a = 300 \text{ kJ/mol}$ to be ~10 msec at 1300 K.

Instead, the low 1st heat ramp E_a values reflect the *evolution* of the site distribution during the heat ramp. Initially, the NPs had a large number of sites contributing to sublimation, resulting in high initial rates. As the NPs were heated, the coverage of such sites dropped, resulting in rates that increased more slowly with T_{NP} than would have been the case for a constant site distribution. Evolution, thus, artificially decreased the slopes in **figure 5**, giving artificially low E_a values.

The measured rates can be used to roughly estimate the average E_a for sites contributing to sublimation during the 1st heat ramp. At 1800 K, the average mass loss rate was ~0.002 C/sec/nm², corresponding to an average surface atom lifetime of ~50 seconds. Using the k_1 expression given above, this would imply $E_a \approx 540 \text{ kJ/mol}$, averaged over the sites contributing to sublimation at that T_{NP} . By the end of the 1st heat ramp, at ~2100 K, the average rate was ~0.04 C/sec/nm², implying an average surface atom lifetime of ~2.5 seconds and $E_a \approx 580 \text{ kJ/mol}$, consistent with the conclusion that the surface site distributions evolved to higher average site stability.

It is useful to compare these values to what is known about the energetics of different graphitic sites and diffusion processes. The net energy to remove an atom from a perfect basal plane, creating a mono-vacancy, is reported to be in the 705 to 725 kJ/mol range,²⁷⁻³⁴ and removing C₂ to create a di-vacancy has net formation energy estimated to be in the 700 - 790 kJ/mol range.³³⁻³⁵ It is likely that the E_a values for these processes are higher yet, thus, under our conditions, sublimation of C or C₂ from perfect basal plane sites should make only minor contributions to the total rate. We were unable to find energetics for loss of larger C_n from basal planes, but given the numbers of bonds that would have to be broken, these are also likely to be minor processes under our conditions.

The fast NP sublimation rates are, instead, attributed to the presence of low-coordination, high formation energy sites on the NP surfaces. Some types of low-coordination sites probably are not important, however. For example, adatoms on top of graphitic basal planes are bound by only 145 to 200 kJ/mol,^{33-34, 36-37} and have E_a values for lateral diffusion in the 34 to 51 kJ/mol range.³⁸ Therefore, any adatoms initially present on the NPs would have desorbed or diffused to defects or edges³⁸ long before the start of our experiments.

One type of site that must contribute strongly to sublimation of NPs are basal plane edges. Several symmetric edge structures are possible, including “armchair” with formation energy estimated to be in the range of 110 - 250 kJ/mol *per* angstrom of edge length, “zigzag” (116 - 300 kJ/mol/angstrom), and Klein (172 kJ/mol/angstrom).^{27, 38-39} Armchair edges expose pairs of doubly coordinated atoms, zigzag edges expose individual doubly coordinated atoms, and the Klein edge exposes a row of singly coordinated atoms. In addition, there are lower symmetry edge structures that can form by reconstruction from the symmetric edge structures with low E_a values (< 200 kJ/mol).^{38, 40} Thus, interconversion between different edge structures should be rapid on our time scale.

Another important type of site is basal plane defects, which are likely to be present to some extent in the reactant NPs. The E_a values for sublimation of strained or under-coordinated atoms at defects are similar to those for edge sites, and as material sublims around the defects, holes or pits form that expose sites similar to those around the basal plane edges.⁴¹⁻⁴⁶

An obvious question is the extent to which annealing is important during sublimation, *i.e.*, is annealing fast enough to significantly modify the surface site distribution, as it evolves during sublimation? The E_a for lateral diffusion of C atoms within perfect basal planes is estimated to be in the ~675 to 780 kJ/mol range,²⁸ and annealing of dislocation loops by a vacancy creation/migration mechanism has $E_a \sim 800 \text{ kJ/mol}$,⁴⁷ both substantially higher than the E_a values for NP sublimation. As already noted, interconversion between different edge structures should be fast, however, that simply converts between different types of under-coordinated sites with similar energies, rather than reducing their numbers. If the NPs have existing mono-vacancies, their E_a values for lateral diffusion are only *ca.* 115 to 135 kJ/mol,^{33-34, 48} which would give diffusion rates fast compared to sublimation. Diffusion of a mono-vacancy to a basal plane edge is energetically favorable

(and for NPs, the distances are small), and since this effectively heals the vacancy, we expect mono-vacancies to be short-lived. Note, however, that merging two mono-vacancies to form a di-vacancy is also energetically favorable, and the energy for lateral diffusion of di-vacancies is estimated to be 580 - 840 kJ/mol,^{33-34, 48} *i.e.*, once formed, di-vacancies are much more stable with respect to diffusion than mono-vacancies. This is presumably also true of larger vacancies. We conclude that atomic-scale transformations (mono-vacancy diffusion, edge interconversion) should be fast on the sublimation time scale, but that large scale restructuring of the NPs in ways that would significantly change the number of under-coordinated surface sites, is probably not. Therefore, sublimation – specifically preferential sublimation from defective/under-coordinated sites – is the dominant process driving the evolution of the surface site distributions during sublimation.

As shown in **figure 6**, in the 3rd heat ramps, the E_a values for a few of the NPs approached that for bulk graphite, but the average remained substantially lower, raising the question of how best to compare our single NP measurements with the bulk sublimation experiments described above.⁹⁻¹² The bulk experiments, on polycrystalline graphite, would also have had contributions from a range of sites, including basal planes, exposed basal plane edges or defects, and grain boundaries. Furthermore, the individual crystallites in the bulk graphite undoubtedly evolved with time, similar to the evolution shown here for single NPs. The bulk rates average over many crystallites, however, and because macroscopic amounts of material were sublimed, the area-averaged site distributions and associated kinetics would have reached steady state.

The obvious question is whether steady state can ever be reached during sublimation of individual graphite or graphene NPs. Consideration of graphitic NP structures, and of experiments like those in **figures 3, 5, 6, and S6**, suggest that the answer may be “only partially”. These figures all show a tendency of rates to slow and E_a values to increase as sublimation proceeds, corresponding to the evolution of the NP surface sites toward greater stability, however, this evolution is not monotonic. Rates were observed to fluctuate with time in the constant T_{NP} experiments (**figures 3 and S6**), and there were a few NPs where the rates accelerated and E_a values decreased in the 3rd heat ramp (**figures 5 and 6**). This behavior suggests that there is a propensity for NP structures to evolve in ways that gen-

erally decreases the number of defective or low coordination surface sites, but that it is possible for there to be temporary increases in the number of such sites.

This behavior is not surprising for graphitic NPs that are initially rough, with irregular edges, defects, and surface asperities. Such NPs should sublime quickly at first, but the combination of preferential sublimation at low-coordination sites, and annealing should tend to reduce the numbers of such sites. On the other hand, there are processes, such as sublimation around basal defects, or sublimation that exposes underlying defective reactions, which increase the numbers of low-coordination sites. Therefore, as sublimation and annealing proceed, the rate should approach a near-steady-state, punctuated by occasional rate accelerations as is observed.

The motivation for studying both graphite and graphene NPs was to examine the effects of changing the ratio of basal plane area to basal plane edge length. The SI discusses the expected numbers and fractions of basal plane vs. edge sites for idealized graphite and graphene NPs, for a mass (52 MDa) typical of the NPs studied here. For idealized cube-shaped graphite, the edge length would be ~ 33.5 nm, and given the unit cell dimensions, just over 50% of the exposed surface atoms would be in edge sites. For graphene with the ~ 5 nm average thickness reported for our NP feedstock, and idealized square NP would have much larger surface area, but with only $\sim 6\%$ of the exposed surface atoms in edge sites. More importantly, the total number of exposed edge atoms in the graphene NP would be $\sim 1/3^{\text{rd}}$ that for the graphite NP. Therefore, if sublimation occurs primarily at exposed edge sites, we might expect graphene NPs to sublime with about $1/3^{\text{rd}}$ the rate of equal mass graphite NPs.

In fact, however, the difference between the average sublimation rates for graphite and graphene is much smaller than the variations within the sets of graphite and graphene NPs. This is not surprising, because the NPs are not idealized structures with regular-shaped, defect-free basal planes. Both irregularities of the basal plane edges, and vacancies and other defects in the basal planes increase the number of low coordination sites, thus increasing the sublimation rates.

Correlations between Emission Intensity and Sublimation Rates: **Figures 1, 2, S4, and S5** show examples in which the integrated emission intensity, I , increased after heating, and in those examples, the sublimation rate, R , also slowed significantly. This raises the question of whether emissivity might be correlated

with sublimation rate, and if so, what the correlation reveals about the factors that control graphitic NP emissivity. One way to extract such correlations would be to compare I and R for all the NPs before and after periods at high T_{NP} where significant mass loss occurred. The difficulty is that our control over T_{NP} was not adequate to hit exactly the same T_{NP} values in different heat ramps and for different NPs. Therefore, the following approach was used. The rates (figure 5) and emission intensities (figure 4) measured in each heat ramp for each NP, were fit to determine how they varied with T_{NP} , using $I \propto T_{NP}^s$ and $R = A \cdot \exp(-E_a/kT_{NP})$, with s , A , and E_a as fitting parameters. The fits were then used to interpolate between the I and R measurements, to estimate the values for $T_{NP} = 2000$ K.

Because of the large NP-to-NP variation in both I and R , it is difficult to deduce much about correlations by comparing the I and R values directly, as shown in figure S9. The correlation is clearer if we compare *changes* in I and R for each NP after heating, because this cancels out the large NP-to-NP variations in absolute intensity and rate. Figure 7 plots the percent change in I vs. the percent change in R for each NP, comparing the interpolated 2000 K I and R values measured in the 2nd and 3rd heat ramps relative to those measured in the 1st. Filled symbols compare I and R values measured in the 2nd and 1st heat ramps, and open symbols compare the net change between the 3rd and 1st heat ramps, with circles and diamonds for graphite and graphene, respectively. Arrows connecting the symbols show how particular NPs evolved. There are a few unconnected points for NPs where only two heat ramps were completed.

It can be seen that most of the points lie in the upper left quadrant, *i.e.*, there is a reasonably strong anti-correlation between changes in sublimation rate and changes in emission intensity, the most common behavior being for intensities to increase while rates decrease. The tendency of the sublimation rates to decrease over time is attributed to evolution of the NP surface site distributions, *i.e.*, to loss of low-coordination/defective sites, as discussed above. Therefore, figure 7 suggests that loss of such sites increases the emission brightness of graphitic NPs. It is not surprising that the NP surface structure should affect emission properties, because defects and low coordination surface sites must affect the NP electronic and vibronic (phonon) state distributions. Understanding the structure-emissivity relationship quantitatively is not so

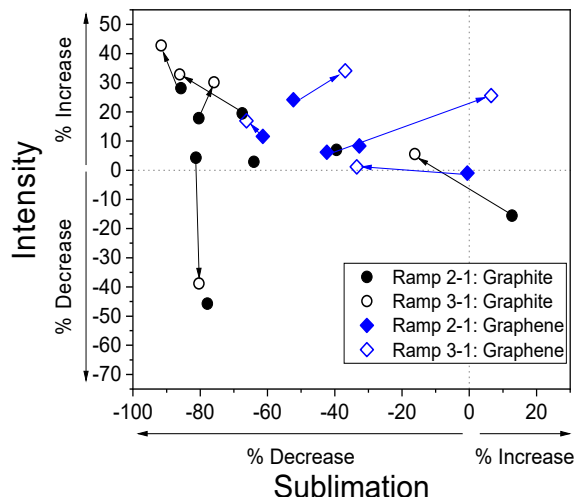


Figure 7: Correlations between heat-induced changes in emission intensity and sublimation rate at 2000 K, where each point represents a different NP. ‘Ramp 2-1’ means the percent change in intensity and rate between the 2nd and 1st heat ramps.

straightforward, and would appear to be an interesting topic for theoretical investigation.

CONCLUSIONS

We have, for the first time, reported sublimation rates as a function of temperature for individual graphite and graphene NPs. The average rates *per* unit area were initially several orders of magnitude faster than that for bulk graphite but decreased significantly as sublimation was driven at high T_{NP} over the course of several hours. There were, however, large NP-to-NP variations in the rates – much larger than the difference between the graphite and graphene rates, for example.

No significant correlations were observed of sublimation rates with NP mass or NP charge, both of which varied significantly as the NPs were repeatedly heated. Instead, the NP-to-NP variations in sublimation kinetics are attributed to the heterogeneity of the NPs and the resulting variations in the numbers of defective/under-coordinated surface sites. The evolution of the kinetics as the NPs were heated is, therefore, attributed to the evolution of the surface site distributions driven by preferential sublimation from less stable sites, and annealing.

The activation energies extracted from the rates increased substantially in repeated heat ramps, reflecting the evolution of the NP surface structure toward greater stability, however, the evolution during both repeated temperature cycling and in long term heating experi-

ments was non-monotonic. The NPs approached a partial steady state in which their surfaces had relatively stable fractions of low coordination and defect sites, but individual NPs never reached a true steady state.

The thermal emission intensity underwent only partially reversible changes as the NP temperature was repeatedly cycled. Most commonly, the emission brightened after heating, while the sublimation rates decreased, suggesting that emission intensity is depressed by high coverage of defects and low coordination surface sites.

ASSOCIATED CONTENT

Supporting Information.

The Supporting Information is available free of charge via the Internet at <http://pubs.acs.org>.

The following files are available free of charge:

Figures S1-S9 show differences in equilibrium and no-equilibrium rates vs temperature, single NP emission spectra, oxidation as a function of time, example of a graphite NP experiment, long term heating experiment, prefactor (A) information, NP charge state vs. activation energy, and how normalized intensity varies for different NPs vs mass loss rate.

Data underlying **Figures 1-7** are provided in tabular form (XLSX).

AUTHOR INFORMATION

Corresponding Author

*Scott L. Anderson, anderson@chem.utah.edu, (801)585-7289

Author Contributions

The manuscript was written through contributions of all authors. All authors have given approval to the final version of the manuscript.

Funding Sources

U.S. Department of Energy, Office of Science, Office of Basic Energy Sciences, under Award Number DE-SC- 0018049.

ACKNOWLEDGMENT

The nIR spectrograph was purchased with funds from the Albaugh Scientific Equipment Endowment of the College of Science, University of Utah. This material is based upon work supported by the U.S. Department of Energy, Office of Science, Office of Basic Energy Sciences, under Award Number DE-SC- 0018049. We thank Dr. Bruce Kay (PNNL) and Prof. Timothy Minton (Montana State University) for helpful discussions.

ABBREVIATIONS

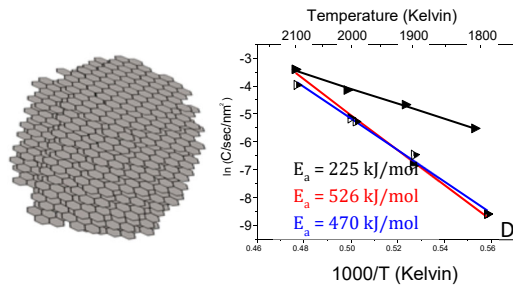
NP, nanoparticle; T_{NP} , nanoparticle temperature;

REFERENCES

- Brewer, L.; Gilles, P. W.; Jenkins, F. A., The Vapor Pressure and Heat of Sublimation of Graphite. *J. Chem. Phys.* **1948**, *16*, 797-807.
- Honig, R. E.; Kramer, D. A., *Vapor Pressure Data for the Solid and Liquid Elements*. RCA Laboratories, David Sarnoff Research Center: 1969.
- Zavitsanos, P. D.; Carlson, G. A., Experimental study of the sublimation of graphite at high temperatures. *J. Chem. Phys.* **1973**, *59* (6), 2966-2973.
- Chupka, W. A.; Berkowitz, J.; Meschi, D. J.; Tasman, H. A., Mass Spectrometric Studies of High Temperature Systems. In *Advances in Mass Spectrometry*, Elliott, R. M., Ed. Pergamon: 1963; pp 99-109.
- Drowart, J.; Burns, R. P.; DeMaria, G.; Inghram, M. G., Mass Spectrometric Study of Carbon Vapor. *J. Chem. Phys.* **1959**, *31* (4), 1131-1132.
- Chupka, W. A.; Inghram, M. G., Molecular Species Evaporating from a Carbon Surface. *J. Chem. Phys.* **1953**, *21* (7), 1313-1313.
- Steele, W. C.; Bourgelas, F. N. *Studies of Graphite Vaporization Using a Modulated Beam Mass Spectrometer, Technical report AFML-TR-72-222, AVSD-0048-73-CR*; Air Force Materials Laboratory, Air Force Systems Command: Wright-Patterson Air Force Base, Ohio, 1972.
- Doehaerd, T.; Goldfinger, P.; Waelbroeck, F., Direct Determination of the Sublimation Energy of Carbon. *J. Chem. Phys.* **1952**, *20*, 757.
- Clarke, J. T.; Fox, B. R., Rate and Heat of Vaporization of Graphite above 3000°K. *J. Chem. Phys.* **1969**, *51* (8), 3231-3240.
- Marshall, A. L.; Norton, F. J., Carbon Vapor Pressure and Heat of Vaporization. *J. Am. Chem. Soc.* **1950**, *72* (5), 2166-2171.
- Tsai, C. C.; Gabriel, T. A.; Haines, J. R.; Rasmussen, D. A., Graphite Sublimation Tests For Target Development For The Muon Collider/Neutrino Factory *IEEE Symp. Fusion Eng.* **2006**, *21*, 377-379.
- Haines, J. R.; Tsai, C. C. *Graphite Sublimation Tests for the Muon Collider/Neutrino Factory Target Development Program*; Oak Ridge, 2002; p 6 pages.
- Pflieger, R.; Sheindlin, M.; Colle, J.-Y., Advances in the mass spectrometric study of the laser vaporization of graphite. *J. Appl. Phys.* **2008**, *104* (5), 054902.
- Long, B. A.; Rodriguez, D. J.; Lau, C. Y.; Schultz, M.; Anderson, S. L., Thermal Emission Spectroscopy of Single, Isolated Carbon Nanoparticles: Effects of Particle Size, Material, Charge, Excitation Wavelength, and Thermal History. *J. Phys. Chem. C* **2020**, *124*, 1704-1716.
- Howder, C. R.; Long, B. A.; Alley, R. N.; Gerlich, D.; Anderson, S. L., Single Nanoparticle Mass Spectrometry as a High Temperature Kinetics Tool: Emission Spectra, Sublimation, and Oxidation of Hot Carbon Nanoparticles. *J. Phys. Chem. A* **2015**, *119*, 12538-12550.
- Long, B. A.; Rodriguez, D. J.; Lau, C. Y.; Anderson, S. L., Thermal emission spectroscopy for single nanoparticle temperature measurement: optical system design and calibration. *Appl. Opt.* **2019**, *58* (3), 642-649.
- Gerlich, D.; Decker, S., Trapping Ions at High Temperatures: Thermal Decay of C_{60}^+ . *Appl. Phys. B: Lasers Opt.* **2014**, *114*, 257-266.
- Rossmann, R. P.; Smith, W. R., Density of Carbon Black by Helium Displacement. *Ind. Eng. Chem. Res.* **1943**, *35* (9), 972-976.
- Bohren, C. F.; Huffman, D. R., *Absorption and Scattering of Light by Small Particles*. Wiley: New York, 1983.
- Siddall, R. G.; McGrath, I. A., The emissivity of luminous flames. *Symp. (Int.) Combust., [Proc.]* **1963**, *9* (1), 102-110.
- Köylü, Ü. Ö.; Faeth, G. M., Optical Properties of Overfire Soot in Buoyant Turbulent Diffusion Flames at Long Residence Times. *J. Heat Transfer* **1994**, *116* (1), 152-159.
- Landstrom, L.; Elihn, K.; Boman, M.; Granqvist, C. G.; Heszler, P., Analysis of Thermal Radiation from Laser-Heated Nanoparticles Formed by Laser-Induced Decomposition of Ferrocene. *Appl. Phys. A* **2005**, *81*, 827-833.
- Landstrom, L.; Heszler, P., Analysis of Blackbody-Like Radiation from Laser-Heated Gas-Phase Tungsten Nanoparticles. *J. Phys. Chem. B* **2004**, *108*, 6216-6221.

24. Michelsen, H. A., Understanding and predicting the temporal response of laser-induced incandescence from carbonaceous particles. *J. Chem. Phys.* **2003**, *118*, 2012-2045.
25. Kaden, W. E.; Kunkel, W. A.; Roberts, F. S.; Kane, M.; Anderson, S. L., CO Adsorption and Desorption on Size-selected Pd_n/TiO₂(110) Model Catalysts: Size Dependence of Binding Sites and Energies, and Support-mediated Adsorption. *J. Chem. Phys.* **2012**, *136*, 204705/1-204705/12.
26. Kolasinski, K. W., *Surface Science. Foundations of Catalysis and Nanoscience*. 3rd ed.; Wiley: Chichester, 2012.
27. Zobelli, A.; Ivanovskaya, V.; Wagner, P.; Suarez-Martinez, I.; Yaya, A.; Ewels, C. P., A comparative study of density functional and density functional tight binding calculations of defects in graphene. *Phys. Stat. Sol. B* **2012**, *249* (2), 276-282.
28. Thrower, P. A.; Mayer, R. M., Point defects and self-diffusion in graphite. *Phys. Stat. Sol. A* **1978**, *47*, 11-37.
29. Kaxiras, E.; Pandey, K. C., Energetics of defects and diffusion mechanisms in graphite. *Phys. Rev. Letts.* **1988**, *61* (23), 2693-2696.
30. El-Barbary, A. A.; Telling, R. H.; Ewels, C. P.; Heggge, M. I.; Briddon, P. R., Structure and energetics of the vacancy in graphite. *Phys. Rev. B* **2003**, *68* (14), 144107.
31. Li, L.; Reich, S.; Robertson, J., Defect energies of graphite: Density-functional calculations. *Physical Review B* **2005**, *72* (18), 184109.
32. Hahn, J. R.; Kang, H., Vacancy and interstitial defects at graphite surfaces: Scanning tunneling microscopic study of the structure, electronic property, and yield for ion-induced defect creation. *Phys. Rev. B* **1999**, *60* (8), 6007-6017.
33. Banhart, F.; Kotakoski, J.; Krashennnikov, A. V., Structural Defects in Graphene. *ACS Nano* **2011**, *5* (1), 26-41.
34. Ivanovskii, A. L., Graphene-based and graphene-like materials. *Russ. Chem. Rev.* **2012**, *81* (7), 571-605.
35. Yamashita, K.; Saito, M.; Oda, T., Atomic Geometry and Stability of Mono-, Di-, and Trivacancies in Graphene. *Jpn. J. Appl. Phys.* **2006**, *45* (8A), 6534-6536.
36. Lehtinen, P. O.; Foster, A. S.; Ayuela, A.; Krashennnikov, A.; Nordlund, K.; Nieminen, R. M., Magnetic Properties and Diffusion of Adatoms on a Graphene Sheet. *Phys. Rev. Letts.* **2003**, *91* (1), 017202.
37. Krashennnikov, A. V.; Lehtinen, P. O.; Foster, A. S.; Nieminen, R. M., Bending the rules: Contrasting vacancy energetics and migration in graphite and carbon nanotubes. *Chem. Phys. Lett.* **2006**, *418*, 132-136.
38. Skowron, S. T.; Lebedeva, I. V.; Popov, A. M.; Bichoutskaia, E., Energetics of atomic scale structure changes in graphene. *Chem. Soc. Rev.* **2015**, *44*, 3143-3176.
39. Suarez-Martinez, I.; Savini, G.; Haffenden, G.; Campanera, J.-M.; Heggge, M. I., Dislocations of Burgers vector $c/2$ in graphite. *Phys. Stat. Sol. C* **2007**, *4* (8), 2958-2962.
40. Li, J.; Li, Z.; Zhou, G.; Liu, Z.; Wu, J.; Gu, B.-L.; Ihm, J.; Duan, W., Spontaneous edge-defect formation and defect-induced conductance suppression in graphene nanoribbons. *Phys. Rev. B* **2010**, *82* (11), 115410.
41. Chang, H.; Bard, A. J., Formation of monolayer pits of controlled nanometer size on highly oriented pyrolytic graphite by gasification reactions as studied by scanning tunneling microscopy. *J. Am. Chem. Soc.* **1990**, *112* (11), 4598-9.
42. McCarroll, B.; McKee, D. W., Reactivity of graphite surfaces with atoms and molecules of hydrogen, oxygen, and nitrogen. *Carbon* **1971**, *9* (3), 301-311.
43. Myers, G. E.; Gordon, M. D., Anomalous hexagonal etch pits produced in the graphite-water vapor reaction. *Carbon (Oxford)* **1968**, *6* (3), 422-3.
44. Patrick, D. L.; Cee, V. J.; Beebe, T. P., Jr., "Molecule corrals" for studies of monolayer organic films. *Science (Washington, D. C.)* **1994**, *265* (5169), 231-4.
45. Hahn, J. R.; Kang, H., Conversion efficiency of graphite atomic-scale defects to etched pits in thermal oxidation reaction. *J. Vac. Sci. Technol., A* **1999**, *17* (4, Pt. 1), 1606-1609.
46. Hahn, J. R.; Kang, H.; Lee, S. M.; Lee, Y. H., Mechanistic Study of Defect-Induced Oxidation of Graphite. *J. Phys. Chem. B* **1999**, *103* (45), 9944-9951.
47. Turnbull, J. A.; Stagg, M. S., Isothermal annealing studies on vacancy and interstitial loops in single crystal graphite. *Philos. Mag.* **1966**, *14* (131), 1049-66.
48. Zhang, H.; Zhao, M.; Yang, X.; Xia, H.; Liu, X.; Xia, Y., Diffusion and coalescence of vacancies and interstitials in graphite: A first-principles study. *Diamond Relat. Mater.* **2010**, *19* (10), 1240-1244.

TOC figure



Sublimation Kinetics for Individual Graphite and Graphene Nanoparticles (NPs): NP-to-NP Variations and Evolving Structure-Kinetics and Structure-Emissivity Relationships

Bryan A. Long, Chris Y. Lau, Daniel J. Rodriguez, Susanna An Tang, and Scott L. Anderson*

Department of Chemistry, University of Utah, 315 S. 1400 E., Salt Lake City, Utah 84112, USA

*Corresponding author: anderson@chem.utah.edu

Supporting Information

Previous work toward the goal of single NP reaction kinetics:

Our single NP kinetics technique is based on earlier NP mass spectrometry and fluorescence spectroscopy work by several groups,¹⁻⁶ which laid a foundation of methods for measuring NP mass and charge using optical detection of the NP secular (motional) frequencies. Some experiments have also examined the kinetics for mass gain or loss, although until now, none could directly measure the NP temperature or vary it quantitatively. For example, in 2004, Schlemmer et al. measured the kinetics for mass gain by a ~500 nm diameter silica NP, as molecules from the vacuum system adsorbed on the NP surface at near room temperature. Recently Esser *et al.*⁹ reported a new instrument and measurements of argon adsorption/desorption for silica NPs at temperatures below 40 K, but without direct temperature measurement.

Our group developed an electrospray ionization (ESI) NP source to introduce CdSe/ZnS core/shell NPs to a trap, detecting them by laser-induced luminescence, and used this instrument

to study changes in the luminescence behavior as the NP lost mass by slow sublimation.¹²⁻¹³ We also previously examined sublimation of hot carbon NPs,¹⁵ however, in that experiment, as with all previous single NP kinetics work, the NP temperature was unknown, so that rates could not be associated with T_{NP} to extract energetic information. Temperature determination required development of an optical system and calibration method capable of measuring visible and near IR spectra for single NPs with quantitative intensity information, and we previously reported the optical system design, as well as the steps necessary to convert raw spectra to temperatures.¹⁶⁻¹⁷ The present report is the first in which single NP kinetic measurements have been done at well-defined and variable temperature.

Bulk graphite sublimation:

Figure S1 presents measured graphite sublimation rates and a fit to an Arrhenius rate law, $R=A\exp(-E_a/kT)$, used to extract an E_a of 862 kJ/mol, and to extrapolate the rate to the T_{NP} range of our experiments.

For materials where the sticking coefficients (S) are unity, sublimation rates can be calculated from the equilibrium vapor pressures, and the figure also shows

the rates that would be obtained if this assumption is erroneously used in conjunction with measured equilibrium vapor pressures.¹⁴ In fact, however, graphite has S values for various C_n

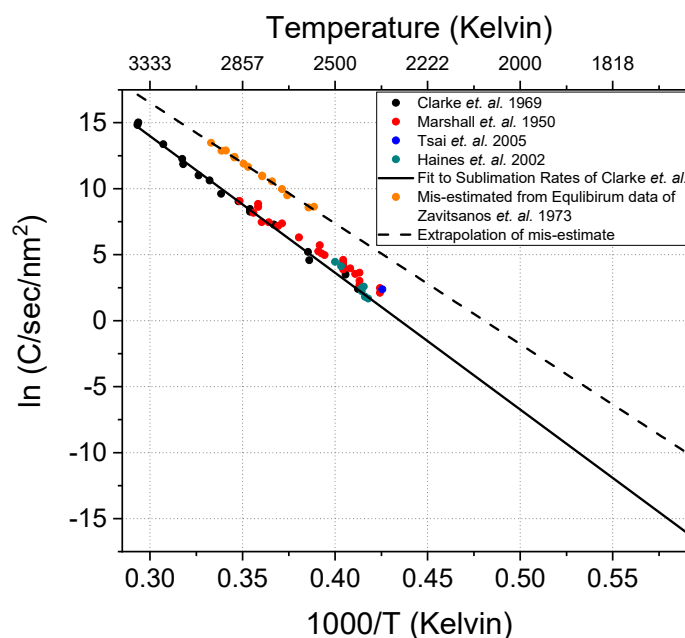


Figure S1: Measurements of the sublimation rates for graphite in vacuum by Clarke *et al.*,⁷ Marshall *et al.*,⁸ Tsai *et al.*,¹⁰ and Haines *et al.*,¹¹ The solid line is an Arrhenius fit to the Clarke data. The orange points and dashed fit line show the sublimation rate that would *incorrectly* be estimated if equilibrium vapor pressure data (in this case, by Zavitsanos *et al.*¹⁴) are analyzed using the common, but in this case, erroneous assumption that the C_n sticking coefficient is unity with hot graphite surfaces. Note, Zavitsanos *et al.* did not make this error – the mis-estimate of the sublimation rate is included only to make the point that graphite sublimation is quite different from that typical for metals.

vapor species that temperature dependent and well below unity.¹⁸⁻²⁰ For example, $S(C)$ was found to vary from 0.7 ± 0.15 at $T_{\text{surface}} = 800$ K, to 0.4 ± 0.2 at 2300 K,¹⁸ and $S(C_3)$ was found to be zero within experimental uncertainty, for surface temperatures above 1000 K.^{18, 20}

Typical Carbon NP spectra:

A few typical emission spectra are shown for a single laser-heated graphite NP (black points), along with fits (colored curves) using the model thermal emission function given in equation 4 in the main text. The T_{NP} and n parameters extracted from the fits are given in the figure legend.

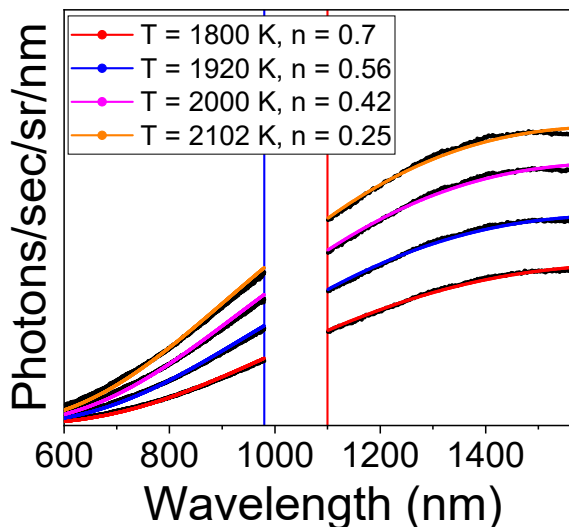


Figure S2: Emission spectra for a single graphite NP. T_{NP} are extracted by fitting the raw emission intensity using a Planckian fitting function. The emissivity parameter n is also shown for each T_{NP} value.

Graphite and Graphene NP purity in the experiments:

The NPMS method only monitors the total NP mass, thus it is important that we work with materials with the highest possible purity, with particular concern regarding any contaminants (*e.g.*, metals) that might survive at high temperatures, and catalyze sublimation or other reactions. The entire ESI source is carefully cleaned whenever the NP material is changed, with parts exposed to the ESI solutions extensively cleaned or replaced. The graphite NPs examined here have stated purity of 99.9999% (metals basis, Alfa Aesar), and the graphene platelet material (US Research Nanomaterials, Inc.) has stated composition of 99.7% C, <0.3% O. As received, the NPs presumably have oxidized surface groups and adventitious adsorbates from air exposure. Electrospray ionization was done from 2 mM ammonium acetate solutions in methanol, thus the electrosprayed NPs likely also have excess ammonium acetate and methanol adsorbed. Most

stable molecules, like water or methanol, desorb from graphite surfaces at low temperatures, and ammonium acetate was chosen specifically because it decomposes to volatile products well below the T_{NP} range of interest here.²¹ Similarly, oxidized surface groups have been shown to desorb as CO or CO₂ below ~1400 K when heated in vacuum,²²⁻²⁵ and adventitious organic contaminants would be expected to pyrolyze to carbon plus gaseous products. Trapped NPs are initially held at $T_{NP} \leq 1300$ K during charge stepping (20 – 60 minutes), then heated over the course of a few minutes to 1800 K for the start of the sublimation experiments. We expect, therefore, both contaminants and heteroatom functional groups on the NP surfaces should have desorbed, i.e., the NPs should be quite pure.

Possible effects of background oxygen on the sublimation rates:

Another consideration is that the presence of O₂ or other oxidizers in the trap chamber background could lead to NP mass change from reactions, interfering with measuring sublimation rates. UHP Ar (99.999%) at pressures of ~1 mTorr is used as a buffer gas to damp NP motion during normal operations, with UHV-compatible gas lines and fittings. The trap chamber is also mostly UHV-compatible but because it is exposed to methanol from the ESI source during every NP injection, its base pressure is typically $\sim 7 \times 10^{-7}$ Torr. To test for the effects of small additions of O₂, experiments were done in which a separate flow controller was used to add O₂ to the Argon buffer gas at pressures ~10,000 times higher than the worst-case O₂ background pressure (i.e., assuming the background is air).

One such experiment is summarized in **Figure S3**, which tests of the effects of deliberately adding O₂ on the mass-loss rates. The mass-loss rates were measured without and with 0.18 mTorr of O₂ added to the argon buffer gas in the trap. From the difference in mass loss rates, the rate of oxidative mass loss can be determined. As has been observed previously²⁶⁻²⁷ the rate for graphite

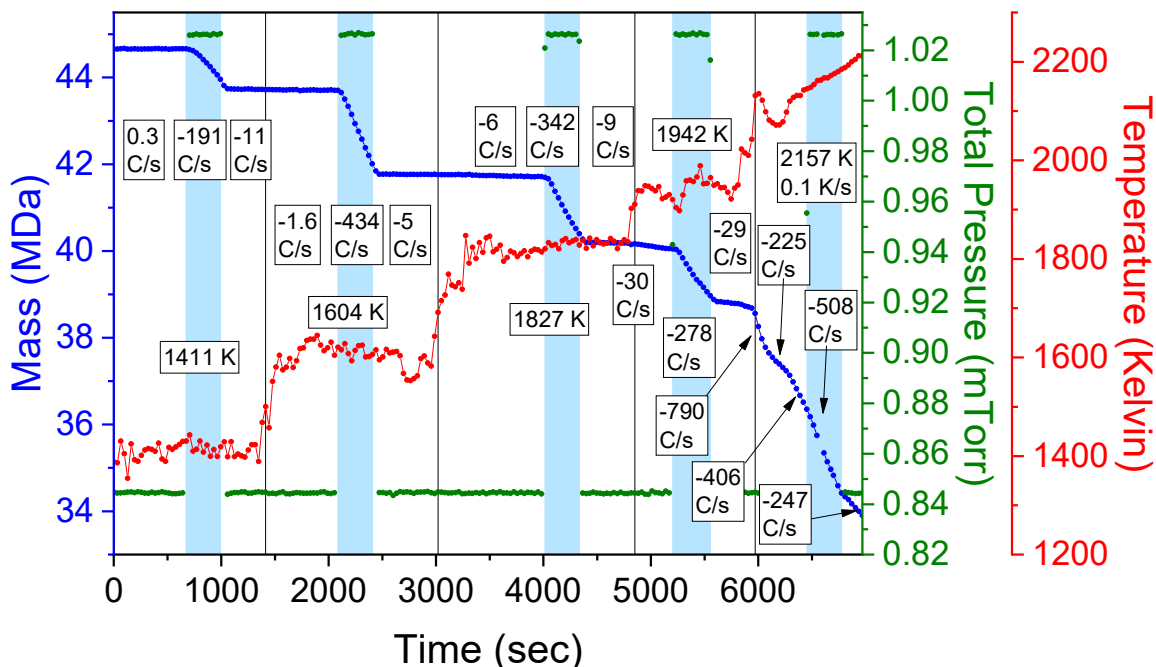


Figure S3: A 44.66 MDa graphite NP was heated to ~ 5 different temperatures, measuring the mass loss rate, with and without added O_2 .

oxidation by O_2 decreases with increasing surface temperature in our T_{NP} range. As a result, in the worst case, where the O_2 pressure would have been $\sim 10^{-4}$ of that used in **figure S3**, background oxidation would have had $< 5\%$ effect on the sublimation rates at our lowest temperatures, decreasing with increasing T_{NP} to $< 0.1\%$ above ~ 1950 K.

Typical experiment for a single graphite NP:

Figure S4 shows an experiment analogous to that shown in **Figure 1** of the main text. A graphite NP with initial mass 38.9 MDa (~ 38 nm diameter, if spherical), was heated in a series of steps, from ~ 1800 K to ~ 2100 K. The initial period, during which the NP was held at ~ 1300 K for Q determination is not shown. Gaps in the data indicate periods when T_{NP} was unstable, and these periods were omitted from further analysis. T_{NP} values and mass loss rates, averaged over the roughly constant T_{NP} periods defined by the solid vertical lines, are given in boxes. In addition to M and T_{NP} , the figure shows the integrated emission intensity (emitted photons/second/sr over the 600 – 1600 nm range) and the value of the n parameter in the power

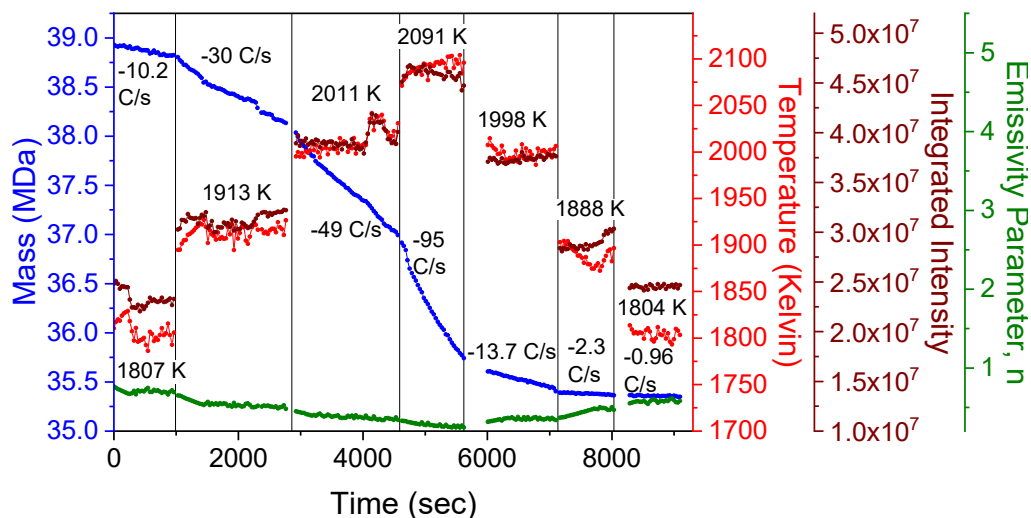


Figure S4: Typical sublimation kinetics experiment, in which a single graphite NP of initial mass of 38.93 MDa was heated in step-wise fashion from ~ 1800 K to ~ 2100 K, then back down to 1800 K. The temperatures and sublimation rates (given as C atoms/sec) indicated in boxes are the values averaged over the time intervals defined by the vertical black lines.

law emissivity function. Note that n decreased as T_{NP} increased, and then increased again as the NP cooled, indicating that emissivity is temperature dependent. Similarly, the integrated emission intensity, I , increased by a factor of ~ 2 as T_{NP} increased by a factor of ~ 1.16 (~ 1800 to ~ 2100 K), corresponding to $I \propto T_{NP}^5$.

The sublimation rate increased with increasing T_{NP} , as expected, however, the rates at similar T_{NP} values measured during the heating and cooling phases of the experiment were significantly different. For example, at ~ 1807 K at the beginning of the experiment, the NP sublimed at a rate of 10.2 C/sec, while during the period with $T_{NP} \approx 1804$ K at the end of the experiment, the rate was only 0.96 C/sec. Decreases in sublimation rate were also observed for other temperatures, although in those cases the T_{NP} values didn't match as well during the heating and cooling phases, complicating the comparison. Note also that during the period at ~ 2091 K, there was a slow increase in T_{NP} . Nonetheless, the sublimation rate slowed significantly. As in the example in **figure 1**, As NPs sublime, some rate slowing is expected due to reduction in NP surface area, however, the mass loss over the entire experiment was only $\sim 9\%$, thus the surface area loss ($\propto \sim M^{2/3}$) would

have been on the order of 6 %. Clearly, this small surface area loss cannot account for rates slowing by up to an order of magnitude.

Figure S5 summarizes the results, as in **figure 2** of the main text. **Figure S5A** shows the

variation of the integrated emission intensity with T_{NP} . Ideal blackbody emission intensity

scales with emitter surface area and the emissivity for small NPs (equation 3)

introduces another factor of r , thus intensity should scale with r^3 . Therefore, to compensate

for the expected effects of decreasing NP mass during the experiment (and to allow

comparisons to NPs with different masses), the intensities have been scaled by the NP mass (\propto

r^3) measured during the spectral measurements. Note that the intensity

increased and decreased with T_{NP} , but the final intensity at 1800 K was ~15% higher than the

intensity measured at the same T_{NP} prior to the heat ramps. Horizontal Error bars based on the $\pm 2\%$ uncertainty in T_{NP} are plotted with each data

point, as explained in the main text. The uncertainties in relative emission intensity are negligible.

Figure S5B plots the n parameter, which decreased with increasing T_{NP} , then recovered as the

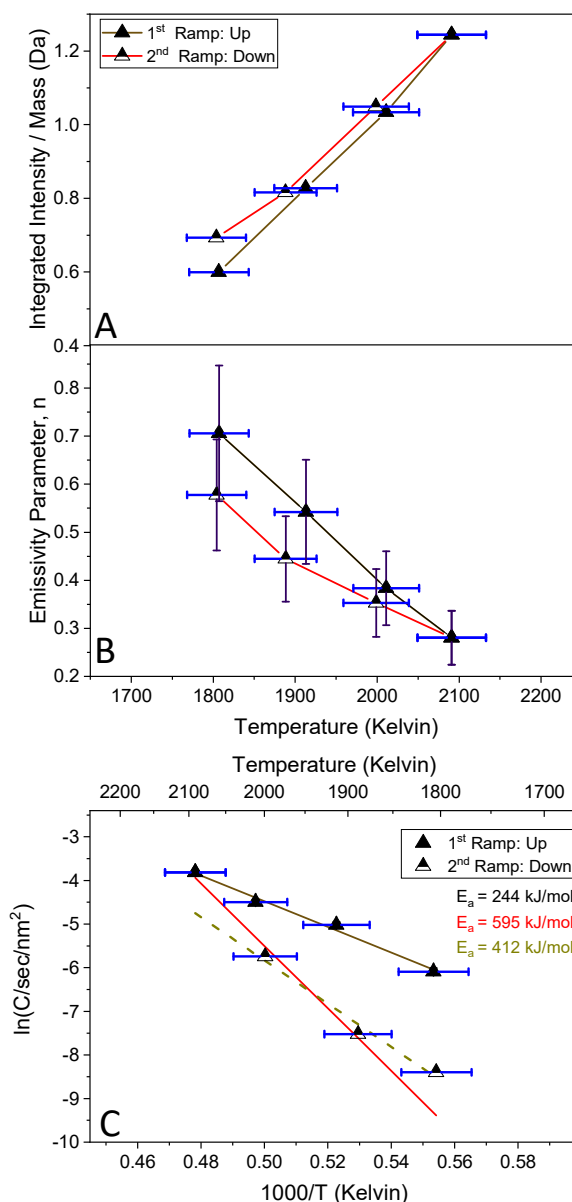


Figure S5: Analysis of the experiment shown in **figure 1**. A: Integrated emission intensity averaged over each constant T_{NP} period along with fits used to extract T_{NP} (colored curves). B: Emissivity parameter, n , averaged over each constant T_{NP} interval. C: Area-normalized sublimation rate vs. T_{NP} , along with fits to extract the effective E_a values shown. For the 2nd ramp, fits are shown to the highest and lowest T_{NP} points.

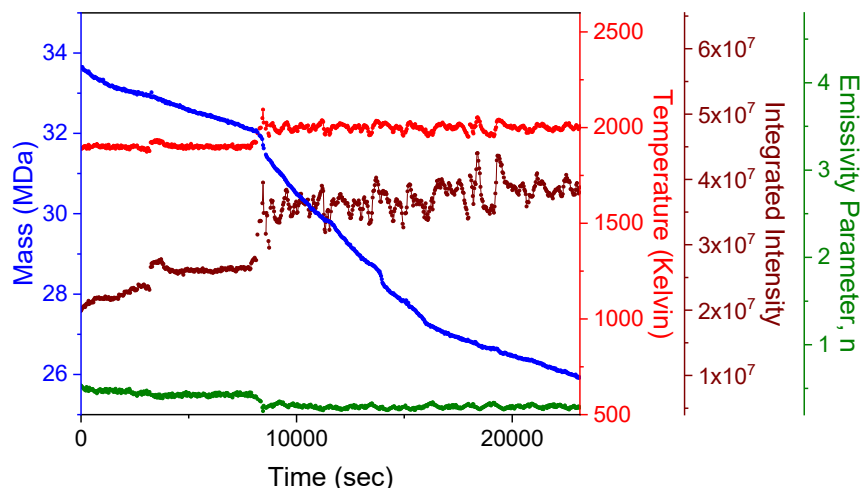
T_{NP} dropped, but only to $\sim 80\%$ of its initial value. These changes in intensity and n parameter indicate that in addition to driving sublimation, heating caused irreversible changes in the NP emissivity. The estimated $\pm 20\%$ uncertainties in n are shown as vertical error bars

Figure S2C plots the sublimation rates measured at each T_{NP} as the NP was heated then cooled. The rates and T_{NP} values are simply the rates and temperatures averaged over the constant T_{NP} intervals indicated by the vertical lines in **figure S1**. To correct for the $\sim 6\%$ surface area loss during the experiment, and to allow comparisons with other NPs, we would ideally normalize rates to the NP surface areas, but these are unknown. We have approximately area-normalized the rates assuming that the NPs are spherical with the bulk density, thus obtaining upper limits on the area-normalized rates, given as $C/\text{sec}/\text{nm}^2$. The data for both the 1st ramp up and 2nd ramp down are reasonably linear when plotted as $\ln(C/\text{sec}/\text{nm}^2)$ vs. $1000/T$, thus the fit lines can be used to extract activation energies, E_a , and prefactors, A , in rate expressions of the type: $R = A \exp(-E_a/RT_{NP})$. For this data, the E_a value extracted from 1st ramp up was 244 kJ/mol. During the 2nd ramp down, the rates are not fit well by a single E_a value. The three highest T_{NP} points are reasonably well fit (red line) to give $E_a = 595$ kJ/mol, and the three lowest T_{NP} points (dashed line) give 412 kJ/mol. In either case, compared to the 1st ramp up, the E_a values are substantially higher, and the rates at low T_{NP} substantially lower, during the 2nd ramp down. Error bars indicate the $\pm 2\%$ uncertainty in T_{NP} . The $\sim \pm 1.3\%$ uncertainty in the mass loss rate is small compared to the size of the symbols.

Another constant T_{NP} sublimation experiment:

Figure S6 shows an experiment in which a graphite NP (initial mass 33.7 MDa, ~ 36.1 nm if spherical) was heated, initially to 1900 K for ~ 2 hours, then increased to 2000 K to drive faster mass loss. In this experiment, heating was initially done with just the 532 nm laser, but when T_{NP} was increased to 2000 K, a cw CO_2 laser was used to help heat the NP. The CO_2 laser is less stable,

and decreased the stability of T_{NP} , which, nonetheless, only fluctuated by ± 40 K, ($\pm 2\%$) with standard deviation of 17 K ($< 1\%$). The total mass



loss was $\sim 23\%$.

Figure S6: Long exposure heating experiments. A graphite NP with initial mass 33.7 MDa initially heated at ~ 1900 K ~ 2 hours, then at 2000 K for an additional ~ 4.4 hours.

During the 2000 K period, the sublimation rate slowed by $\sim 67\%$, from an average of 51 C/sec over the first 10 minutes to 17 C/sec over the final 10 minutes, whereas the surface area (assuming spherical shape) would have decreased by only $\sim 13\%$. Note also that there were significant fluctuations in the sublimation rate (*e.g.*, at $\sim 14,000$ sec) that are not correlated with fluctuations in either T_{NP} or the emission intensity. The emission intensity generally tracked the fluctuations in T_{NP} , as expected, but the intensity also slowly increased during each constant T_{NP} period. For this NP, the n parameter decreased with time at 1900 K but was roughly constant at 2000 K.

A factors extracted from fitting rates in

Figure 5 of the main text.

The A factors extracted by fitting the rates

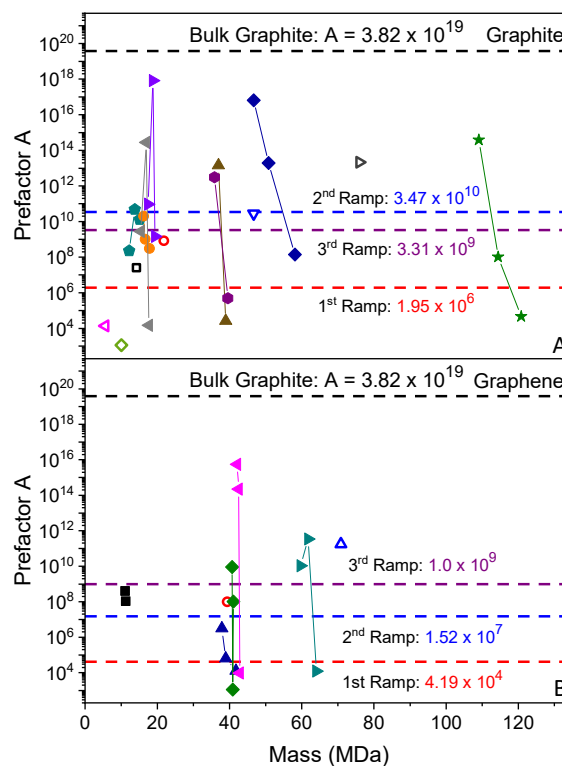


Figure S7: Prefactor, A, values for the graphite and graphene NP fits found in **figure 6** in. Also shown in all figures are the average values for the NPs and the values obtained by fitting bulk graphite data.

shown in **figure 5** of the main text are shown in **figure S7**. The logs of the A factors are correlated with the E_a values, as can be seen by comparing to **figure 6** of the main text. The A factors tended to increase substantially from heat ramp to heat ramp, but remained well below the A factor value extracted by fitting the bulk graphite sublimation rate data shown in **figure S1**.

Relation between NP charge (Q) and kinetics.

Figure S8 shows the E_a values for all the graphite NPs plotted vs. the Q value at the beginning of each heat ramp. The Q values generally increased, particularly between the 1st and 2nd heat ramps, due to thermionic emission at high T_{NP} . The inherent effects of Q can be judged by comparing the E_a values measured for each of

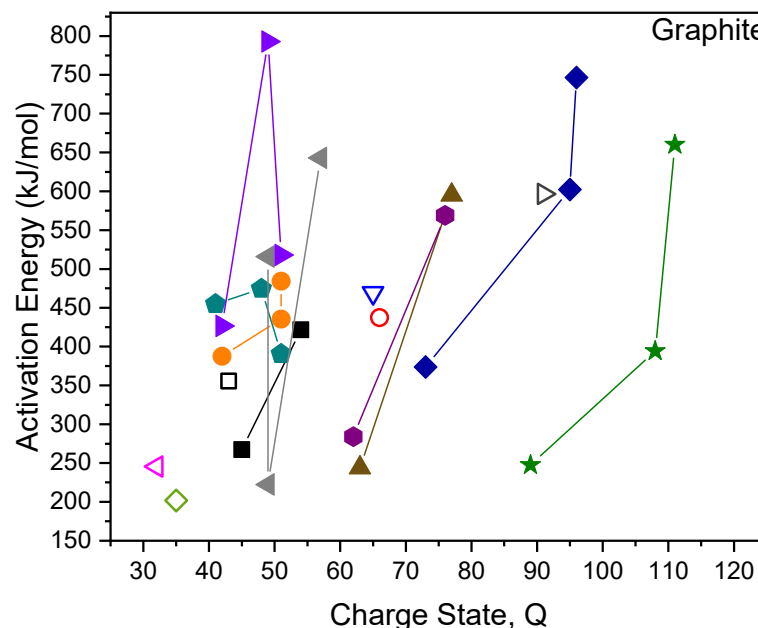


Figure S8: Showing E_a vs Q. In this case it seems that there no noticeable changes due to Q state changes. In the figure the initial Q state was use for each E_a that was determined for each heat ramp.

the heat ramps across the ensemble of NPs. As with the situation for NP mass, the large variations in Q across the ensemble are clearly not correlated to the kinetics. For individual NPs, Q tends to increase in successive heat ramps, and E_a also increases, however, we believe these are simply the consequences of two unrelated processes that occur at high T_{NP} – thermionic emission that increases Q, and sublimation that changes the surface site distribution, thus changing the sublimation kinetics. The effects of Q on the actual rates can be observed by comparing **figure 5** and **figure S8**, which allows the Q value for each NP in **figure 5** to be

identified, because the symbol colors and shapes are consistent. Again, there is no correlation between Q and the rates.

Comparison of the fraction of under-coordinated edge sites for graphite and graphene NPs:

The sublimation rate for an NP is expected to be strongly influenced by the number of defective or under-coordinated sites exposed on the NP surface because such sites have lower stability, and therefore should have lower activation energy (E_a) for sublimation. For NPs, the class of such sites that clearly must be present in large numbers is edge sites. An idealized graphite NP might consist of a cubical stack of graphene layers. For example, given graphite's 0.3353 nm interlayer spacing and 0.2461 nm basal plane unit cell edge length (2 C/unit cell),²⁸ a stack with thickness of 100 layers would be ~33.53 nm thick, and if we assume square layers with 33.53 nm edges, then the resulting cubical NP would have mass of ~52 MDa – in the mass range for our NPs.

This cubical NP would have $\sim 8.7 \times 10^4$ fully coordinated C atoms in the exposed top and bottom basal planes, and $\sim 9.4 \times 10^4$ under-coordinated atoms in the edges of the stacked basal planes. Thus, for idealized graphite NPs with aspect ratios near unity, roughly 50% of the NP surface consists of under-coordinated atoms in basal plane edge sites. This ratio is independent of NP size but is strongly affected by the NP shape. For example, for the same NP thickness and basal plane area (i.e., the same mass), if the basal planes are elongated or irregularly shaped such that the perimeter/area ratio increases, the fraction of under-coordinated edge sites would also increase. On the other hand, if the NP is thinner, with fewer but larger basal planes (to keep the same mass), the fraction of edge sites decreases.

Consider graphene NPs. Our graphene NPs feedstock is stated to have 2 to 8 nm thickness, i.e., the average thickness is ~5 nm. A 5.03 nm thick NP would have 15 layers. If these layers

were square, they would need to have a lateral dimension of 86.5 nm to give the same 52 MDa mass as the cubical NP discussed above. In such a particle, there would be $\sim 3.6 \times 10^4$ under-coordinated atoms in the edges of the 15 stacked layers, with $\sim 5.8 \times 10^5$ fully coordinated atoms exposed in the top and bottom basal planes. Thus the idealized graphene NP would have only $\sim 6.3\%$ of its surface atoms in under-coordinated edge sites. More importantly, the total number of under-coordinated edge atoms would be about one third the number in an idealized graphite NP with an aspect ratio of 1.0.

Of course, real graphite and graphene NPs would have additional under-coordinated sites due to irregular shapes and to defects in the basal planes. Nonetheless, we expect that graphene NPs should have a significantly smaller fraction of under-coordinated surface atoms than graphite NPs, which should result in slower sublimation kinetics.

Another factor that must be taken into account in comparing the sublimation rates for graphite and graphene NPs is that the reported rates for each NP have been normalized to the nominal surface area, calculated as the surface area of a spherical particle with the same mass, assuming the bulk density. This sets a lower limit on the surface area, hence giving area-normalized rates that are upper limits. For the cubical NP discussed above, the actual surface area would be 1.23 times greater than the nominal area, and for the 5 nm graphene NP, the actual area would be 1.68 times greater than the nominal area. Roughness or other irregularities would further increase the actual surface areas.

Comparison of integrated intensities and sublimation rates in the three heat ramps:

Figure S9 plots the 2000 K integrated intensities vs. sublimation rates for all the NP. Because of the large NP-to-NP variations, it is difficult to see much correlation, other than a general tendency for sublimation rates to decrease in subsequent heat ramps.

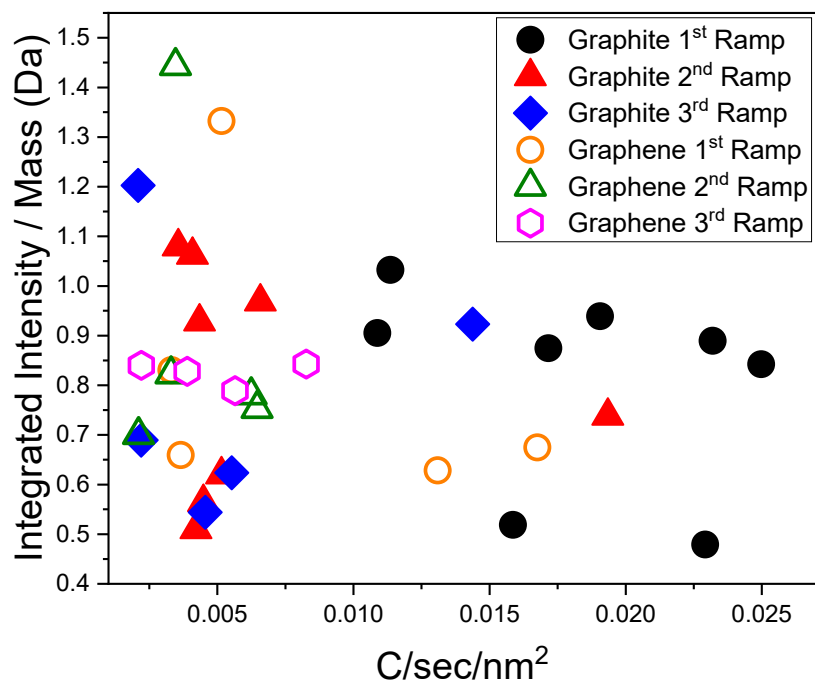


Figure S9: Interpolated integrated intensities plotted vs. area-normalized sublimation rates, both at 2000 K, for all NPs where more than one temperature ramp was completed. On average, the rates decreased substantially from the 1st to 2nd heat ramps, and the NP-to-NP spread in emission brightness increased. Comparing the 2nd and 3rd ramps, the effects on rates and intensities were much smaller, making generalizations difficult.

References

1. Schlemmer, S.; Illema, J.; Wellert, S.; Gerlich, D., Nondestructive High-Resolution And Absolute Mass Determination Of Single Charged Particles In A Three-Dimensional Quadrupole Trap. *J. Appl. Phys.* **2001**, *90* (10), 5410-5418.
2. Cai, Y.; Peng, W. P.; Kuo, S. J.; Lee, Y. T.; Chang, H. C., Single-Particle Mass Spectrometry of Polystyrene Microspheres and Diamond Nanocrystals. *Anal. Chem.* **2002**, *74* (1), 232-238.
3. Gerlich, D., Molecular Ions and Nanoparticles in RF and AC Traps. *Hyperfine Interact.* **2003**, *146/147* (1-4/1-4), 293-306.
4. Trevitt, A. J.; Wearne, P. J.; Bieske, E. J.; Schuder, M. D., Observation of Nondegenerate Cavity Modes for a Distorted Polystyrene Microsphere. *Opt. Lett.* **2006**, *31* (14), 2211-2213.
5. Graf, C.; Lewinski, R.; Dembski, S.; Langer, B.; Ruehl, E., Experiments on single levitated particles: a novel approach for investigations of electronic properties of structured II-VI-semiconductor nanoparticles in selected environments. *Phys. Status Solidi C* **2007**, *4* (9), 3244-3259.
6. Nagornykh, P.; Coppock, J. E.; Kane, B. E., Cooling of levitated graphene nanoplatelets in high vacuum. *Appl. Phys. Lett.* **2015**, *106* (24), 244102.
7. Clarke, J. T.; Fox, B. R., Rate and Heat of Vaporization of Graphite above 3000°K. *J. Chem. Phys.* **1969**, *51* (8), 3231-3240.
8. Marshall, A. L.; Norton, F. J., Carbon Vapor Pressure and Heat of Vaporization. *J. Am. Chem. Soc.* **1950**, *72* (5), 2166-2171.
9. Esser, T. K.; Hoffmann, B.; Anderson, S. L.; Asmis, K. R., A cryogenic single nanoparticle action spectrometer. *Review of Scientific Instruments* **2019**, *90* (12), 125110.
10. Tsai, C. C.; Gabriel, T. A.; Haines, J. R.; Rasmussen, D. A., Graphite Sublimation Tests For Target Development For The Muon Collider/Neutrino Factory *IEEE Symp. Fusion Eng.* **2006**, *21*, 377-379.
11. Haines, J. R.; Tsai, C. C. *Graphite Sublimation Tests for the Muon Collider/Neutrino Factory Target Development Program*; Oak Ridge, 2002; p 6 pages.
12. Bell, D. M.; Howder, C. R.; Johnson, R. C.; Anderson, S. L., Single CdSe/ZnS Nanocrystals in an Ion Trap: Charge and Mass Determination and Photophysics Evolution with Changing Mass, Charge, and Temperature. *ACS Nano* **2014**, *8*, 2387-2398.
13. Howder, C. R.; Bell, D. M.; Anderson, S. L., Optically Detected, Single Nanoparticle Mass Spectrometer With Pre-Filtered Electrospray Nanoparticle Source. *Rev. Sci. Instrum.* **2014**, *85*, 014104 -014110.
14. Zavitsanos, P. D.; Carlson, G. A., Experimental study of the sublimation of graphite at high temperatures. *J. Chem. Phys.* **1973**, *59* (6), 2966-2973.

15. Howder, C. R.; Long, B. A.; Alley, R. N.; Gerlich, D.; Anderson, S. L., Single Nanoparticle Mass Spectrometry as a High Temperature Kinetics Tool: Emission Spectra, Sublimation, and Oxidation of Hot Carbon Nanoparticles. *J. Phys. Chem. A* **2015**, *119*, 12538–12550.
16. Long, B. A.; Rodriguez, D. J.; Lau, C. Y.; Anderson, S. L., Thermal emission spectroscopy for single nanoparticle temperature measurement: optical system design and calibration. *Appl. Opt.* **2019**, *58* (3), 642-649.
17. Long, B. A.; Rodriguez, D. J.; Lau, C. Y.; Schultz, M.; Anderson, S. L., Thermal Emission Spectroscopy of Single, Isolated Carbon Nanoparticles: Effects of Particle Size, Material, Charge, Excitation Wavelength, and Thermal History. *J. Phys. Chem. C* **2020**, *124*, 1704-1716.
18. Chupka, W. A.; Berkowitz, J.; Meschi, D. J.; Tasman, H. A., Mass Spectrometric Studies of High Temperature Systems. In *Advances in Mass Spectrometry*, Elliott, R. M., Ed. Pergamon: 1963; pp 99-109.
19. Doehaerd, T.; Goldfinger, P.; Waelbroeck, F., Direct Determination of the Sublimation Energy of Carbon. *J. Chem. Phys.* **1952**, *20*, 757.
20. Steele, W. C.; Bourgelas, F. N. *Studies of Graphite Vaporization Using a Modulated Beam Mass Spectrometer, Technical report AFML-TR-72-222, AVSD-0048-73-CR*; Air Force Materials Laboratory, Air Force Systems Command: Wright-Patterson Air Force Base, Ohio, 1972.
21. Olszak-Humienik, M., On the thermal stability of some ammonium salts. *Thermochim. Acta* **2001**, *378* (1), 107-112.
22. Tremblay, G.; Vastola, F. J.; Walker, P. L., Jr., Characterization of Graphite Surface Complexes by Temperature-Programmed Desorption. *Extended Abstracts - Biennial Conf. on Carbon* **1975**, *12*, 177-178.
23. Marchon, B.; Carrazza, J.; Heinemann, H.; Somorjai, G. A., TPD and XPS studies of O₂, CO₂, and H₂O adsorption on clean polycrystalline graphite. *Carbon* **1988**, *26* (4), 507-514.
24. Nowakowski, M. J.; Vohs, J. M.; Bonnell, D. A., Surface reactivity of oxygen on cleaved and sputtered graphite. *Surf. Sci.* **1992**, *271* (3), L351-L356.
25. Pan, Z.; Yang, R. T., Strongly Bonded Oxygen in Graphite: Detection by High-Temperature TPD and Characterization *Ind. Eng. Chem. Res.* **1992**, *31*, 2675-2680.
26. Olander, D. R.; Siekhaus, W.; Jones, R.; Schwarz, J. A., Reactions of Modulated Molecular Beams with Pyrolytic Graphite. I. Oxidation of the Basal Plane. *J. Chem. Phys.* **1972**, *57* (1), 408-420.
27. Murray, V. J.; Smoll, E. J.; Minton, T. K., Dynamics of Graphite Oxidation at High Temperature. *J. Phys. Chem. C* **2018**, *122* (12), 6602-6617.
28. Bacon, G. E., The interlayer spacing of graphite. *Acta Crystallogr. A* **1951**, *4* (6), 558-561.

Figure 1 Graphene Experiment

Time (sec)	M (Mda)	Time (sec)	Integration	n	T
0	64.03095	-1	1.61E+07	0.88158	1783.647
31	64.01698	32	1.60E+07	0.8435	1794.097
63	64.02718	64	1.60E+07	0.85637	1789.552
95	63.99884	96	1.62E+07	0.86252	1790.65
122	63.98377	128	1.69E+07	0.84647	1793.929
165	63.99905	160	1.75E+07	0.85355	1802.868
192	63.98872	192	1.79E+07	0.83089	1810.943
219	63.97677	224	1.82E+07	0.81364	1816.617
261	63.9404	256	1.83E+07	0.85311	1802.99
289	63.97053	288	1.84E+07	0.8322	1808.295
320	63.93606	321	1.82E+07	0.82052	1813.213
358	63.93691	353	1.77E+07	0.80522	1818.126
379	63.95389	385	1.76E+07	0.81945	1813.529
416	63.8977	417	1.77E+07	0.84643	1803.605
449	63.94471	449	1.79E+07	0.82281	1811.945
475	63.91391	481	1.84E+07	0.78552	1819.799
518	63.90223	513	1.84E+07	0.81008	1813.514
539	63.84826	545	1.98E+07	0.79365	1822.623
572	63.84357	578	2.06E+07	0.77625	1829.492
615	63.84325	610	2.05E+07	0.77441	1827.048
641	63.82505	642	2.04E+07	0.78625	1821.399
668	63.82035	674			
706	63.77752	706			
743	63.7502	738			
770	63.78432	770			
802	63.72711	802			
835	63.72515	835	2.86E+07	0.69425	1923.923
861	63.66925	867	3.00E+07	0.70444	1921.671
894	63.76052	899	3.03E+07	0.68823	1922.264
935	63.6043	931	2.99E+07	0.65605	1924.964
964	63.558	963	2.97E+07	0.67692	1912.164
996	63.59515	995	2.94E+07	0.6801	1908.744
1026	63.51324	1027	2.95E+07	0.66276	1917.622
1060	63.51948	1059	2.94E+07	0.7035	1901.511
1091	63.49712	1092	2.94E+07	0.68749	1909.779
1123	63.44715	1124	2.95E+07	0.68132	1909.167
1156	63.45754	1156	2.93E+07	0.69803	1902.692
1187	63.39956	1188	2.94E+07	0.65941	1915.53
1220	63.4053	1220	2.95E+07	0.69456	1904.033
1252	63.35105	1252	2.93E+07	0.68373	1906.672
1284	63.3312	1284	2.92E+07	0.6788	1908.297
1317	63.39275	1317	2.92E+07	0.67514	1910.375
1348	63.36893	1349	2.94E+07	0.687	1905.333
1380	63.3074	1381	2.94E+07	0.69241	1904.396
1413	63.29213	1413	2.93E+07	0.6643	1910.369

1445	63.29467	1445	2.95E+07	0.66523	1910.597
1476	63.25211	1477	2.95E+07	0.68842	1904.525
1504	63.24926	1509			
1546	63.2294	1541			
1573	63.2148	1573			
1605	63.21553	1605			
1631	63.17339	1637			
1674	63.07437	1670			
1697	63.07411	1702			
1738	62.9803	1734			
1766		1766			
1795		1798			
1828	62.78631	1830	4.19E+07	0.54787	2003.595
1867	62.68979	1862	4.22E+07	0.52985	2008.22
1889	62.66752	1894	4.29E+07	0.52552	2010.825
1931	62.60146	1926	4.30E+07	0.51438	2013.813
1958	62.58499	1958	4.24E+07	0.53752	2001.343
1989	62.51765	1990	4.26E+07	0.52199	2007.306
2022	62.50095	2022	4.26E+07	0.53514	2001.792
2048	62.44316	2054	4.31E+07	0.5192	2006.838
2092	62.39154	2087	4.31E+07	0.52188	2005.904
2119	62.38311	2119	4.32E+07	0.51223	2007.898
2150	62.345	2151	4.30E+07	0.5287	2001.641
2183	62.31073	2183	4.31E+07	0.51235	2007.955
2214	62.25511	2215	4.30E+07	0.5214	2002.735
2247	62.2345	2247	4.28E+07	0.51925	2002.722
2279	62.25354	2279	4.29E+07	0.50863	2006.732
2305	62.17728	2311	4.41E+07	0.4899	2015.867
2349	62.12605	2344	4.42E+07	0.51639	2004.182
2375	62.08019	2376	4.37E+07	0.50774	2007.355
2408	62.05093	2408	4.41E+07	0.49525	2011.096
2440	62.03061	2440			
2471	61.95349	2472			
2504	61.87553	2504			
2536	61.79144	2536	5.30E+07	0.41298	2101.201
2562	61.70892	2568	5.50E+07	0.38591	2115.308
2605	61.55329	2600	5.43E+07	0.39441	2106.902
2633	61.45257	2632	5.38E+07	0.40669	2098.571
2659	61.38159	2665	5.46E+07	0.39509	2103.501
2701	61.25246	2697	5.47E+07	0.38933	2104.122
2729	61.18941	2729	5.40E+07	0.40787	2095.046
2760	61.10189	2761	5.40E+07	0.40131	2097.423
2793	61.02709	2793	5.46E+07	0.38495	2106.652
2825		2825			
2856		2857			
2892	60.78997	2889	5.48E+07	0.38462	2102.089
2923	60.74515	2921	5.49E+07	0.37024	2105.818

2953	60.65148	2953	5.43E+07	0.38442	2098.844
2985	60.55817	2986	5.45E+07	0.3884	2098.322
3018	60.53887	3018	5.40E+07	0.39487	2093.799
3049	60.45837	3050	5.39E+07	0.39026	2093.171
3082	60.39976	3082	5.45E+07	0.39277	2092.884
3114	60.33373	3114	5.37E+07	0.39223	2091.472
3146	60.26894	3146	5.41E+07	0.39125	2092.288
3178		3178			
3209		3210			
3245	60.0586	3242			
3270	60.01174	3274	4.59E+07	0.45265	2010.921
3312	60.00127	3306	4.63E+07	0.4525	2009.783
3338	60.01456	3338	4.62E+07	0.46343	2005.49
3370	59.97458	3371	4.57E+07	0.46809	2003.355
3402	59.95672	3403	4.57E+07	0.45973	2005.307
3434	59.94235	3435	4.60E+07	0.48711	1996.933
3466	59.9044	3467	4.59E+07	0.46438	2004.303
3499	59.90518	3499	4.60E+07	0.46799	2002.625
3531	59.9186	3531	4.54E+07	0.47129	1999.825
3563	59.90563	3563	4.57E+07	0.46367	2002.595
3595	59.87819	3595	4.57E+07	0.47808	1996.804
3627	59.84872	3627	4.55E+07	0.47423	1998.048
3659	59.82662	3659	4.48E+07	0.48404	1992.833
3692	59.84193	3692	4.54E+07	0.46827	1999.231
3723	59.81958	3724	4.54E+07	0.46928	1999.28
3755	59.80091	3756	4.52E+07	0.48582	1991.874
3788	59.84651	3788	4.49E+07	0.4879	1991.838
3818	59.77022	3820	4.53E+07	0.47418	1996.657
3852	59.78083	3852	4.59E+07	0.45681	2005.406
3884	59.75885	3884	4.55E+07	0.46282	2002.648
3916		3916			
3948	59.74964	3948	3.73E+07	0.56761	1907.056
3980	59.73987	3981	3.75E+07	0.57815	1903.39
4013	59.73569	4013	3.74E+07	0.56368	1909.655
4044	59.72923	4045	3.69E+07	0.56356	1908.345
4077	59.72244	4077	3.65E+07	0.60425	1889.85
4109	59.73472	4109	3.74E+07	0.55182	1911.949
4140	59.71927	4141	3.64E+07	0.56541	1901.842
4173	59.7182	4173	3.62E+07	0.5917	1891.045
4205	59.72163	4205	3.63E+07	0.59032	1893.58
4237	59.72067	4237	3.65E+07	0.59193	1893.388
4269	59.73438	4269	3.63E+07	0.59651	1892.068
4301	59.72008	4302	3.67E+07	0.6057	1888.893
4333	59.71497	4334	3.62E+07	0.57547	1897.527
4365	59.70106	4366	3.69E+07	0.59625	1894.125
4398	59.72507	4398	3.72E+07	0.56015	1907.388
4429	59.68347	4430	3.68E+07	0.59166	1894.545

4462	59.72222	4462	3.66E+07	0.58933	1896.268
4493	59.68614	4494	3.67E+07	0.58494	1896.295
4526	59.69527	4526	3.66E+07	0.57185	1901.683
4558	59.66192	4558			
4591	59.68379	4591			
4622	59.655	4623			
4655	59.68696	4655			
4686	59.68667	4687			
4725		4719			
4750	59.67103	4751	2.87E+07	0.69961	1794.504
4789	59.68508	4783	2.84E+07	0.70201	1792.185
4814	59.65858	4815	2.84E+07	0.69048	1795.926
4847	59.69945	4847	2.85E+07	0.73012	1783.513
4878	59.66195	4879	2.84E+07	0.71549	1787.72
4912	59.68198	4911	2.82E+07	0.68026	1796.793
4943	59.66885	4944	2.83E+07	0.675	1799.189
4975	59.67679	4976	2.84E+07	0.69116	1793.871
5007	59.64229	5008	2.83E+07	0.68861	1793.439
5040	59.63728	5040	2.81E+07	0.69764	1790.344
5072	59.67505	5072	2.82E+07	0.68438	1795.722
5103	59.64604	5104	2.80E+07	0.67787	1797.068
5136	59.66615	5136	2.80E+07	0.69506	1791.113
5168	59.67583	5168	2.80E+07	0.72722	1781.593
5200	59.68072	5200	2.78E+07	0.69662	1790.504
5232	59.6773	5233	2.78E+07	0.7365	1777.023
5264	59.68709	5265	2.80E+07	0.6937	1791.68
5296	59.66811	5297	2.82E+07	0.71133	1787.044
5329	59.65836	5329	2.81E+07	0.67897	1797.416
5361	59.65762	5361	2.82E+07	0.68329	1795.588
5393	59.67842	5393	2.80E+07	0.71403	1786.638
5425	59.68	5425	2.84E+07	0.70724	1789.203
5457	59.6562	5457	2.83E+07	0.70416	1790.2
5489	59.6403	5489	2.82E+07	0.66839	1799.962
5522	59.66641	5521	2.83E+07	0.71855	1786.046
5551		5554			
5585	59.66074	5586	3.53E+07	0.58422	1885.461
5615	59.67859	5618	3.50E+07	0.59688	1879.409
5649	59.63097	5650	3.48E+07	0.62429	1870.146
5682	59.64157	5682	3.50E+07	0.586	1883.98
5714	59.66973	5714	3.55E+07	0.59168	1885.611
5745	59.63879	5746	3.54E+07	0.63109	1871.348
5778	59.63917	5778	3.61E+07	0.59972	1885.654
5810	59.63588	5810	3.63E+07	0.58294	1895.606
5842	59.61007	5842	3.67E+07	0.58536	1894.386
5875	59.63893	5875	3.67E+07	0.59325	1892.308
5906	59.5848	5907	3.74E+07	0.59429	1897.099
5939	59.60672	5939	3.73E+07	0.5716	1905.788

5971	59.60679	5971	3.73E+07	0.56719	1907.95
6003	59.60473	6003	3.75E+07	0.56147	1909.983
6035	59.60809	6035	3.71E+07	0.59222	1898.253
6067	59.60754	6067	3.73E+07	0.57618	1904.393
6099	59.604	6099	3.77E+07	0.55735	1910.919
6131	59.60594	6132	3.78E+07	0.55157	1913.136
6163	59.59731	6164	3.76E+07	0.58265	1900.734
6196	59.60313	6196	3.74E+07	0.57871	1902.911
6227	59.57467	6228	3.74E+07	0.57149	1904.502
6260	59.58173	6260	3.75E+07	0.56393	1908.045
6292	59.57874	6292	3.73E+07	0.56732	1906.53
6324	59.5762	6324	3.78E+07	0.55085	1914.555
6356	59.57442	6356	3.72E+07	0.57342	1903.548
6388	59.5715	6388	3.71E+07	0.56439	1904.937
6420	59.5627	6421			
6452	59.55663	6453			
6484	59.55287	6485			
6516	59.55459	6517	4.44E+07	0.4884	1985.364
6548	59.54266	6549	4.46E+07	0.45909	1997.161
6581	59.53505	6581	4.46E+07	0.48623	1986.069
6613	59.51345	6613	4.48E+07	0.48123	1988.061
6645	59.51523	6645	4.49E+07	0.4832	1989.386
6677	59.51199	6677	4.47E+07	0.49707	1983.307
6709	59.51669	6709	4.49E+07	0.49485	1984.976
6741	59.48614	6742	4.56E+07	0.47826	1993.052
6773	59.46047	6774	4.57E+07	0.47941	1993.815
6806	59.47832	6806	4.57E+07	0.47611	1994.208
6838	59.48351	6838	4.52E+07	0.47159	1993.666
6869	59.43204	6870	4.51E+07	0.49097	1986.463
6902	59.41359	6902	4.52E+07	0.46843	1996
6934	59.40436	6934	4.51E+07	0.48292	1989.144
6966	59.40264	6966	4.56E+07	0.46319	2000.093
6998	59.39271	6999	4.53E+07	0.47871	1992.64
7030	59.39619	7031	4.59E+07	0.4634	1999.732
7062	59.37447	7063	4.55E+07	0.48358	1991.598
7094	59.33555	7095	4.55E+07	0.47681	1992.157
7127	59.30594	7127	4.57E+07	0.46619	1998.027
7159	59.33103	7159	4.58E+07	0.46474	1998.927
7190	59.28857	7191			
7223		7223			
7248		7255			
7285	59.03108	7287			
7324	58.93498	7319			
7352	58.89805	7351	5.70E+07	0.36573	2099.096
7383	58.87045	7384	5.69E+07	0.35351	2101.71
7415	58.80675	7416	5.67E+07	0.35724	2099.6
7448	58.7753	7448	5.72E+07	0.33614	2109.519

7479	58.70892	7480	5.64E+07	0.36347	2096.2
7512	58.671	7512	5.59E+07	0.35901	2095.173
7544	58.64068	7544	5.72E+07	0.36778	2093.829
7575	58.5758	7576	5.62E+07	0.34666	2101.578
7608	58.54636	7608	5.64E+07	0.36313	2093.896
7640	58.48357	7640	5.64E+07	0.35446	2096.786
7672	58.42762	7672	5.67E+07	0.35844	2097.293
7704	58.3899	7705	5.60E+07	0.35475	2097.352
7737	58.37112	7737	5.66E+07	0.35736	2096.432
7768	58.33925	7769	5.60E+07	0.36993	2089.825
7800	58.29131	7801	5.70E+07	0.35606	2096.706
7833	58.23771	7833	5.68E+07	0.3513	2098.118
7865	58.21165	7865	5.62E+07	0.36328	2091.535
7896	58.16551	7898	5.69E+07	0.35356	2098.134

Figure 2A

T avg	lavg/Mi
1808.947	0.28177
1911.173	0.46236
2006.727	0.68556
2099.856	0.87808
2000.788	0.7601
1898.889	0.6152
1791.371	0.47266
1897.584	0.61588
1992.088	0.75949
2097.377	0.96054

Figure 2B

T avg	n
1808.947	0.8245
1911.173	0.682
2006.727	0.51922
2099.856	0.39264
2000.788	0.46961
1898.889	0.58107
1791.371	0.69871
1897.584	0.58077
1992.088	0.47783
2097.377	0.35732

Figure 2C 1st Ramp: UP

1000/T	Fit data	Exp Data
0.55281	-5.5152	-5.51999
0.52324	-4.71678	-4.66442
0.49832	-4.04401	-4.13881
0.47622	-3.44725	-3.40003

2nd Ramp: Down

1000/T	Fit data	Exp data
0.47622	-3.53839	-3.40E+00
0.4998	-5.02902	-5.16E+00
0.52662	-6.7245	-6.85E+00
0.55823	-8.72262	-8.61E+00

3rd Ramp: Up

1000/T	Fit data	Exp Data
0.55823	-8.46645	-8.61109
0.52699	-6.70072	-6.47127
0.50199	-5.28795	-5.27756
0.47679	-3.86389	-3.9591

Figure 3

Time (sec)	M(Mda)	Time (sec)	Integration	n	T
64	82.8823	1	6.33E+07	0.68703	1904.586
97	82.8405	33	6.86E+07	0.67902	1923.848
129	82.8185	65	6.87E+07	0.67095	1928.852
158	82.9673	97	6.34E+07	0.6715	1908.618
191	82.6584	129	6.34E+07	0.71542	1894.623
231	82.6561	161	6.98E+07	0.71903	1917.587
257	82.5882	193	6.76E+07	0.6652	1922.113
290	82.5934	226	6.67E+07	0.654	1923.515
321	82.5495	258	7.29E+07	0.65078	1945.863
354	82.5322	290	6.94E+07	0.71493	1914.812
386	82.5011	322	6.56E+07	0.71483	1899.784
418	82.4649	354	6.97E+07	0.65535	1931.729
451	82.4772	386	6.81E+07	0.65388	1927.426
482	82.4407	419	6.68E+07	0.71185	1904.793
515	82.4088	451	6.48E+07	0.72467	1893.694
547	82.418	483	6.26E+07	0.72672	1887.051
579		515	6.34E+07	0.66043	1907.139
611	82.3883	547	6.25E+07	0.66073	1904.983
643	82.3626	579	6.28E+07	0.73172	1886.124
675	82.3364	611	6.47E+07	0.66581	1911.201
708	82.3291	644	6.48E+07	0.66753	1910.86
740	82.3168	676	6.44E+07	0.71111	1898.964
772	82.3225	708	6.33E+07	0.65301	1909.458
804	82.2838	740	6.11E+07	0.67042	1895.042
832	82.2547	772	5.95E+07	0.65984	1892.873
873	82.2213	804	5.95E+07	0.706	1878.666
901	82.2122	837	6.34E+07	0.71408	1892.13
933	82.1727	869	6.65E+07	0.64664	1922.345
965	82.1757	901	6.75E+07	0.64774	1924.127
997	82.1694	933	6.74E+07	0.64111	1927.112
1025	82.1222	966	6.68E+07	0.64383	1923.196
1066	82.0847	998	6.59E+07	0.64348	1919.625
1094	82.0944	1030	6.41E+07	0.67679	1902.118
1126	82.0707	1062	6.28E+07	0.68312	1895.048
1158	82.0547	1094	6.14E+07	0.69055	1889.587
1190	82.0502	1126	6.03E+07	0.67162	1889.543
1223	82.0453	1159	5.94E+07	0.70677	1875.417
1255	82.0343	1191	5.94E+07	0.72006	1872.352
1287	82.009	1223	6.01E+07	0.72914	1872.922
1319	81.9769	1255	6.02E+07	0.70112	1878.561
1352		1287	6.03E+07	0.74103	1869.484
1383	81.9947	1319	6.11E+07	0.68364	1888.676
1416	81.9673	1352	6.14E+07	0.67925	1891.845
1448	81.9401	1384	6.11E+07	0.74218	1873.532
1480	81.9469	1416	6.08E+07	0.74491	1868.602

1512	81.9406	1448	6.04E+07	0.70661	1877.004
1544	81.9269	1480	6.02E+07	0.74688	1867.181
1576	81.9348	1512	6.17E+07	0.68777	1888.48
1608	81.9214	1544	6.20E+07	0.68939	1888.909
1641		1576	6.20E+07	0.75087	1870.213
1674	81.9326	1609	6.19E+07	0.69596	1887.163
1705	81.8917	1641	6.34E+07	0.68807	1894.648
1738	81.8722	1673	6.37E+07	0.73753	1883.056
1770	81.838	1706	6.32E+07	0.68166	1896.049
1802	81.8163	1738	6.26E+07	0.68041	1893.58
1834	81.7986	1770	6.33E+07	0.66725	1901.551
1866	81.7857	1802	6.31E+07	0.72553	1884.957
1899	81.8105	1834	6.32E+07	0.67392	1898.823
1930	81.7708	1867	6.30E+07	0.72004	1883.658
1963	81.7039	1899	6.31E+07	0.65974	1901.733
1995	81.715	1931	6.37E+07	0.65483	1905.659
2027	81.7356	1963	6.45E+07	0.65247	1910.048
2059	81.6769	1995	6.66E+07	0.64161	1920.657
2092	81.6794	2027	6.82E+07	0.69903	1908.721
2123	81.6571	2059	7.04E+07	0.62846	1939.275
2156	81.6363	2092	7.19E+07	0.68804	1926.016
2188	81.6353	2124	7.29E+07	0.62883	1946.507
2220	81.6041	2156	7.31E+07	0.62433	1948.487
2252	81.5797	2188	7.31E+07	0.62105	1948.738
2284	81.5837	2220	7.28E+07	0.67005	1933.443
2316	81.5341	2252	7.28E+07	0.61541	1950.508
2349	81.5294	2284	7.25E+07	0.66353	1935.682
2381	81.5116	2317	7.16E+07	0.67082	1929.671
2413	81.4963	2349	7.06E+07	0.68058	1921.99
2445	81.4868	2381	6.92E+07	0.69308	1916.557
2477	81.4739	2413	6.84E+07	0.64393	1925.223
2509	81.4286	2445	6.68E+07	0.70391	1901.773
2541	81.4159	2477	6.55E+07	0.71239	1894.375
2573	81.4208	2509	6.41E+07	0.72112	1886.404
2605	81.4236	2541	6.35E+07	0.67864	1896.321
2638	81.4438	2574	6.29E+07	0.7266	1880.269
2669	81.3981	2606	6.15E+07	0.69894	1884.061
2702	81.4017	2638	6.06E+07	0.74291	1868.221
2734	81.407	2670	6.15E+07	0.74932	1870.443
2766	81.3782	2702	6.53E+07	0.68332	1903.434
2799	81.3613	2734	6.75E+07	0.68421	1910.869
2831	81.3435	2767	6.82E+07	0.67615	1915.464
2863	81.3524	2799	6.87E+07	0.67183	1918.127
2895	81.3495	2831	6.83E+07	0.65832	1921.248
2927	81.3342	2863	6.75E+07	0.7085	1905.309
2959	81.2954	2895	6.60E+07	0.71379	1895.843
2991	81.2712	2927	6.55E+07	0.65642	1911.311

3023	81.2976	2959	6.53E+07	0.64768	1914.093
3055	81.2815	2992	6.47E+07	0.66612	1905.287
3088	81.2828	3024	6.47E+07	0.66394	1905.604
3120	81.2337	3056	6.40E+07	0.66095	1903.886
3152	81.2532	3088	6.36E+07	0.64771	1907.3
3184	81.234	3120	6.31E+07	0.69014	1892.165
3216	81.2452	3152	6.24E+07	0.69906	1889.319
3248	81.2262	3185	6.22E+07	0.70598	1885.875
3281	81.1981	3217	6.18E+07	0.71481	1883.867
3313	81.2054	3249	6.29E+07	0.66868	1899.109
3345	81.1619	3281	6.48E+07	0.73052	1888.301
3377	81.1805	3313	6.48E+07	0.66862	1905.819
3409	81.1642	3345	6.40E+07	0.66528	1903.436
3441	81.1304	3377	6.36E+07	0.72406	1886.698
3474	81.1382	3409	6.25E+07	0.66977	1896.451
3505	81.1148	3442	6.18E+07	0.67127	1893.564
3538		3474	6.13E+07	0.66984	1891.534
3570	81.1197	3506	6.04E+07	0.71405	1876.218
3602	81.1102	3538	5.93E+07	0.68294	1880.473
3634	81.0595	3570	5.84E+07	0.71565	1868.244
3667	81.0784	3602	5.73E+07	0.69142	1869.538
3698	81.0857	3634	5.73E+07	0.66596	1878.635
3730	81.0608	3667	6.26E+07	0.6593	1900.945
3763	81.0384	3699	7.01E+07	0.65372	1927.455
3795	81.0092	3731	7.36E+07	0.71107	1926.021
3827	80.9995	3763	7.60E+07	0.71011	1932.17
3854	80.9339	3795	7.63E+07	0.64603	1952.199
3896	80.8816	3827	7.56E+07	0.64225	1949.467
3924	80.8849	3859	7.41E+07	0.63901	1943.986
3955	80.8777	3892	7.15E+07	0.63621	1937.941
3987	80.854	3924	6.94E+07	0.68746	1915.703
4020	80.8463	3956	6.61E+07	0.64309	1916.182
4052	80.8456	3988	6.40E+07	0.68208	1896.752
4084	80.8248	4020	6.91E+07	0.63536	1928.984
4116	80.7899	4052	7.20E+07	0.624	1942.102
4148	80.7895	4084	7.24E+07	0.68712	1926.075
4180	80.7811	4116	7.10E+07	0.62161	1940.858
4212	80.7678	4149	7.02E+07	0.68254	1920.768
4245	80.7743	4181	6.96E+07	0.68263	1918.609
4277	80.7387	4213	6.91E+07	0.6266	1932.059
4309	80.7424	4245	6.76E+07	0.63487	1923.804
4341	80.7173	4277	6.67E+07	0.68213	1907.906
4373	80.7098	4309	6.59E+07	0.69484	1899.894
4405		4341	6.53E+07	0.69743	1896.737
4438	80.714	4374	6.39E+07	0.70053	1893.333
4469	80.6881	4406	6.31E+07	0.64786	1905.57
4502	80.6719	4438	6.24E+07	0.65687	1898.866

4534	80.6683	4470	6.46E+07	0.66913	1902.803
4566	80.6642	4502	6.48E+07	0.70808	1894.659
4598	80.6371	4534	6.40E+07	0.64726	1907.949
4630	80.6351	4566	6.34E+07	0.65967	1901.877
4662	80.6312	4598	6.23E+07	0.70161	1887.212
4694	80.5994	4631	6.17E+07	0.64894	1898.989
4727	80.5973	4663	6.17E+07	0.64616	1899.852
4759	80.6115	4695	6.50E+07	0.62769	1917.413
4791	80.5855	4727	6.84E+07	0.68965	1913.684
4823	80.5452	4759	7.07E+07	0.69595	1919.449
4855	80.5196	4791	7.24E+07	0.6286	1943.857
4887	80.4921	4823	7.28E+07	0.69049	1928.53
4919	80.4636	4855	7.36E+07	0.63315	1945.988
4951	80.454	4888	7.32E+07	0.63419	1944.71
4984		4920	7.27E+07	0.6256	1945.095
5012		4952	7.27E+07	0.67453	1929.252
5049	80.393	4984	7.24E+07	0.68417	1925.313
5081	80.381	5016	7.42E+07	0.61876	1949.848
5112	80.3444	5048	7.10E+07	0.67982	1923.732
5144	80.3418	5080	7.11E+07	0.63347	1936.46
5176	80.3161	5113	7.01E+07	0.69106	1917.408
5209	80.3232	5145	6.88E+07	0.69453	1909.701
5240	80.2979	5177	6.77E+07	0.69671	1907.272
5273	80.3096	5209	6.81E+07	0.65424	1919.047
5305	80.3022	5241	6.87E+07	0.7077	1905.021
5337	80.2827	5273	6.80E+07	0.66124	1917.053
5369	80.2705	5305	6.81E+07	0.66102	1916.656
5401	80.2633	5337	6.82E+07	0.64237	1923.961
5433		5369	6.77E+07	0.69858	1906.713
5466	80.2634	5402	6.70E+07	0.70789	1897.66
5497	80.2872	5434	6.66E+07	0.70793	1897.093
5529	80.2081	5466	6.70E+07	0.65954	1913.485
5562	80.2255	5498	6.59E+07	0.66142	1909.457
5594	80.1955	5530	6.56E+07	0.72143	1891.896
5626		5562	6.63E+07	0.65706	1912.677
5658	80.1948	5594	6.64E+07	0.71555	1893.831
5690	80.1646	5626	6.50E+07	0.66718	1904.537
5723	80.1884	5658	6.53E+07	0.71875	1889.564
5754	80.1626	5691	6.33E+07	0.68644	1891.056
5787	80.1678	5723	6.37E+07	0.67016	1898.592
5819	80.1561	5755	6.58E+07	0.7262	1891.446
5851	80.1572	5787	6.57E+07	0.67201	1905.448
5883	80.1283	5819	6.56E+07	0.67649	1903.066
5916	80.1602	5851	6.58E+07	0.72057	1891.136
5947	80.1086	5883	6.55E+07	0.72774	1888.406
5980	80.128	5915	6.54E+07	0.68064	1900.328
6011	80.0923	5948	6.60E+07	0.73026	1889.218

6043	80.0627	5980	6.68E+07	0.67178	1909.012
6076	80.0618	6012	6.67E+07	0.74151	1889.722
6108	80.0493	6044	6.72E+07	0.67487	1909.461
6136		6076	6.81E+07	0.7348	1897.439
6176	80.0175	6108	6.67E+07	0.67577	1908.762
6204	80.0021	6140	6.76E+07	0.73473	1894.907
6236	79.989	6172	6.71E+07	0.74795	1888.271
6268	80.0035	6204	6.63E+07	0.68155	1902.978
6300	79.9742	6237	6.77E+07	0.67921	1910.086
6333	79.9677	6269	6.73E+07	0.67491	1909.23
6365	79.9553	6301	6.64E+07	0.69028	1900.891
6397	79.9371	6333	6.63E+07	0.67615	1905.273
6429	79.9562	6365	6.65E+07	0.66088	1910.662
6461	79.8994	6397	6.57E+07	0.7101	1894.615
6494	79.909	6429	6.46E+07	0.71659	1889.6
6526	79.9291	6462	6.26E+07	0.72534	1876.838
6557	79.8916	6494	6.26E+07	0.7327	1877.918
6590	79.8938	6526	6.33E+07	0.68229	1893.029
6622	79.9043	6558	6.43E+07	0.74908	1878.197
6654	79.8852	6590	6.55E+07	0.75726	1879.269
6686		6622	6.68E+07	0.69485	1900.119
6718	79.8853	6654	6.82E+07	0.68707	1908.297
6751	79.8783	6687	6.92E+07	0.6784	1914.355
6782	79.8506	6719	7.05E+07	0.67766	1919.321
6815	79.8417	6751	7.02E+07	0.734	1904.302
6847	79.8207	6783	6.83E+07	0.65968	1918.057
6879	79.8185	6815	6.48E+07	0.72173	1888.279
6911	79.8009	6847	6.61E+07	0.72901	1890.4
6943	79.7965	6879	6.90E+07	0.6692	1917.253
6975	79.7736	6911	7.21E+07	0.73786	1908.035
7008	79.7645	6944	7.37E+07	0.66832	1933.633
7039	79.7547	6976	7.50E+07	0.66996	1937.078
7072	79.7651	7008	7.24E+07	0.72962	1911.589
7104	79.7403	7040	6.63E+07	0.66024	1910.836
7136	79.7264	7072	6.06E+07	0.72786	1870.443
7168	79.7202	7104	6.32E+07	0.67706	1892.944
7200	79.6907	7136	6.66E+07	0.6583	1912.344
7232	79.6628	7168	6.91E+07	0.65608	1921.513
7265	79.686	7200	7.04E+07	0.64211	1929.92
7296	79.649	7232	6.94E+07	0.63867	1927.045
7329	79.6471	7265	6.56E+07	0.68717	1901.513
7361		7297	5.98E+07	0.68929	1876.848
7392	79.6576	7329	5.93E+07	0.6958	1871.978
7425	79.6644	7361	6.10E+07	0.70414	1875.873
7457	79.6502	7393	6.26E+07	0.67936	1889.235
7489	79.6411	7425	6.42E+07	0.68315	1895.63
7521	79.6433	7457	6.48E+07	0.72486	1886.464

7553	79.6291	7489	6.30E+07	0.73233	1877.923
7586	79.6235	7522	6.04E+07	0.70008	1876.485
7618	79.6147	7554	6.22E+07	0.67573	1891.224
7650	79.6238	7586	6.38E+07	0.69361	1889.84
7682		7618	6.55E+07	0.67623	1902.086
7714	79.6023	7650	6.66E+07	0.73038	1891.753
7746	79.6069	7682	6.84E+07	0.66044	1917.541
7778	79.595	7714	7.02E+07	0.65291	1925.974
7810	79.5533	7746	7.17E+07	0.71685	1913.214
7843	79.565	7779	7.19E+07	0.65299	1930.752
7875	79.554	7811	7.10E+07	0.71685	1912.299
7907	79.5304	7843	6.74E+07	0.71401	1898.023
7939	79.5316	7875	6.28E+07	0.67791	1892.312
7971	79.5268	7907	5.83E+07	0.73051	1861.067
8003	79.4988	7939	5.41E+07	0.73338	1840.602
8035	79.5073	7971	5.58E+07	0.71029	1854.576
8067	79.5128	8003	5.85E+07	0.70684	1865.854
8099	79.4776	8036	6.02E+07	0.69374	1876.617
8132	79.4951	8068	6.17E+07	0.7507	1867.361
8164	79.5144	8100	6.26E+07	0.70555	1881.455
8196	79.4831	8132	6.44E+07	0.74909	1878.387
8228	79.4988	8164	6.40E+07	0.75724	1873.704
8260	79.4674	8196	6.22E+07	0.76783	1863.958
8292	79.4839	8228	5.96E+07	0.70878	1870.811
8324	79.4838	8260	6.18E+07	0.70081	1882.328
8356	79.4727	8293	6.13E+07	0.69991	1881.311
8389	79.4813	8325	5.84E+07	0.76326	1851.692
8420	79.4267	8357	5.75E+07	0.69846	1865.656
8453	79.4707	8389	5.83E+07	0.71771	1863.867
8484	79.4136	8421	5.98E+07	0.71287	1870.735
8517	79.4285	8453	6.05E+07	0.68252	1882.633
8549	79.4317	8485	6.13E+07	0.75071	1866.972
8581	79.3909	8517	6.22E+07	0.68922	1886.187
8614	79.4106	8550	6.21E+07	0.74614	1870.542
8645	79.402	8582	6.18E+07	0.75211	1867.884
8678	79.4088	8614	6.11E+07	0.69865	1879.195
8710	79.4009	8646	6.01E+07	0.691	1877.789
8742	79.3545	8678	5.77E+07	0.70074	1864.942
8774	79.345	8710	5.72E+07	0.72472	1856.328
8806	79.3675	8742	6.04E+07	0.68403	1882.273
8838	79.3568	8774	6.16E+07	0.73482	1871.516
8870	79.3473	8806	6.31E+07	0.67171	1895.225
8902	79.3495	8839	6.37E+07	0.73837	1878.637
8934	79.349	8871	6.50E+07	0.67519	1899.948
8967		8903	6.59E+07	0.73587	1888.303
8999	79.3264	8935	6.75E+07	0.67563	1910.384
9031	79.2836	8967	6.91E+07	0.73432	1899.916

9063	79.3023	8999	7.05E+07	0.67628	1919.882
9095	79.2863	9031	7.14E+07	0.66448	1927.743
9127	79.2555	9063	7.14E+07	0.66245	1926.959
9159	79.2714	9095	7.11E+07	0.71677	1912.089
9191	79.2719	9128	7.05E+07	0.7254	1905.668
9223	79.231	9160	6.96E+07	0.65462	1924.148
9256	79.246	9192	6.54E+07	0.71898	1891.228
9288	79.229	9224	6.40E+07	0.73043	1880.128
9320	79.2077	9256	6.44E+07	0.7447	1880.964
9352	79.1708	9288	6.50E+07	0.69807	1892.48
9384	79.1867	9320	6.45E+07	0.68019	1898.269
9416	79.1655	9352	6.35E+07	0.7502	1875.02
9449	79.1659	9385	6.29E+07	0.68468	1889.452
9481	79.1754	9417	6.37E+07	0.67599	1895.819
9513	79.175	9449	6.40E+07	0.67018	1897.636
9545	79.1585	9481	6.41E+07	0.67267	1898.061
9577	79.157	9513	6.44E+07	0.72528	1886.382
9609	79.1334	9545	6.48E+07	0.72005	1887.127
9641	79.1342	9577	6.51E+07	0.72747	1887.163
9673	79.1324	9610	6.57E+07	0.6733	1903.604
9706	79.1354	9642	6.57E+07	0.66857	1905.881
9738	79.1158	9674	6.59E+07	0.73808	1886.753
9770	79.1163	9706	6.62E+07	0.74077	1886.798
9802	79.1076	9738	6.63E+07	0.74512	1885.996
9834		9770	6.60E+07	0.67751	1904.054
9867	79.1267	9802	6.48E+07	0.67831	1899.841
9898	79.109	9834	6.46E+07	0.68016	1897.809
9930	79.0817	9866	6.48E+07	0.67006	1901.565
9962	79.0589	9899	6.56E+07	0.72474	1887.277
9995	79.0624	9931	6.65E+07	0.72046	1893.168
10027	79.0574	9963	6.66E+07	0.66001	1910.4
10059	79.0462	9995	6.63E+07	0.72564	1892.13
10091	79.0255	10027	6.63E+07	0.66517	1908.451
10123	79.0027	10059	6.54E+07	0.73417	1887.458
10156	79.0412	10091	6.64E+07	0.73615	1889.924
10187	79.0121	10124	6.66E+07	0.66902	1908.213
10220	79.0196	10156	6.61E+07	0.67073	1905.755
10252	79.0076	10188	6.67E+07	0.7298	1892.021
10284	79.0111	10220	6.58E+07	0.67257	1903.575
10316	78.9751	10252	6.49E+07	0.67726	1898.853
10348	79.0145	10284	6.44E+07	0.71807	1885.881
10380	78.9709	10316	6.38E+07	0.72837	1880.281
10412	78.952	10348	6.40E+07	0.66995	1899.021
10445	78.993	10380	6.52E+07	0.72791	1888.34
10476	78.9897	10413	6.40E+07	0.6691	1899.38
10508	78.9476	10445	6.39E+07	0.67786	1896.3
10541	78.933	10477	6.41E+07	0.72937	1883.103

10573	78.9515	10509	6.42E+07	0.72958	1883.199
10605	78.9511	10541	6.41E+07	0.7421	1879.809
10637	78.9666	10573	6.46E+07	0.67412	1900.026
10669	78.9439	10605	6.48E+07	0.67508	1900.284
10701	78.9142	10637	6.44E+07	0.67455	1898.71
10733	78.9288	10669	6.47E+07	0.67593	1898.708
10765	78.9228	10701	6.57E+07	0.72277	1888.806
10797	78.9317	10734	6.65E+07	0.66337	1909.09
10829	78.8895	10766	6.70E+07	0.64876	1916.034
10862	78.8997	10798	6.69E+07	0.65717	1912.504
10894	78.8932	10830	6.72E+07	0.64869	1916.592
10926	78.8615	10862	6.71E+07	0.64992	1915.776
10958	78.8617	10894	6.68E+07	0.64636	1916.752
10990	78.8739	10926	6.67E+07	0.68269	1904.363
11022	78.8611	10958	6.61E+07	0.68981	1902.617
11054	78.87	10991	6.58E+07	0.69667	1897.106
11086	78.8262	11023	6.46E+07	0.70674	1891.875
11119	78.8489	11055	6.53E+07	0.67051	1903.565
11150	78.8121	11087	6.77E+07	0.66544	1912.462
11183	78.8037	11119	7.00E+07	0.72013	1906.172
11215	78.7664	11151	7.02E+07	0.72649	1904.249
11247	78.7759	11183	7.18E+07	0.66297	1927.791
11279	78.7582	11215	7.29E+07	0.72356	1915.32
11311	78.7389	11248	7.30E+07	0.66473	1931.565
11343	78.7227	11280	7.32E+07	0.73456	1911.869
11376	78.7404	11312	7.33E+07	0.73759	1911.478
11408	78.7132	11344	7.30E+07	0.66945	1930.777
11440	78.6639	11376	7.25E+07	0.67068	1928.871
11472	78.6982	11408	7.24E+07	0.66063	1931.602
11504	78.6914	11440	7.16E+07	0.65985	1928.997
11536	78.6284	11472	7.19E+07	0.71362	1914.639
11569	78.6228	11504	7.15E+07	0.70859	1912.591
11600	78.6091	11537	7.10E+07	0.64854	1930.355
11633	78.5863	11569	7.06E+07	0.71216	1909.783
11665	78.6193	11601	7.05E+07	0.65412	1926.189
11696	78.6043	11633	7.00E+07	0.65304	1926.822
11729	78.5966	11665	6.92E+07	0.70905	1905.099
11761	78.5899	11697	6.93E+07	0.64211	1926.194
11793	78.5917	11729	6.87E+07	0.64836	1922.455
11825	78.572	11762	6.86E+07	0.6944	1908.914
11858		11794	6.84E+07	0.64872	1920.636
11889	78.5501	11826	6.74E+07	0.70196	1904.24
11922	78.5485	11858	6.76E+07	0.70047	1903.275
11954	78.5563	11890	6.72E+07	0.653	1914.774
11986	78.5461	11922	6.67E+07	0.71369	1894.466
12018	78.5394	11954	6.61E+07	0.64939	1911.871
12050	78.4948	11986	6.58E+07	0.71789	1890.453

12078	78.4569	12018	6.54E+07	0.6683	1902.466
12119	78.4469	12051	6.46E+07	0.66248	1903.586
12147	78.4767	12083	6.39E+07	0.71647	1884.259
12178	78.4568	12115	6.38E+07	0.71705	1885.695
12211	78.4336	12147	6.39E+07	0.73126	1879.168
12243	78.4312	12179	6.42E+07	0.69069	1891.949
12275	78.4369	12211	6.40E+07	0.68219	1894.13
12307	78.3993	12243	6.33E+07	0.74291	1873.541
12340	78.4114	12275	6.34E+07	0.67718	1893.96
12371	78.4055	12307	6.43E+07	0.6719	1897.464
12404	78.3672	12340	6.48E+07	0.72762	1884.946
12436	78.3644	12372	6.41E+07	0.67649	1896.149
12468	78.3447	12404	6.48E+07	0.73418	1883.217
12500	78.3573	12436	6.50E+07	0.73235	1881.573
12532	78.3385	12468	6.56E+07	0.67309	1901.908
12564	78.3312	12500	6.64E+07	0.67331	1904.437
12596	78.2845	12533	6.67E+07	0.73278	1888.043
12629	78.325	12565	6.76E+07	0.7446	1887.968
12660	78.2881	12597	6.76E+07	0.74679	1887.817
12693	78.2866	12629	6.75E+07	0.74982	1887.053
12725	78.2607	12661	6.86E+07	0.69298	1905.42
12757	78.2251	12693	6.94E+07	0.77006	1886.065
12789	78.249	12725	7.04E+07	0.70381	1909.384
12821	78.1877	12757	7.09E+07	0.69606	1912.497
12854	78.1788	12790	7.19E+07	0.68642	1919.212
12886	78.1593	12822	7.26E+07	0.67437	1926.192
12918	78.1852	12854	7.22E+07	0.67084	1925.593
12950	78.1641	12886	7.20E+07	0.72061	1909.679
12982	78.1124	12918	7.17E+07	0.72414	1909.526
13014	78.1152	12950	7.15E+07	0.73004	1907.37
13046	78.0723	12982	7.09E+07	0.6688	1920.445
13079	78.0813	13015	7.16E+07	0.66774	1924.138
13110	78.0849	13047	7.09E+07	0.73738	1901.542
13142	78.0436	13079	6.99E+07	0.7409	1896.778
13175	78.008	13111	6.85E+07	0.74442	1892.379
13207		13143	6.66E+07	0.74744	1885.338
13239	78.0175	13175	6.31E+07	0.76396	1867.61
13271	78.0007	13207	6.26E+07	0.70948	1880.251
13303	77.984	13239	6.35E+07	0.70418	1884.624
13335	77.9745	13272	6.44E+07	0.6972	1889.898
13367	77.9679	13304	6.32E+07	0.68823	1888.716
13400	77.9522	13336	6.20E+07	0.69025	1882.576
13432	77.9401	13368	6.17E+07	0.68225	1884.913
13464	77.9518	13400	6.23E+07	0.68499	1886.327
13496	77.9158	13432	6.28E+07	0.72301	1878.477
13528	77.873	13464	6.30E+07	0.72844	1876.958
13561	77.9002	13496	6.28E+07	0.73688	1874.6

13592	77.8818	13529	6.10E+07	0.69737	1877.481
13624	77.8802	13561	6.18E+07	0.69139	1882.43
13656	77.86	13593	6.33E+07	0.69198	1887.515
13689	77.8263	13625	6.43E+07	0.68857	1891.927
13721	77.8369	13657	6.60E+07	0.66618	1905.854
13753	77.8124	13689	6.78E+07	0.65274	1916.421
13785	77.8075	13721	6.84E+07	0.64427	1921.047
13817	77.7998	13753	6.90E+07	0.64508	1923.571
13849	77.7985	13785	6.93E+07	0.69234	1909.223
13881	77.7905	13818	6.89E+07	0.69313	1909.471
13913	77.7512	13850	6.90E+07	0.69878	1904.649
13946	77.7329	13882	6.90E+07	0.70845	1904.343
13978	77.7118	13914	6.92E+07	0.65318	1919.978
14010	77.7195	13946	6.90E+07	0.65472	1918.881
14042	77.7045	13978	6.85E+07	0.64835	1919.581
14074		14010	6.78E+07	0.70633	1901.768
14106	77.679	14042	6.63E+07	0.64167	1914.001
14138	77.6615	14075	6.40E+07	0.69389	1889.164
14170	77.6449	14107	6.17E+07	0.70244	1879.827
14203	77.6332	14139	6.17E+07	0.71246	1877.308
14235	77.6427	14171	6.12E+07	0.72593	1869.501
14267	77.6222	14203	6.16E+07	0.68263	1883.515
14299	77.6049	14235	6.20E+07	0.73864	1871.258
14331	77.5936	14267	6.25E+07	0.74804	1869.107
14363	77.5731	14299	6.26E+07	0.68546	1887.965
14395	77.5663	14332	6.26E+07	0.75195	1867.222
14428	77.5413	14364	6.46E+07	0.68528	1894.741
14460	77.5199	14396	6.58E+07	0.68578	1899.169
14492	77.5191	14428	6.68E+07	0.74687	1884.889
14524	77.5278	14460	6.67E+07	0.74662	1884.977
14556	77.5174	14492	6.52E+07	0.68714	1896.226
14588	77.4897	14524	6.63E+07	0.67482	1903.435
14620	77.4863	14557	6.76E+07	0.67283	1909.747
14652	77.4592	14589	6.85E+07	0.67037	1913.298
14685	77.4444	14621	6.94E+07	0.65584	1920.325
14717	77.42	14653	6.94E+07	0.70581	1907.74
14749	77.4168	14685	6.94E+07	0.70973	1903.691
14781	77.3942	14717	6.79E+07	0.71706	1897.06
14813	77.3717	14749	6.69E+07	0.72635	1893.163
14845	77.3802	14781	6.77E+07	0.73811	1890.802
14877	77.372	14814	6.85E+07	0.68344	1909.163
14909	77.3553	14846	6.87E+07	0.67919	1912.206
14942	77.3333	14878	6.84E+07	0.67339	1912.228
14974	77.3183	14910	6.86E+07	0.7351	1894.814
15006	77.3005	14942	6.83E+07	0.73694	1894.114
15038	77.2723	14974	6.94E+07	0.73669	1898.061
15070	77.2806	15006	6.95E+07	0.74788	1895.034

15102	77.2722	15038	7.01E+07	0.6897	1913.431
15134	77.268	15071	7.14E+07	0.6928	1916.172
15166	77.222	15103	7.10E+07	0.68476	1916.683
15199	77.1959	15135	7.10E+07	0.74588	1900.723
15231	77.1644	15167	7.16E+07	0.67659	1923.369
15263	77.1353	15199	7.19E+07	0.66305	1926.057
15295	77.1161	15231	7.22E+07	0.65799	1930.096
15327	77.1301	15263	7.26E+07	0.65137	1933.391
15359	77.0954	15295	7.24E+07	0.71293	1915.287
15391	77.0868	15327	7.19E+07	0.63877	1934.918
15423	77.0646	15360	7.21E+07	0.63189	1936.604
15456	77.0812	15392	7.09E+07	0.63009	1934.048
15487	77.0398	15424	7.08E+07	0.68566	1919.48
15520	77.0348	15456	7.03E+07	0.69286	1912.524
15552	77.0059	15488	6.96E+07	0.68865	1910.692
15584	77.0009	15520	6.97E+07	0.63438	1928.54
15616	76.991	15552	6.98E+07	0.63982	1926.492
15643	76.9746	15584	6.98E+07	0.70169	1907.663
15685		15616	6.97E+07	0.63791	1928.306
15712	76.9415	15648	6.92E+07	0.69351	1907.132
15744	76.9062	15681	6.86E+07	0.63648	1923.52
15777	76.9274	15713	6.80E+07	0.69498	1904.316
15808	76.9008	15745	6.74E+07	0.64724	1915.93
15841	76.8969	15777	6.72E+07	0.69513	1902.189
15873	76.8417	15809	6.72E+07	0.70714	1899.49
15906		15841	6.66E+07	0.71001	1893.368
15937	76.8332	15873	6.60E+07	0.72544	1886.689
15969	76.8474	15906	6.57E+07	0.66214	1905.157
16001	76.833	15938	6.45E+07	0.66497	1899.758
16033	76.8019	15970	6.38E+07	0.72864	1878.257
16066	76.793	16002	6.38E+07	0.66333	1898.722
16098	76.7865	16034	6.52E+07	0.65446	1906.13
16125	76.746	16066	6.58E+07	0.66136	1906.252
16167	76.746	16098	6.67E+07	0.64724	1914.788
16194	76.7578	16130	6.61E+07	0.70456	1893.14
16226	76.7312	16162	6.56E+07	0.6995	1895.033
16259	76.7365	16195	6.58E+07	0.66021	1905.223
16290	76.7121	16227	6.54E+07	0.7083	1889.945
16323	76.7225	16259	6.42E+07	0.71816	1885.892
16354	76.6803	16291	6.41E+07	0.66799	1896.435
16387	76.6811	16323	6.35E+07	0.67891	1890.837
16419	76.6811	16355	6.26E+07	0.72105	1877.342
16451	76.6669	16387	6.27E+07	0.66504	1892.568
16483	76.687	16419	6.21E+07	0.68264	1885.5
16515	76.6676	16452	6.13E+07	0.71728	1871.528
16548	76.6619	16484	6.20E+07	0.72763	1873.406
16580	76.6415	16516	6.18E+07	0.67234	1886.51

16612	76.6556	16548	6.24E+07	0.68444	1884.786
16644	76.6423	16580	6.25E+07	0.73171	1871.909
16676	76.641	16612	6.23E+07	0.74202	1869.308
16708	76.6409	16644	6.27E+07	0.68573	1886.29
16740	76.6034	16676	6.24E+07	0.68377	1886.326
16773	76.5997	16709	6.25E+07	0.68319	1886.138
16805	76.5919	16741	6.21E+07	0.74055	1868.234
16837	76.6057	16773	6.18E+07	0.67463	1886.251
16869	76.5815	16805	6.14E+07	0.72825	1871.087
16901	76.602	16837	6.16E+07	0.73718	1869.211
16933		16869	6.17E+07	0.6849	1882.721
16965	76.5512	16902	6.15E+07	0.74876	1865.357
16998	76.5526	16934	6.16E+07	0.75048	1864.771
17029	76.5303	16966	6.16E+07	0.69342	1880.986
17062	76.5554	16998	6.15E+07	0.70671	1874.973
17094	76.5325	17030	6.18E+07	0.68475	1884.018
17126	76.5148	17062	6.11E+07	0.69117	1878.252
17158	76.5113	17094	6.10E+07	0.74057	1866.23
17190	76.5034	17127	6.13E+07	0.73849	1867.648
17223	76.4834	17159	6.14E+07	0.74796	1864.889
17255	76.4981	17191	6.12E+07	0.69284	1878.886
17287	76.5185	17223	6.17E+07	0.75832	1863.211
17319	76.489	17255	6.12E+07	0.77242	1856.911
17351	76.5101	17287	6.19E+07	0.7049	1878.643
17383	76.4713	17319	6.33E+07	0.69852	1885.806
17415	76.4624	17352	6.25E+07	0.69608	1882.541
17447	76.4671	17384	6.26E+07	0.68975	1885.289
17479	76.4255	17416	6.25E+07	0.74795	1869.695
17512	76.4184	17448	6.46E+07	0.67207	1898.827
17544	76.4065	17480	6.29E+07	0.73591	1873.865
17576	76.4133	17512	6.30E+07	0.68122	1888.51
17608	76.4056	17544	6.28E+07	0.67568	1890.14
17640	76.3661	17576	6.24E+07	0.67975	1887.64
17673	76.3745	17608	6.28E+07	0.72337	1876.44
17704	76.3737	17641	6.17E+07	0.73415	1869.392
17736	76.3366	17673	6.21E+07	0.68821	1884.474
17769	76.353	17705	6.20E+07	0.73524	1871.271
17800	76.3185	17737	6.23E+07	0.68814	1884.918
17833	76.306	17769	6.18E+07	0.68167	1885.051
17865	76.3095	17801	6.13E+07	0.69172	1879.395
17897	76.2728	17833	6.14E+07	0.67972	1883.928
17929	76.2779	17865	6.13E+07	0.68797	1881.246
17961	76.2983	17897	6.12E+07	0.72014	1871.359
17993	76.2706	17929	6.19E+07	0.72686	1874.217
18026	76.27	17962	6.19E+07	0.73634	1871.225
18057	76.2428	17994	6.25E+07	0.74571	1870.903
18090	76.2686	18026	6.19E+07	0.69165	1881.951

18122	76.2477	18058	6.27E+07	0.68793	1888.178
18154	76.2394	18090	6.18E+07	0.68854	1883.24
18186		18122	6.28E+07	0.74554	1871.934
18219	76.2251	18154	6.28E+07	0.67628	1890.906
18250	76.1905	18187	6.25E+07	0.73289	1873.323
18283	76.1975	18219	6.20E+07	0.69439	1882.297
18314	76.1955	18251	6.20E+07	0.74291	1870.35
18347	76.2096	18283	6.22E+07	0.68248	1887.074
18379	76.2229	18315	6.21E+07	0.6788	1887.382
18411	76.1993	18347	6.22E+07	0.74161	1871.586
18443	76.1949	18379	6.22E+07	0.74344	1870.709
18475	76.1785	18412	6.18E+07	0.68195	1886.097
18508	76.1603	18444	6.15E+07	0.74094	1869.054
18540	76.1625	18476	6.15E+07	0.68815	1883.059
18572	76.1706	18508	6.17E+07	0.68326	1885.792
18604	76.1413	18540	6.13E+07	0.69744	1879.277
18636	76.1481	18572	6.18E+07	0.67849	1887.808
18668	76.1583	18604	6.17E+07	0.68679	1884.448
18700	76.1476	18636	6.11E+07	0.72117	1871.601
18732	76.161	18668	6.14E+07	0.7281	1872.708
18764	76.1488	18701	6.15E+07	0.73752	1869.858
18796	76.1255	18733	6.15E+07	0.74593	1868.52
18829	76.1128	18765	6.14E+07	0.69297	1881.526
18861	76.0987	18797	6.18E+07	0.76139	1864.646
18893	76.0878	18829	6.20E+07	0.70528	1879.933
18925	76.0915	18861	6.16E+07	0.76505	1860.532
18957	76.0895	18893	6.14E+07	0.69742	1879.009
18989	76.11	18926	6.15E+07	0.6882	1882.739
19021	76.0986	18958	6.15E+07	0.70352	1877.615
19054	76.1124	18990	6.14E+07	0.69072	1881.67
19085	76.0979	19022	6.18E+07	0.74443	1869.001
19118	76.066	19054	6.17E+07	0.7401	1870.443
19150	76.0769	19086	6.17E+07	0.74906	1865.603
19182	76.0764	19118	6.17E+07	0.6936	1881.535
19214	76.0634	19150	6.20E+07	0.68741	1884.59
19246	76.0776	19182	6.21E+07	0.75907	1865.778
19278	76.0295	19215	6.29E+07	0.68956	1887.691
19311	76.0464	19247	6.37E+07	0.67995	1893.634
19343	76.0367	19279	6.39E+07	0.73701	1877.468
19375	76.0059	19311	6.51E+07	0.68614	1896.584
19407	76.0077	19343	6.51E+07	0.74586	1881.449
19439	75.9908	19375	6.50E+07	0.68183	1897.337
19472	75.9975	19408	6.58E+07	0.74147	1883.318
19503	75.9704	19440	6.61E+07	0.68254	1901.629
19536	75.9357	19472	6.60E+07	0.67219	1904.05
19568	75.9517	19504	6.59E+07	0.66954	1905.103
19600	75.9485	19536	6.63E+07	0.72399	1890.35

19632	75.9368	19568	6.65E+07	0.66305	1908.467
19664	75.9115	19601	6.63E+07	0.71637	1892.087
19697	75.9255	19633	6.66E+07	0.72348	1890.332
19728	75.9052	19665	6.65E+07	0.66819	1906.814
19761	75.9111	19697	6.62E+07	0.73397	1888.416
19793	75.9096	19729	6.47E+07	0.73606	1882.021
19825	75.8882	19761	6.39E+07	0.67983	1894.409
19857	75.8968	19793	6.34E+07	0.68758	1890.279
19889	75.8579	19825	6.34E+07	0.73618	1877.5
19922	75.8827	19858	6.36E+07	0.75046	1873.625
19954	75.8791	19890	6.42E+07	0.68212	1894.924
19986	75.8698	19922	6.52E+07	0.7426	1882.196
20018	75.8762	19954	6.53E+07	0.6838	1898.387
20050	75.8549	19986	6.51E+07	0.75499	1877.48
20082	75.835	20018	6.48E+07	0.68665	1895.016
20114	75.8359	20050	6.46E+07	0.67598	1898.317
20146	75.8282	20083	6.47E+07	0.67336	1898.567
20179	75.8384	20115	6.52E+07	0.67562	1898.857
20211	75.7988	20147	6.55E+07	0.65995	1905.473
20243	75.7996	20179	6.65E+07	0.70803	1894.884
20275	75.7833	20211	6.67E+07	0.64756	1915.44
20307	75.773	20243	6.71E+07	0.64939	1914.748
20340	75.7257	20276	6.74E+07	0.70152	1899.971
20373	75.7422	20308	6.71E+07	0.64647	1915.602
20404	75.7543	20340	6.77E+07	0.70412	1899.978
20436	75.7379	20373	6.80E+07	0.7033	1902.834
20469	75.7142	20405	6.78E+07	0.71501	1899.715
20501	75.7142	20437	6.90E+07	0.72879	1899.202
20533	75.7133	20469	6.95E+07	0.66456	1919.522
20566	75.7343	20501	6.96E+07	0.668	1917.115
20597	75.6994	20534	6.90E+07	0.66114	1917.879
20630	75.6999	20566	6.89E+07	0.72187	1902.097
20662	75.6975	20598	6.83E+07	0.65906	1916.269
20694	75.6739	20630	6.60E+07	0.70867	1893.84
20726	75.6556	20662	6.58E+07	0.71793	1890.415
20758	75.6463	20694	6.63E+07	0.65905	1908.947
20791	75.6535	20727	6.69E+07	0.65865	1911.826
20823	75.6113	20759	6.67E+07	0.65393	1912.052
20855	75.6305	20791	6.65E+07	0.65023	1912.293
20887	75.5826	20823	6.63E+07	0.70136	1898.888
20920	75.6313	20856	6.56E+07	0.69787	1894.977
20951	75.6049	20888	6.66E+07	0.70603	1897.084
20984	75.5692	20920	6.74E+07	0.71598	1898.17
21016	75.5949	20952	6.67E+07	0.66358	1908.717
21048	75.5686	20984	6.59E+07	0.73181	1886.353
21080	75.5567	21016	6.57E+07	0.6825	1900.485
21112	75.5512	21049	6.68E+07	0.67091	1906.79

21145	75.5619	21081	6.59E+07	0.67271	1903.441
21176	75.5272	21113	6.62E+07	0.71852	1893.017
21209	75.5582	21145	6.67E+07	0.66053	1910.323
21241	75.5205	21177	6.86E+07	0.64698	1921.132
21273	75.5102	21209	6.93E+07	0.70763	1904.033
21305	75.514	21241	6.89E+07	0.65248	1920.642
21337	75.5026	21274	6.92E+07	0.71109	1906.011
21370	75.5396	21306	6.92E+07	0.70953	1906.666
21401	75.5192	21338	6.92E+07	0.65563	1921.148
21434	75.5056	21370	6.90E+07	0.65291	1921.324
21466		21402	6.87E+07	0.71014	1902.665
21498		21434	6.80E+07	0.65927	1914.797
21535	75.4665	21466	6.79E+07	0.65347	1916.358
21558	75.456	21499	6.79E+07	0.6385	1921.347
21595	75.4588	21531	6.73E+07	0.696	1903.089
21627	75.4148	21563	6.63E+07	0.70505	1898.807
21660	75.4442	21595	6.56E+07	0.70398	1896.681
21691	75.4263	21627	6.57E+07	0.71337	1893.49
21723	75.3766	21660	6.54E+07	0.65681	1908.684
21756	75.37	21692	6.49E+07	0.72979	1884.149
21788		21724	6.43E+07	0.67946	1897.009
21819	75.3327	21756	6.44E+07	0.66185	1902.856
21853	75.3589	21788	6.47E+07	0.72267	1887.553
21884	75.3237	21820	6.54E+07	0.72462	1889.703
21917	75.32	21853	6.61E+07	0.73886	1885.437
21949	75.3262	21885	6.80E+07	0.74077	1893.295
21981	75.29	21917	6.82E+07	0.75364	1890.378
22013	75.2966	21949	6.86E+07	0.77292	1885.09
22045		21981	6.87E+07	0.70885	1902.69
22078	75.2772	22013	6.86E+07	0.78016	1882.909
22110	75.2686	22046	6.89E+07	0.71371	1903.705
22142	75.2533	22078	6.90E+07	0.70856	1905.16
22174	75.2143	22110	6.89E+07	0.77368	1885.309
22206	75.1948	22142	6.86E+07	0.77384	1884.403
22239	75.2146	22174	6.87E+07	0.71249	1902.099
22271	75.2212	22207	6.81E+07	0.77328	1884.621
22303	75.1869	22239	6.57E+07	0.71095	1893.064
22335	75.1971	22271	6.34E+07	0.71141	1884.336
22367	75.2045	22303	6.30E+07	0.77321	1865.59
22399	75.2065	22336	6.56E+07	0.69946	1895.617
22432	75.204	22368	6.45E+07	0.69698	1892.692
22464	75.2035	22400	6.33E+07	0.75432	1873.124
22496	75.1946	22432	6.25E+07	0.69137	1885.898
22529	75.1697	22464	6.17E+07	0.70858	1878.636
22561	75.158	22496	6.19E+07	0.67794	1888.662
22593	75.146	22529	6.19E+07	0.67262	1889.846
22625	75.1621	22561	6.13E+07	0.73601	1870.614

22657	75.1525	22593	6.14E+07	0.73217	1872.483
22690		22626	6.16E+07	0.68753	1884.168
22722	75.1267	22658	6.17E+07	0.73632	1872.464
22754	75.1486	22690	6.18E+07	0.74858	1869.675
22786	75.122	22722	6.11E+07	0.69988	1879.253
22819	75.1176	22755	6.09E+07	0.75694	1861.352
22851	75.1149	22787	5.98E+07	0.71727	1869.095
22883	75.1051	22819	5.88E+07	0.76839	1852.702
22915	75.0842	22851	5.83E+07	0.77512	1848.066
22948	75.1182	22883	5.76E+07	0.70903	1862.672
22979	75.1022	22915	5.81E+07	0.73826	1855.851
23012	75.0431	22948	5.86E+07	0.72722	1860.656
23046	75.0634	22980	5.92E+07	0.70642	1870.647
23077	75.1025	23013	5.99E+07	0.69465	1876.306
23109	75.0868	23046	6.10E+07	0.69958	1880.051
23142	75.1029	23078	6.11E+07	0.67862	1885.591
23174	75.0765	23110	6.10E+07	0.73636	1867.498
23207	75.0898	23142	6.09E+07	0.73828	1869.309
23238	75.0771	23174	6.11E+07	0.67909	1886.467
23271	75.0632	23207	6.07E+07	0.69863	1878.301
23303	75.0565	23239	6.05E+07	0.74151	1866.981
23335	75.0625	23271	6.07E+07	0.69577	1878.936
23367	75.055	23303	6.00E+07	0.69407	1877.532
23399	75.0402	23335	6.03E+07	0.7369	1866.834
23432	75.0444	23368	6.22E+07	0.69436	1884.539
23465		23400	6.44E+07	0.74815	1878.512
23496	75.0498	23433	6.71E+07	0.74954	1888.571
23530	75.0786	23465	6.78E+07	0.76083	1887.593
23561	75.0538	23497	7.15E+07	0.70106	1916.869
23594	75.0325	23530	7.33E+07	0.76733	1902.587
23626	75.0028	23562	7.43E+07	0.70811	1923.634
23659	74.9845	23594	7.45E+07	0.77424	1905.076
23691	74.9648	23627	7.45E+07	0.7052	1925.833
23723		23659	7.46E+07	0.69463	1928.463
23757	74.9496	23691	7.39E+07	0.69341	1926.499
23788	74.929	23724	7.36E+07	0.67936	1930.204
23821	74.9145	23756	7.33E+07	0.6739	1931.188
23853	74.8988	23789	7.33E+07	0.72376	1917.024
23886	74.9012	23821	7.29E+07	0.65836	1934.255
23918	74.8767	23854	7.28E+07	0.72005	1914.332
23950	74.8517	23886	7.29E+07	0.72564	1915.102
23983	74.8415	23918	7.20E+07	0.66533	1928.76
24015	74.8231	23950	7.19E+07	0.6637	1928.941
24047	74.8104	23983	7.05E+07	0.65235	1927.93
24079	74.8044	24015	7.06E+07	0.71968	1906.985
24112		24047	7.02E+07	0.65107	1927.426
24143	74.7974	24080	6.93E+07	0.6369	1928.819

24176	74.7903	24112	6.92E+07	0.6315	1931.229
24208	74.7707	24144	6.85E+07	0.69122	1908.572
24241		24177	6.75E+07	0.69938	1905.567
24273	74.7711	24209	6.83E+07	0.69512	1909.76
24305	74.7609	24241	6.82E+07	0.70437	1904.034
24337	74.7169	24273	6.79E+07	0.71853	1898.745
24370	74.7161	24305	6.85E+07	0.66664	1916.473
24402	74.714	24338	6.82E+07	0.66197	1917.2
24434	74.6854	24370	6.81E+07	0.65486	1920.215
24464		24402	6.78E+07	0.65591	1917.545
24499		24435	6.69E+07	0.70516	1899.646
24533	74.6599	24467	6.87E+07	0.70235	1906.04
24563	74.6716	24499	6.60E+07	0.70985	1894.09
24595	74.6675	24531	6.48E+07	0.71991	1888.924
24628	74.6501	24563	6.55E+07	0.73357	1886.748
24660	74.6304	24596	6.51E+07	0.69189	1895.314
24692	74.6389	24628	6.48E+07	0.67788	1899.816
24724	74.6342	24660	6.42E+07	0.67823	1896.74
24757	74.6133	24693	6.39E+07	0.73531	1878.608
24789	74.6056	24725	6.38E+07	0.67955	1894.577
24821	74.5885	24757	6.38E+07	0.7272	1882.634
24853	74.5822	24789	6.34E+07	0.73462	1879.45
24886	74.5599	24821	6.29E+07	0.74653	1872.743
24919	74.5745	24854	6.34E+07	0.69267	1889.005
24951	74.5465	24886	6.37E+07	0.68031	1894.043
24984		24919	6.36E+07	0.75208	1875.151
25017	74.5549	24952	6.28E+07	0.70415	1884.248
25048	74.5329	24984	6.36E+07	0.69532	1889.485
25081		25017	6.24E+07	0.74015	1873.121
25113	74.508	25049	6.41E+07	0.67868	1898.375
25146	74.4811	25081	6.89E+07	0.67837	1915.714
25178	74.4748	25114	7.25E+07	0.7343	1912.721
25205	74.4272	25146	7.54E+07	0.6701	1939.59
25247	74.3465	25178	7.83E+07	0.66531	1951.163
25276	74.3745	25211	8.06E+07	0.65109	1961.984
25307	74.3208	25243	8.20E+07	0.64584	1967.548
25340	74.3597	25275	8.26E+07	0.63966	1971.885
25371	74.3286	25308	8.27E+07	0.68712	1959.552
25404	74.3098	25340	8.23E+07	0.62491	1975.593
25436	74.2965	25372	8.17E+07	0.61724	1976.092
25469	74.299	25404	8.14E+07	0.6751	1956.586
25501	74.2572	25437	8.10E+07	0.61637	1973.577
25533	74.2473	25469	7.98E+07	0.67635	1951.464
25565	74.2192	25501	7.93E+07	0.67409	1950.156
25598	74.1841	25533	7.84E+07	0.61924	1964.655
25630	74.1593	25566	7.78E+07	0.61962	1963.193
25663	74.191	25598	7.64E+07	0.67319	1944.039

25694	74.184	25630	7.60E+07	0.68512	1937.338
25727	74.1877	25663	7.45E+07	0.68697	1933.537
25759	74.152	25695	7.48E+07	0.62399	1951.268
25792	74.1587	25728	7.44E+07	0.69067	1932.43
25824	74.1297	25760	7.40E+07	0.70559	1924.86
25856	74.1222	25792	7.39E+07	0.64454	1941.509
25889	74.133	25824	7.37E+07	0.70387	1926.018
25921	74.1379	25856	7.33E+07	0.70742	1922.941
25953	74.0946	25889	7.32E+07	0.6559	1936.722
25986	74.0746	25921	7.24E+07	0.71763	1914.917
26018	74.0659	25953	7.21E+07	0.65327	1932.468
26050	74.0537	25986	7.14E+07	0.65324	1931.443
26082	74.0619	26018	7.02E+07	0.71136	1909.659
26115	74.0486	26050	7.02E+07	0.71219	1908.853
26147		26083	6.96E+07	0.65506	1924.05
26180	74.0511	26115	6.76E+07	0.71088	1903.093
26212	74.0138	26147	6.70E+07	0.72297	1894.349
26245	74.0076	26180	6.75E+07	0.73762	1892.283
26277	74.0254	26212	6.82E+07	0.67236	1914.519
26309	74.0049	26245	6.90E+07	0.73477	1899.298
26342	73.9886	26277	6.81E+07	0.67993	1911.411
26374	73.9918	26310	6.74E+07	0.74501	1890.853
26407	73.9975	26342	6.66E+07	0.67824	1907.623
26439	73.9704	26374	6.56E+07	0.67716	1903.237
26471	73.9676	26407	6.53E+07	0.73817	1884.599
26504	73.9733	26439	6.26E+07	0.73889	1872.861
26536	73.9559	26472	6.02E+07	0.75127	1862.999
26569	73.9779	26504	6.06E+07	0.75258	1861.01
26600	73.957	26536	6.01E+07	0.71628	1869.526
26633	73.946	26569	5.83E+07	0.73322	1858.163
26666	73.989	26601	5.69E+07	0.77537	1842.845
26698	73.9988	26633	5.62E+07	0.78303	1837.977
26730	73.9869	26666	5.30E+07	0.76511	1828.592
26763	73.9762	26698	5.36E+07	0.79233	1822.597
26795		26731	5.29E+07	0.75519	1830.077
26828	73.9581	26763	5.48E+07	0.77294	1833.388
26860	73.9819	26796	5.38E+07	0.74074	1838.475
26892	73.9522	26828	5.41E+07	0.75646	1834.113
26925	73.9571	26860	5.52E+07	0.80171	1828.248
26957	73.9533	26893	5.57E+07	0.73342	1847.86
26989	73.9476	26925	5.71E+07	0.7991	1834.801
27022	73.9673	26957	5.91E+07	0.72797	1864.066
27054	73.9491	26990	6.10E+07	0.80192	1850.489
27087	73.9232	27022	6.24E+07	0.73418	1874.444
27120	73.9542	27055	6.34E+07	0.72135	1881.486
27151	73.9184	27087	6.46E+07	0.71906	1887.349
27184	73.9016	27119	6.48E+07	0.70385	1892.104

27217	73.9557	27152	6.55E+07	0.69927	1895.991
27248	73.9238	27184	6.61E+07	0.75132	1885.205
27281	73.9175	27217	6.65E+07	0.68302	1904.795
27313	73.8917	27249	6.69E+07	0.74687	1887.996
27346	73.9122	27281	6.69E+07	0.68625	1905.608
27378	73.8963	27314	6.55E+07	0.74901	1882.613
27411	73.8868	27346	6.51E+07	0.69737	1896.11
27443	73.8625	27379	6.47E+07	0.74813	1881.864
27476	73.8904	27411	6.51E+07	0.69651	1895.502
27508	73.8695	27443	6.61E+07	0.67968	1905.63
27540	73.8506	27476	6.57E+07	0.68792	1900.56
27573	73.8475	27508	6.63E+07	0.73702	1889.924
27605	73.8357	27541	6.65E+07	0.74535	1889.654
27638	73.8458	27573	6.72E+07	0.74476	1892.383
27670	73.827	27605	6.77E+07	0.75489	1889.749
27702	73.8191	27638	6.79E+07	0.69729	1906.513
27735	73.8367	27670	6.84E+07	0.69907	1907.422
27767	73.8502	27702	6.88E+07	0.76468	1891.717
27799	73.8497	27735	6.83E+07	0.6963	1906.872
27832	73.8113	27767	6.88E+07	0.68632	1911.966
27865	73.8127	27800	6.89E+07	0.74417	1895.582
27897	73.8182	27832	6.90E+07	0.6822	1913.563
27929	73.8089	27865	6.95E+07	0.75048	1895.455
27962	73.7981	27897	6.96E+07	0.6763	1918.421
27994	73.8128	27929	6.99E+07	0.6725	1920.255
28026	73.828	27962	7.00E+07	0.66987	1920.944
28059	73.8067	27994	7.00E+07	0.72479	1906.846
28091	73.7582	28027	7.05E+07	0.66385	1926.097
28124	73.795	28059	7.06E+07	0.71554	1910.408
28156	73.7523	28092	7.11E+07	0.65484	1929.703
28188	73.7668	28124	7.07E+07	0.72007	1908.099
28220	73.7319	28156	7.10E+07	0.73061	1909.196
28253	73.7336	28188	7.14E+07	0.66213	1929.185
28285	73.7266	28221	7.18E+07	0.73147	1908.818
28318	73.6975	28253	7.25E+07	0.66483	1932.771
28351	73.7271	28286	7.21E+07	0.66673	1930.068
28383	73.7089	28318	7.23E+07	0.6566	1933.955
28415	73.7126	28351	7.10E+07	0.71017	1913.908
28448	73.6722	28383	7.07E+07	0.72026	1909.227
28481	73.7114	28416	7.11E+07	0.7179	1911.441
28512		28448	7.07E+07	0.65963	1927.193
28545	73.6556	28481	6.98E+07	0.66303	1922.036
28578	73.654	28513	6.90E+07	0.65949	1921.803
28611	73.6866	28545	6.90E+07	0.71827	1903.012
28642	73.6442	28578	6.87E+07	0.71785	1902.332
28675	73.6254	28610	6.91E+07	0.71784	1904.066
28708	73.6391	28643	6.89E+07	0.73006	1902.182

28740	73.6348	28675	6.79E+07	0.74413	1893.118
28772	73.6117	28708	6.76E+07	0.68935	1906.862
28805	73.6102	28740	6.77E+07	0.75584	1889.554
28837	73.6026	28772	6.75E+07	0.69107	1907.156
28870	73.6088	28805	6.82E+07	0.75819	1890.491
28902	73.604	28837	6.82E+07	0.7641	1889.252
28934	73.5692	28870	6.75E+07	0.69512	1905.181
28967	73.5536	28902	6.78E+07	0.76951	1886.275
29000	73.5701	28935	6.74E+07	0.77238	1883.167
29032	73.5892	28967	6.71E+07	0.71427	1899.302
29064	73.5638	29000	6.65E+07	0.70592	1899.066
29092	73.5275	29032	6.67E+07	0.69487	1903.743
29134		29065	6.61E+07	0.69482	1900.199
29162	73.525	29097	6.64E+07	0.75228	1885.608
29194	73.5118	29129	6.58E+07	0.74805	1885.692
29226	73.4942	29162	6.63E+07	0.75515	1884.284
29259	73.4845	29194	6.68E+07	0.69258	1902.328
29291	73.4748	29227	6.72E+07	0.765	1884.616
29324	73.473	29259	6.77E+07	0.70548	1903.92
29356	73.4538	29292	6.73E+07	0.69659	1904.425
29389	73.4439	29324	6.69E+07	0.68681	1904.245
29421	73.4266	29357	6.72E+07	0.67385	1910.316
29454	73.4177	29389	6.65E+07	0.74082	1890.177
29486	73.4123	29421	6.61E+07	0.73575	1887.971
29519	73.4334	29454	6.57E+07	0.68576	1901.671
29551	73.4238	29486	6.48E+07	0.73983	1881.944
29584	73.4044	29519	6.52E+07	0.69293	1897.559
29616	73.4251	29551	6.51E+07	0.68406	1899.496
29648	73.3959	29584	6.51E+07	0.74305	1883.123
29681	73.3769	29616	6.44E+07	0.74458	1878.857
29713	73.3904	29649	6.47E+07	0.68763	1896.965
29746	73.4111	29681	6.47E+07	0.74597	1879.522
29778	73.4031	29713	6.41E+07	0.68556	1895.675
29811	73.4064	29746	6.43E+07	0.68776	1894.953
29843	73.3824	29778	6.36E+07	0.69658	1890.934
29876	73.3644	29811	6.38E+07	0.66846	1900.457
29908	73.3709	29844	6.37E+07	0.73171	1881.801
29941	73.407	29876	6.37E+07	0.72872	1883.764
29973	73.3664	29908	6.26E+07	0.73778	1874.917
30006	73.3575	29941	6.29E+07	0.69441	1889.367
30038	73.3356	29973	6.35E+07	0.74782	1877.234
30071	73.3586	30006	6.40E+07	0.76449	1873.759
30102	73.3275	30038	6.42E+07	0.77138	1871.936
30136	73.3283	30071	6.47E+07	0.78034	1871.827
30168	73.3204	30103	6.52E+07	0.78927	1871.819
30200	73.3184	30136	6.55E+07	0.73213	1887.222
30232	73.29	30168	6.58E+07	0.8059	1867.802

30265	73.2889	30200	6.59E+07	0.73701	1887.712
30298	73.3053	30232	6.56E+07	0.80737	1866.181
30330	73.2913	30265	6.54E+07	0.73562	1885.997
30362		30298	6.54E+07	0.72543	1888.601
30395	73.2815	30330	6.60E+07	0.72415	1891.17
30427	73.2713	30363	6.60E+07	0.70862	1896.142
30460	73.2785	30395	6.61E+07	0.77725	1878.358
30492	73.2627	30427	6.61E+07	0.6975	1899.508
30525	73.2468	30460	6.61E+07	0.69026	1902.064
30557	73.2248	30492	6.64E+07	0.68771	1903.049
30591	73.2351	30525	6.65E+07	0.74788	1887.175
30623	73.2311	30558	6.67E+07	0.68977	1903.114
30655	73.1958	30590	6.63E+07	0.67539	1906.918
30689	73.2002	30623	6.63E+07	0.73311	1889.651
30721		30656	6.62E+07	0.74211	1887.005
30753	73.2186	30688	6.59E+07	0.68177	1903.232
30785	73.1859	30721	6.62E+07	0.73965	1889.017
30819	73.2359	30753	6.63E+07	0.67868	1905.795
30850	73.1867	30786	6.65E+07	0.67931	1906.907
30884	73.2065	30819	6.67E+07	0.73952	1891.716
30915	73.1641	30851	6.67E+07	0.73898	1890.46
30948	73.1713	30883	6.64E+07	0.68186	1905.838
30981	73.1632	30916	6.66E+07	0.73886	1889.602
31013	73.1393	30949	6.69E+07	0.75149	1888.15
31046	73.1433	30981	6.67E+07	0.76665	1883.069
31078	73.1492	31013	6.67E+07	0.69879	1900.933
31111	73.1337	31046	6.65E+07	0.69115	1903.002
31144	73.1316	31078	6.70E+07	0.69292	1906.559
31176	73.1068	31111	6.67E+07	0.68841	1903.807
31208	73.1289	31144	6.64E+07	0.74296	1886.498
31240	73.0808	31176	6.66E+07	0.73799	1891.086
31274	73.0925	31209	6.73E+07	0.74622	1890.305
31305	73.0768	31241	6.72E+07	0.68562	1906.391
31338	73.0469	31273	6.74E+07	0.68423	1909.127
31372	73.0698	31306	6.77E+07	0.68343	1908.187
31404	73.0426	31338	6.75E+07	0.67212	1911.197
31437	73.0552	31371	6.75E+07	0.72904	1895.185
31469	73.047	31404	6.72E+07	0.72543	1896.646
31502	73.0289	31437	6.75E+07	0.66391	1915.118
31535	73.0217	31469	6.67E+07	0.72953	1891.768
31567	73.0076	31502	6.63E+07	0.66881	1908.232
31600	73.0098	31534	6.64E+07	0.66926	1908.887
31632	72.9876	31567	6.66E+07	0.66346	1911.135
31664	72.9697	31599	6.60E+07	0.71294	1893.782
31697	72.9804	31632	6.64E+07	0.72324	1894.97
31729		31665	6.64E+07	0.72192	1895.843
31761		31697	6.68E+07	0.73307	1894.685

31794	72.968	31730	6.60E+07	0.74647	1884.176
31827	72.9621	31762	6.69E+07	0.69115	1904.026
31859	72.9322	31794	6.61E+07	0.68701	1903.157
31892	72.9369	31827	6.58E+07	0.75172	1885.141
31925	72.9398	31859	6.59E+07	0.75798	1883.681
31957	72.9232	31892	6.58E+07	0.69052	1901.514
31990	72.9191	31925	6.58E+07	0.67989	1903.61
32022	72.9186	31958	6.56E+07	0.68647	1900.465
32055	72.9357	31990	6.58E+07	0.74898	1884.673
32088	72.9259	32023	6.74E+07	0.74841	1891.075
32121	72.8927	32055	6.79E+07	0.67531	1913.506
32153	72.8907	32088	6.79E+07	0.67242	1913.29
32185	72.8892	32121	6.81E+07	0.671	1914.443
32218	72.8705	32153	6.86E+07	0.73839	1898.036
32251	72.8701	32186	6.92E+07	0.73616	1898.72
32283	72.8643	32218	6.89E+07	0.66373	1919.145
32316	72.8556	32251	6.93E+07	0.73116	1899.633
32349	72.8288	32284	6.95E+07	0.67268	1917.718
32381		32316	7.01E+07	0.673	1920.412
32414	72.8116	32349	7.02E+07	0.66058	1924.192
32446	72.7982	32382	6.95E+07	0.71424	1907.791
32479		32414	6.83E+07	0.65616	1918.975
32511	72.7835	32447	6.64E+07	0.7091	1896.331
32545	72.8315	32479	6.61E+07	0.71675	1894.605
32576	72.8137	32512	6.66E+07	0.6568	1912.026
32609	72.7886	32544	6.66E+07	0.72514	1891.866
32642		32577	6.64E+07	0.72743	1892.982
32674	72.7474	32610	6.70E+07	0.67169	1909.82
32708	72.7603	32642	6.79E+07	0.73454	1894.238
32740	72.756	32675	6.86E+07	0.66796	1916.697
32772	72.7259	32707	6.91E+07	0.74062	1898.303
32805	72.7436	32740	7.00E+07	0.67302	1920.724
32837	72.7123	32772	7.10E+07	0.73245	1907.409
32870	72.7174	32805	7.24E+07	0.67423	1927.301
32902	72.685	32838	7.36E+07	0.66277	1935.295
32936	72.6762	32870	7.47E+07	0.66179	1939.149
32968	72.6529	32903	7.61E+07	0.7149	1930.325
33001		32935	7.80E+07	0.65477	1953.392
33032	72.6414	32968	7.91E+07	0.70738	1939.439
33066	72.6286	33001	8.00E+07	0.71434	1941.864
33098	72.6119	33033	8.06E+07	0.6561	1961.214
33131		33066	8.02E+07	0.72397	1939.123
33163	72.5816	33098	7.98E+07	0.65674	1959.165
33197	72.5771	33131	7.96E+07	0.65712	1957.085
33229	72.5819	33164	7.90E+07	0.64757	1957.315
33261	72.591	33196	7.76E+07	0.63489	1957.86
33294	72.5754	33229	7.57E+07	0.69726	1933.6

33327	72.5772	33261	7.12E+07	0.69165	1921.945
33360	72.5665	33294	7.09E+07	0.69898	1918.77
33392	72.5233	33327	6.94E+07	0.64037	1928.509
33426	72.5553	33360	6.50E+07	0.70626	1895.336
33458	72.5841	33393	6.18E+07	0.72125	1879.519
33490	72.5622	33425	6.05E+07	0.72629	1873.047
33523	72.6191	33458	5.74E+07	0.73356	1857.748
33554	72.5659	33490	5.63E+07	0.74082	1851.443
33588	72.5664	33523	5.66E+07	0.76192	1844.521
33620	72.5628	33555	5.69E+07	0.77361	1844.283
33653	72.5675	33588	5.80E+07	0.74245	1855.06
33686	72.5499	33620	5.87E+07	0.71295	1866.451
33718	72.546	33653	5.88E+07	0.71717	1865.081
33751	72.5792	33686	5.92E+07	0.7787	1851.488
33783	72.5526	33718	5.89E+07	0.7118	1867.834
33817		33751	5.89E+07	0.76924	1853.729
33849	72.5427	33784	5.85E+07	0.77487	1849.959
33882		33817	5.98E+07	0.71284	1872.487
33913	72.5069	33849	6.01E+07	0.71202	1872.747
33948	72.5314	33882	6.47E+07	0.69935	1894.544
33980	72.4959	33914	6.92E+07	0.69698	1910.576
34013	72.512	33947	7.14E+07	0.68325	1922.827
34045	72.4933	33980	7.19E+07	0.73593	1909.56
34078	72.4729	34013	7.01E+07	0.74078	1901.873
34111		34046	6.94E+07	0.67569	1917.55
34143	72.4697	34078	7.09E+07	0.6712	1923.93
34176	72.4673	34111	7.04E+07	0.6663	1923.977
34209	72.4845	34144	7.01E+07	0.66308	1924.711
34241	72.4654	34176	6.73E+07	0.71758	1901.155
34274	72.4819	34209	6.28E+07	0.71271	1882.803
34306	72.4737	34241	6.24E+07	0.72049	1879.784
34339	72.4624	34274	6.04E+07	0.73083	1868.787
34372	72.4247	34307	6.27E+07	0.6861	1891.319
34405	72.4238	34339	6.48E+07	0.74922	1882.022
34438		34372	6.75E+07	0.68388	1909.458
34469	72.4333	34405	6.81E+07	0.6784	1912.858
34502	72.3997	34438	6.76E+07	0.6704	1913.471
34535	72.4807	34470	6.57E+07	0.65892	1909.841
34566	72.3627	34502	6.56E+07	0.65375	1912.356
34600	72.3217	34535	6.35E+07	0.70252	1889.457
34634	72.4596	34568	6.18E+07	0.70644	1880.635
34664	72.4279	34600	6.02E+07	0.71233	1875.799
34698	72.3778	34633	5.82E+07	0.72113	1862.669
34731	72.3823	34665	5.97E+07	0.7342	1867.362
34763	72.3788	34698	5.88E+07	0.75109	1857.99
34796	72.3819	34731	5.77E+07	0.76129	1852.072
34828	72.3553	34763	5.55E+07	0.77281	1838.658

34862	72.3685	34796	5.60E+07	0.7213	1853.246
34894	72.3454	34829	5.65E+07	0.73196	1852.456
34927		34862	5.75E+07	0.72577	1858.309
34958	72.3525	34894	5.70E+07	0.72177	1857.016
34992	72.3412	34927	5.71E+07	0.72818	1856.022
35024	72.3591	34959	5.73E+07	0.76209	1849.938
35057	72.3578	34992	5.76E+07	0.71139	1863.288
35090	72.3651	35024	5.75E+07	0.76633	1846.532
35122	72.3493	35057	5.72E+07	0.77485	1844.638
35155	72.3574	35090	5.65E+07	0.786	1839.087
35187	72.3617	35123	5.77E+07	0.72971	1857.729
35220	72.3331	35155	5.77E+07	0.71597	1861.353
35253	72.3449	35188	5.69E+07	0.72649	1855.576
35285		35220	5.77E+07	0.71611	1862.638
35319	72.3667	35253	5.76E+07	0.7716	1848.449
35350	72.3347	35286	5.96E+07	0.76857	1856.515
35384	72.3392	35318	5.95E+07	0.7054	1872.939
35416	72.3062	35351	6.03E+07	0.70075	1877.862
35449	72.3063	35384	5.91E+07	0.76911	1855.631
35481		35417	5.97E+07	0.70814	1873.031
35514	72.3245	35449	5.97E+07	0.76692	1857.98
35546	72.3076	35482	6.00E+07	0.76657	1857.291
35579	72.3124	35514	6.19E+07	0.77941	1862.243
35611	72.3046	35547	6.01E+07	0.72013	1871.17
35644	72.3004	35579	6.01E+07	0.71082	1874.683
35677	72.3132	35612	6.30E+07	0.71133	1884.513
35709	72.2722	35644	6.59E+07	0.70077	1898.421
35742	72.2902	35677	6.97E+07	0.68827	1914.849
35774	72.2942	35710	7.27E+07	0.67095	1930.865
35807	72.2416	35742	7.15E+07	0.66161	1928.864
35841	72.2513	35775	7.36E+07	0.65225	1939.638
35873	72.2615	35808	7.51E+07	0.64103	1949.384
35906	72.2311	35841	7.70E+07	0.69596	1940.784
35939	72.2591	35873	7.78E+07	0.63114	1960.823
35970	72.1992	35906	7.70E+07	0.68922	1943.65
36004	72.2042	35939	7.58E+07	0.62882	1955.98
36036	72.188	35971	7.60E+07	0.6901	1939.805
36069	72.1817	36004	7.63E+07	0.6337	1956.162
36101		36037	7.62E+07	0.68733	1940.78
36133	72.1277	36069	7.64E+07	0.63254	1956.838
36167	72.1363	36102	7.54E+07	0.68722	1934.881
36199	72.1428	36134	7.23E+07	0.63287	1942.435
36232	72.1461	36167	7.10E+07	0.68747	1920.781
36265	72.1277	36200	6.95E+07	0.63221	1932.451
36298	72.1148	36233	6.96E+07	0.68719	1915.323
36330	72.1015	36265	7.24E+07	0.69866	1923.72
36363	72.0986	36298	7.32E+07	0.70106	1927.564

36395	72.0937	36330	7.51E+07	0.64725	1947.383
36428	72.0623	36363	7.62E+07	0.63961	1954.665
36461	72.075	36396	7.65E+07	0.70849	1936.559
36493	72.0465	36428	7.65E+07	0.64506	1953.05
36527	72.0479	36461	7.57E+07	0.63488	1954.558
36559	72.0245	36494	7.49E+07	0.68781	1938.301
36592	72.0363	36526	7.27E+07	0.69633	1925.733
36624	72.032	36559	6.92E+07	0.70824	1911.595
36657	72.0574	36592	7.00E+07	0.64074	1932.54
36689	72.0234	36624	6.85E+07	0.70728	1909.306
36723	72.0341	36657	6.63E+07	0.66393	1912.353
36755		36690	6.66E+07	0.71747	1897.957
36788	71.9994	36722	6.61E+07	0.66142	1913.245
36821	72.025	36755	6.56E+07	0.71208	1898.365
36853	71.9989	36788	6.58E+07	0.65782	1914.031
36886	72.0133	36821	6.12E+07	0.71667	1880.178
36919	71.9975	36854	6.27E+07	0.72775	1880.853
36952	72.0149	36886	6.40E+07	0.66102	1905.375
36984	72.0031	36919	6.29E+07	0.6722	1898.281
37017	71.9833	36952	6.09E+07	0.72145	1876.313
37050	71.9636	36985	5.91E+07	0.73481	1864.857
37082	71.9464	37017	6.00E+07	0.73862	1869.443
37116		37050	5.80E+07	0.7409	1859.272
37147	71.9928	37083	6.40E+07	0.68551	1898.27
37181	72.0063	37115	6.35E+07	0.76047	1875.146
37213	72.0015	37148	6.28E+07	0.69546	1890.149
37246	71.9857	37181	5.91E+07	0.7604	1856.886
37279	71.9867	37214	6.12E+07	0.76497	1863.153
37311	71.9738	37246	6.19E+07	0.77003	1867.122
37344	71.9878	37279	6.46E+07	0.71275	1890.86
37376	71.9635	37311	6.05E+07	0.70369	1879.135
37409		37344	6.20E+07	0.70525	1883.239
37440	71.9506	37377	6.16E+07	0.69477	1885.431
37475	71.958	37409	6.21E+07	0.75316	1870.783
37507	71.9149	37442	5.76E+07	0.74962	1855.125
37540	71.9528	37474	5.66E+07	0.75736	1847.175
37572	71.9522	37507	5.87E+07	0.69543	1875.899
37604	71.9152	37540	6.27E+07	0.69357	1890.619
37638	71.9271	37572	6.20E+07	0.69334	1888.946
37671	71.9853	37605	6.36E+07	0.68837	1895.327
37702	71.9346	37638	6.24E+07	0.7409	1876.013
37736	71.8904	37671	6.37E+07	0.67435	1900.786
37769	71.8965	37703	6.21E+07	0.73301	1876.219
37802	71.8994	37736	6.13E+07	0.74129	1872.109
37835	71.9278	37769	5.97E+07	0.75136	1862.876
37867	71.8885	37802	6.09E+07	0.76459	1865.524
37901	71.8971	37835	6.16E+07	0.76957	1866.344

37933	71.8754	37867	6.32E+07	0.71437	1887.24
37966	71.8577	37900	6.40E+07	0.71083	1890.056
37999	71.8421	37934	6.93E+07	0.70504	1911.947
38032		37966	7.31E+07	0.76952	1906.998
38063	71.8739	37999	7.39E+07	0.69717	1929.357
38097	71.8219	38032	7.59E+07	0.68341	1941.609
38130	71.8152	38064	7.65E+07	0.67753	1943.683
38163	71.8041	38097	7.56E+07	0.67121	1944.004
38196		38130	7.57E+07	0.66478	1945.993
38227	71.7904	38163	7.62E+07	0.64488	1953.831
38262	71.7861	38196	7.69E+07	0.63495	1958.019
38294	71.7956	38229	7.86E+07	0.6916	1946.846
38326	71.77	38261	7.91E+07	0.62841	1967.919
38360	71.7715	38294	7.94E+07	0.68557	1950.505
38392	71.7502	38327	7.88E+07	0.62423	1967.264
38425	71.7504	38360	7.82E+07	0.6856	1948.593
38458		38392	7.76E+07	0.62993	1962.677
38490		38425	7.73E+07	0.61821	1966.271
38524	71.7446	38458	7.58E+07	0.68114	1941.077
38557	71.7557	38491	7.48E+07	0.68021	1940.889
38589	71.7361	38524	7.39E+07	0.69197	1935.184
38622	71.7078	38557	7.42E+07	0.69331	1934.82
38655	71.698	38590	7.33E+07	0.70662	1927.516
38688	71.6785	38622	7.32E+07	0.65612	1940.546
38720	71.6673	38655	7.16E+07	0.65136	1936.195
38754	71.6756	38688	7.05E+07	0.71387	1913.376

Graphite Data Figure 4A		Graphite Data Figure 4C		Graphene Data Figure 4B		Graphene Data Figure 4D	
T avg	lavg/Mi	T avg	Emissivity Parameter, n	T avg	lavg/Mi	T avg	Emissivity Parameter, n
1812.94787	0.52104	1812.94787	0.92197	1925.80261	1.06172	1925.80261	0.58017
1902.57648	0.71115	1902.57648	0.77167	1954.81185	1.23212	1954.81185	0.5892
2006.89379	0.91229	2006.89379	0.62154	2003.01204	1.3617	2003.01204	0.5303
2080.73537	1.08538	2080.73537	0.52346	2140.85915	1.76694	2140.85915	0.34939
T avg	lavg/Mi	T avg	n	T avg	lavg/Mi	T avg	n
1793.90168	0.59474	1793.90168	0.83404	2140.85915	1.76694	2140.85915	0.34939
1893.8928	0.75276	1893.8928	0.71028	1969.90275	1.40486	1969.90275	0.53877
2015.90787	0.97367	2015.90787	0.56332	1729.9279	0.78726	1729.9279	0.81734
2232.13757	1.46208	2232.13757	0.33077	1637.87023	0.5955	1637.87023	0.92972
T avg	lavg/Mi	T avg	n	T avg	lavg/Mi	T avg	n
1910.57947	0.70945	1910.57947	0.59607	1869.4201	1.87254	1869.4201	0.32537
2019.54073	0.98146	2019.54073	0.43751	1896.3167	2.05556	1896.3167	0.29487
2095.5591	1.20947	2095.5591	0.32353	1933.05436	2.41554	1933.05436	0.28314
T avg	lavg/Mi	T avg	n	T avg	lavg/Mi	T avg	n
1904.73075	1.42324	1904.73075	0.36469	1957.30791	2.67071	1957.30791	0.27541
2004.29508	1.7483	2004.29508	0.23764	1924.04544	2.48714	1924.04544	0.30441
2104.20153	2.19528	2104.20153	0.12677	2199.78351	4.63578	2199.78351	0.13901
2181.60988	2.59535	2181.60988	0.09192	T avg	lavg/Mi	T avg	n
T avg	lavg/Mi	T avg	n	1815.31168	1.76364	1815.31168	0.45089
1807.21116	0.59927	1807.21116	0.70571	2040.25966	2.91101	2040.25966	0.20872
1913.09339	0.82796	1913.09339	0.54238	1962.12547	2.74473	1962.12547	0.32549
2011.0964	1.03358	2011.0964	0.38377	2215.22794	4.33478	2215.22794	0.00139
2091.13587	1.244	2091.13587	0.2808	T avg	lavg/Mi	T avg	n
T avg	lavg/Mi	T avg	n	1881.15027	0.31964	1881.15027	0.72559
2091.13587	1.244	2091.13587	0.2808	2017.6305	0.74081	2017.6305	0.52295
1998.86577	1.04945	1998.86577	0.35315	2130.57911	0.91831	2130.57911	0.37578
1888.48525	0.81605	1888.48525	0.44452	T avg	lavg/Mi	T avg	n
1804.2565	0.69331	1804.2565	0.57764	2130.57911	0.91831	2130.57911	0.37578
T avg	lavg/Mi	T avg	n	2054.09987	0.77959	2054.09987	0.38724
1816.6796	0.45408	1816.6796	0.64803	1881.44809	0.69686	1881.44809	0.81789
1850.41986	0.49726	1850.41986	0.61784	T avg	lavg/Mi	T avg	n
1907.03962	0.56625	1907.03962	0.53133	1881.44809	0.69686	1881.44809	0.81789
2011.65633	0.76362	2011.65633	0.41492	1952.5489	0.76392	1952.5489	0.67247
T avg	lavg/Mi	T avg	n	2197.05722	1.08966	2197.05722	0.29344
1914.95414	0.22332	1914.95414	0.49566	T avg	lavg/Mi	T avg	n
1950.33472	0.30857	1950.33472	0.45233	1911.88077	0.67543	1911.88077	0.50718
2007.86418	0.47301	2007.86418	0.38736	2031.68143	0.88793	2031.68143	0.39642
2066.33719	0.57567	2066.33719	0.32015	2062.49722	0.93109	2062.49722	0.35024
T avg	lavg/Mi	T avg	n	T avg	lavg/Mi	T avg	n
1834.00836	0.27712	1834.00836	0.97192	2062.49722	0.93109	2062.49722	0.35024
1957.78381	0.44802	1957.78381	0.75699	1932.42258	0.69659	1932.42258	0.47208
2077.98058	0.58617	2077.98058	0.57543	1786.59117	0.45111	1786.59117	0.52945
T avg	lavg/Mi	T avg	n	T avg	lavg/Mi	T avg	n
1791.51129	0.35457	1791.51129	0.76023	1786.59117	0.45111	1786.59117	0.52945
1899.948	0.47144	1899.948	0.63051	1930.36183	0.70054	1930.36183	0.48213
1950.10993	0.52911	1950.10993	0.58901	2033.686	0.89621	2033.686	0.39405
2012.1849	0.6197	2012.1849	0.54152	2108.19491	1.04937	2108.19491	0.33287
T avg	lavg/Mi	T avg	n	T avg	lavg/Mi	T avg	n
1911.16464	0.70863	1911.16464	0.68727	1806.11444	0.27981	1806.11444	0.65754
2031.59671	1.04463	2031.59671	0.53749	1898.53523	0.45427	1898.53523	0.56332
2112.79093	1.2285	2112.79093	0.42348	2004.415	0.65489	2004.415	0.45161
2173.09917	1.41818	2173.09917	0.35341	2062.86757	0.78344	2062.86757	0.38243
T avg	lavg/Mi	T avg	n	T avg	lavg/Mi	T avg	n
1837.75104	0.33243	1837.75104	0.75333	2062.86757	0.78344	2062.86757	0.38243
1891.62185	0.35987	1891.62185	0.73126	1976.97512	0.6651	1976.97512	0.42787
				1930.796	0.62477	1930.796	0.51201
				1887.02754	0.56931	1887.02754	0.55841

1998.72679	0.51533	1998.72679	0.68952	1810.39881	0.48182	1810.39881	0.66126
2101.26115	0.65307	2101.26115	0.56224				
T avg	lavg/Mi	T avg	n	T avg	lavg/Mi	T avg	n
1812.80194	0.16609	1812.80194	0.8584	1810.39881	0.48182	1810.39881	0.66126
1908.7598	0.356	1908.7598	0.73431	1911.73767	0.60937	1911.73767	0.54402
2021.79725	0.55746	2021.79725	0.64617	2101.37029	1.02982	2101.37029	0.46304
2031.07336	0.60644	2031.07336	0.54986				
T avg	lavg/Mi	T avg	n	T avg	lavg/Mi	T avg	n
1804.341	0.3824	1804.341	0.66985	1808.94671	0.28177	1808.94671	0.8245
1912.95433	0.50069	1912.95433	0.55964	1911.17276	0.46236	1911.17276	0.682
2005.92659	0.62354	2005.92659	0.46987	2006.72732	0.68556	2006.72732	0.51922
2062.062	0.7003	2062.062	0.40713	2099.85628	0.87808	2099.85628	0.39264
2102.03614	0.76546	2102.03614	0.36244				
T avg	lavg/Mi	T avg	n	T avg	lavg/Mi	T avg	n
1928.25571	0.58538	1928.25571	0.52555	2000.7878	0.7601	2000.7878	0.46961
2016.55175	0.70879	2016.55175	0.43708	1898.88905	0.6152	1898.88905	0.58107
2128.52844	0.91083	2128.52844	0.35948	1791.37136	0.47266	1791.37136	0.69871
T avg	lavg/Mi	T avg	n	T avg	lavg/Mi	T avg	n
1770.84544	0.39601	1770.84544	0.81446	1791.37136	0.47266	1791.37136	0.69871
1905.542	0.61669	1905.542	0.68495	1897.58431	0.61588	1897.58431	0.58077
1980.20358	0.79062	1980.20358	0.56876	1992.0879	0.75949	1992.0879	0.47783
2051.76829	0.95684	2051.76829	0.48259	2097.37678	0.96054	2097.37678	0.35732
T avg	lavg/Mi	T avg	n				
1768.71524	0.32821	1768.71524	0.7962				
1895.10273	0.53047	1895.10273	0.79984				
1971.94773	0.6388	1971.94773	0.66358				
2117.1979	1.00741	2117.1979	0.51305				
T avg	lavg/Mi	T avg	n				
1783.17246	0.46709	1783.17246	0.68869				
1885.10191	0.69557	1885.10191	0.72845				
2009.20633	0.94568	2009.20633	0.63787				
2107.40065	1.15692	2107.40065	0.48295				
T avg	lavg/Mi	T avg	n				
1810.97731	0.39756	1810.97731	0.81428				
1973.53413	0.69406	1973.53413	0.64432				
2067.19067	0.95196	2067.19067	0.50022				
2200.12836	1.47119	2200.12836	0.34695				
T avg	lavg/Mi	T avg	n				
1813.75131	0.52275	1813.75131	0.40586				
1868.78471	0.70569	1868.78471	0.50946				
1940.2738	0.91651	1940.2738	0.52113				
2113.57813	1.37227	2113.57813	0.39287				
2222.59346	1.74156	2222.59346	0.30926				
T avg	lavg/Mi	T avg	n				
1813.13689	0.58416	1813.13689	0.39858				
1907.16446	0.89011	1907.16446	0.4932				
2008.60925	1.20887	2008.60925	0.47286				
2199.87307	1.85581	2199.87307	0.36372				
T avg	lavg/Mi	T avg	n				
1809.30126	0.50094	1809.30126	0.91347				
1884.95574	0.63884	1884.95574	0.79164				
1836.59233	0.57928	1836.59233	0.82418				
1940.065	0.76291	1940.065	0.73034				
2120.87767	1.13411	2120.87767	0.51507				
T avg	lavg/Mi	T avg	n				
1988.22033	0.88386	1988.22033	0.63022				
2061.57845	1.07028	2061.57845	0.54358				
1990.78448	0.93173	1990.78448	0.6059				
2067.5995	1.1117	2067.5995	0.54032				

2116.3208	1.19737	2116.3208	0.46835
T avg	lavg/Mi	T avg	n
1803.23565	0.31884	1803.23565	0.84765
1863.37417	0.38093	1863.37417	0.78571
1955.46471	0.44777	1955.46471	0.63939
2112.47811	0.68197	2112.47811	0.52761
T avg	lavg/Mi	T avg	n
1812.07972	0.22429	1812.07972	0.92217
1885.40783	0.2994	1885.40783	0.85852
1955.85308	0.37606	1955.85308	0.80997
2037.44133	0.5303	2037.44133	0.67069
2134.44329	0.70163	2134.44329	0.50502
T avg	lavg/Mi	T avg	n
2134.44329	0.70163	2134.44329	0.50502
2024.95862	0.59447	2024.95862	0.53679
1883.99942	0.4348	1883.99942	0.65144
T avg	lavg/Mi	T avg	n
1796.7533	0.36182	1796.7533	0.7755
1911.14691	0.48268	1911.14691	0.66274
2032.23155	0.65014	2032.23155	0.5677
2144.65911	0.85719	2144.65911	0.45681
T avg	lavg/Mi	T avg	n
1805.57536	0.34218	1805.57536	1.35814
1851.6055	0.35246	1851.6055	1.06385
1904.37085	0.36029	1904.37085	0.88522
2006.86817	0.48171	2006.86817	0.77354
2177.47533	0.91703	2177.47533	0.62753
T avg	lavg/Mi	T avg	n
2177.47533	0.91703	2177.47533	0.62753
2116.5406	0.77301	2116.5406	0.54759
2040.0975	0.66488	2040.0975	0.60887
T avg	lavg/Mi	T avg	n
2253.35911	1.05627	2253.35911	0.4283
1858.02567	0.55259	1858.02567	0.81197
1792.11705	0.47525	1792.11705	0.90636

Figure 6A Graphite Data

M_I	Ea (kJ/mol)
22.16349	267.14402
20.65761	421.54101
14.26879	355.58903
21.83925	437.36601
38.93047	243.9166506
36.91668	595.4463931
46.71086	469.19336
10.02041	201.85678
5.55622	245.40743
75.96802	596.51555
39.55572	283.95802
35.86965	568.92825
120.82357	247.65209
114.41283	394.22492
109.06675	659.98583
15.14995	454.93622
13.78304	474.55585
12.22539	390.53929
58.11882	373.64122
50.80775	602.34573
46.66514	746.4811
17.83133	387.46435
16.65207	435.43481
16.24699	484.2215
17.663499	222.4248456
16.897197	643.0542578
15.436965	448.0165869
19.35606	426.59304
18.80892	792.80297
17.45237	517.98512

Figure 6B Graphene Data

M_I	Ea (kJ/mol)
11.26089	394.9702
11.08014	423.6423
39.37613	373.4958
70.86106	482.1347
41.79014	229.4739
38.94829	268.3702
37.87616	328.4503
41.06963	401.3761
40.87548	211.7857
40.70118	482.9261
42.84934	245.7435
42.53173	651.5733
42.12453	695.0297
64.03095	224.5084
61.79144	525.6055
59.67103	469.8583

Figure 7 Graphite Data

S2-s1/S1	I2-I1/I1	Percent Change
-0.39501	0.06966	6.966
-0.64032	0.02886	2.886
-0.77881	-0.4572	-45.72
-0.67502	0.19491	19.491
0.12692	-0.15574	-15.574
-0.85718	0.28134	28.134
-0.81267	0.0431	4.31
-0.80408	0.17835	17.835

Figure 7 Graphite Data

S3-S1/S1	I3-I1/I1	Percent Change
-0.86121	0.32832	32.832
-0.16221	0.05557	5.557
-0.91624	0.42786	42.786
-0.80368	-0.3883	-38.83
-0.759	0.30172	30.172

Figure 7 Graphene Data

grapheneS2-s1/S1	grapheneI2-I1/I1	Percent Change
-0.32714	0.08361	8.361
-0.52312	0.24147	24.147
-0.00556	-0.00953	-0.953
-0.42353	0.06164	6.164
-0.61411	0.11622	11.622

Figure 7 Graphene Data

grapheneS3-S1/S1	grapheneI3-I1/I1	Percent Change
-0.36892	0.34088	34.088
-0.33467	0.01181	1.181
0.06485	0.25604	25.604
-0.66259	0.16956	16.956